Proteomic Profiling of Animal Models of Myotonia and Motor Neuron Disease

Submitted to National University of Ireland Maynooth for the degree of Doctor of Philosophy

NUI MAYNOOTH

Ollscoil na hÉireann Má Nuad

Lisa Staunton, B. Sc

Head of Department
Professor Kay Ohlendieck,
Department of Biology,
NUIM Maynooth,
Co. Kildare.

Supervisor
Professor Kay Ohlendieck,
Department of Biology,
NUIM Maynooth,
Co. Kildare.

Publications

Staunton L , Jockusch H , Ohlendieck K . 2011. Proteomic analysis of muscle affected by motor neuron degeneraion; the wobbler mouse model of amytrophic lateral schlerosis. Biochem Biophys Res Commun. 406 (4): 595-600.

Staunton L , Jockusch H , Wiegand C , Albrecht T , Ohlendieck K . 2011. Identification of secondary effects of hyperexcitabilty by proteomic profiling of myotonic mouse muscle. Mol. Biosyst. DOI: 10.1039/C1MB05043E. (in press)

Staunton L , and Ohlendieck K. 2011. Mass spectrometric characterization of the sarcoplasmic reticulum from rabbit skeletal muscle by on-membrane digestion. Protein Pept. Lett. Sept 20 PMID: 21933128 (in press)

Staunton L , O' Connell K , Ohlendieck K . 2011. Proteomic profiling of mitochondrial enzymes during skeletal muscle aging. J. Aging Res. Mar 7; 2011: 908035.

Staunton L , Donoghue P , Mullen E , Manning G , Ohlendieck K . 2010. DIGE analysis of rat skeletal muscle proteins using nonionic detergent phase extraction of young adult versus aged gastrocnemius tissue. J. Proteomics. 73 (8): 1441-1453.

Gannon J , **Staunton L** , O' Connell K , Doran P , Ohlenieck K . 2008. Phosphoproteomic analysis of aged skeletal muscle. Int J Mol. Med. 22 (1): 33-42.

Presentations

Poster presentation:

Identification of Novel Biomarkers in Muscle Diseases. Staunton, L., H. Jockusch, K. Ohlendieck. European Proteomics association 2010, Estoril, Portugal.

Staunton L., C. Lewis, S . Carberry, E. Mullen, and K. Ohlendieck. 2011. Mass spectrometry-based proteomic profiling of neuro-muscular disorders. J Mol. Med (abstract).

Departmental Seminars

Animal Models of myotonia. 2009. National University of Ireland, Maynooth.

Fiber type switching in skeletal muscle. 2010. National University of Ireland, Maynooth.

Table of contents

1.Introduction

2. Materials and methods

2.2 Methods

List of figures

List of tables

Acknowledgements

To Professor Kay Ohlendieck for giving me the opportunity to carry out this work in his laboratory and his guidance and support throughout the past three years.

To all members of the Muscle Biology laboratory past and present Joan, Kathy, Caroline, Edel, Pam, Phil and Steven for who all have been helpful and provided numerous laughs. I would especially like to thank Dr. Joan Gannon who supervised during my fourth year project in the lab.

To all the staff of the Biology Department at NUI Maynooth who keep the department running. I would also like to thank all the students (Blanaid, Patrick, Amy and Andrea) who worked on the project with me.

This work was supported by a grant from the Health Research Board, as well as equipment grants from the Irish Health Research Board.

To all my friends for listening to me talk about gels and me complaining when experiments didn't work out. Thank you for your time and encouragement.

To Daniel for his patience the times I would be another ten minutes that turned into an hour and the understanding when I didn't go home because of work. Thank you for your help and support.

I would also like to thank my family, especially my parents Sean and Mary for their constant support throughout my education for encouraging me do transition year during secondary school. You both have always been there for help and advice when I needed it. It is to them that I dedicate this work.

Declaration

This thesis has not been submitted in whole or in part to this or any other university for any degree, and is the original work of the author except where stated.

Signed_____

Date_____

Abbreviations

Ach	Acetylcholine
AChR	Acetylcholine receptor
ADP	Adenosine Diphosphate
ADR	Arrested development of righting response
AK	Adenylate Kinase
ALS	Amytrophic lateral sclerosis
ATP	Adenosine triphosphate
BSA	Bovine serum albumin
Ca^{2+}	Calcium ions
CBB	Coomassie brilliant blue
CHAPS	3-[3-chlolamidopropyl-Dimethylammonio-1-propane sulfonate
Cl^-	Chloride ions
CLC_1	Chloride channel
CLFS	Chronic low-frequency stimulation
CSF	Cerebral spinal fluid
CSQ	Calsequestrin
Cu/Zn SOD	Copper/Zinc Superoxide dismutase
2DE	Two dimensional gel electrophoresis
DHPR	Dihydropyridine Receptors
DIGE	Difference In Gel Electrophoresis
DM	Myotonic Dystrophy
DMF	Dimethlformamide
DTT	Dithiothretiol
EAAT2	Excitatory amino-acid transporter 2
ECL	Enhanced chemiluminescence
EDL	Extensor Digitorum Longus
EDTA	Ethylenediaminetetraacetic acid
ESI	Electrospray ionization
FABP	Fatty acid binding protein
FALS	Familial Amytrophic Lateral Sclerosis
FHL-1	Four and a half LIM domain
G	g force
GAPDH	Glyceraldehyde 3-phosphate dehydrogenase
GARP	Golgi-associated retograde protein
H	Hours
H^+	Hydrogen Ions
HPLC	High performance liquid chromatography
HRP	Horse radish peroxidase
Hsp	Heat shock protein
IEF	Isoelectric focusing

IPG	Immobilised pH Gradient
K^+	Potassium Ions
kDa	Kilodaltons
LCMS	Liquid-chromatography mass spectrometry
M	Molar
MAPK	Mitogen-activated protein kinase
MHC	Myosin heavy chain
MHC_{emb}	Myosin heavy chain embryonic
Min	Minute
Ml	Milliliter
MLC	Myosin light chain
MLC phospho	Myosin light Chain phosphorylatable
mRNA	Messenger ribonucleic acid
MS	Mass Spectrometry
MTO	Myotonia
MYBP	Myosin Binding Protein
MW	Molecular Weight
µL	Microlitre
µg	Microgram
µM	Micromolar
mM	Millimolar
mAb	Monoclonal antibody
Na^+	Sodium Ions
NADH	Nicotinamide Adenine Dinucleotide
NFAT	Nuclear factor of activated T cells
PAGE	Polyacrylamide gel electrophoresis
PBS	Phosphate buffered saline
PGC-1	Peroxisome proliferator γ coactivator 1
Pi	Inorganic phosphate
p*I*	Isoelectric point
PPARδ	Peroxisome proliferator-activated receptor δ
ROS	Reactive Oxygen Species
RuBPs	Ruthenium II[Bathophenathroline Disulfonate]
RyR	Ryanodine Receptor
S	Second
SALS	Sporadic Amytrophic Lateral Sclerosis
SAR	Sarcalumenin
SDS	Sodium dodecyl sulfate
SERCA	Sarcoplasmic/Endoplasmic reticulum Ca^{2+}-ATPase
SMN	Survival motor neuron
SR	Sarcoplasmic Reticulum
Temed	Tetramethylethylenendiamine
TnI	Troponin I
TnT	Troponin T

TnC	Troponin C
TPI	Triosphosphate isomerase
TRIC-A	Trimeric intracellular cation-selective channel
T-tubules	Transverse tubules
UPP	Ubiquitin-proteasome pathway
V	Volts
VAPB	Vesicle associated protein B
VDAC	Voltage dependent anion channel
Vsp	Vesicle sorting protein
WR	Wobbler

Abstract

Skeletal muscle provides an organism with a means of reacting to its environments. It is a complex and versatile tissue that is capable of change under a variety of conditions. For example extensive literature has shown muscle transformation from slow-to-fast by decreased motor nerve activity, hypogravity, physical inactivity and in diseased states. Similarly muscle transformation from fast-to-slow can be evoked by increased muscle nerve activity or exercise. The multitude of protein changes that has been identified by muscle transformation indicates it is a complex process that can change a wide variety of the muscle tissues architecture, metabolism and function.

Proteomic profiling of two very different diseased states has allowed the identification of muscle transformation occurring in opposite directions. Myotonia a common feature found in myotonic dystrophies is characterized by skeletal muscle membrane hyperexcitability. Proteomic profiling was carried out on three independent spontaneous mutant mice and allowed us to compare secondary effects of hyperexcitabilty on skeletal muscle. Severly myotonic mice MTO and ADR displayed a muscle transformation from fast-to-slow. The more mildly affected MTO*5J mutant showed slight changes in proteins associated with fast and slow muscle.

In comparison to the myotonic diseased state we carried out proteomic profiling of skeletal muscle tissue from the Wobbler mouse; an animal model of motor neuron degeneration. In contrast to myotonia the WR protein profile displayed a slow-to-fast muscle transformation.

The detailed MS-based analysis of diseased skeletal muscle has shown that proteomics is highly suitable to determine change in the isoform expression pattern of muscle proteins. Identified proteins can be used as potential factors for the establishment of comprehensive biomarker signature of myotonic and motor neuron diseases.

1. Introduction

1.1 Muscle Biology

Muscle tissue is defined by its ability to use chemical energy to produce force and movement. The ability to move provides an organism with a means of reacting to the environment. Muscle tissue can be categorized into four distinct classes: skeletal muscle, cardiac muscle, smooth muscle and myoepithelial cells, all differing in function and location. Cardiac muscle forms the walls of the heart and is striated like skeletal muscle. The striations found in cardiac and skeletal muscle are due to the arrangement of contractile proteins, and for this reason cardiac and skeletal muscle have similar mechanisms of contraction. Skeletal muscle functions in short bursts of contraction and its contraction is voluntary whereas cardiac, smooth and myoepithelial muscle is involuntary (i.e. not controlled by the somatic nervous system). Cardiac muscle has continuous activity and is resistant to fatigue due to its high concentration of mitochondria. Myoepithelial muscle can be found in areas of the body such as the glands and eye, whereas skeletal muscle is attached to the bones of the skeleton via tendons, and is found throughout the body.

1.2 Skeletal Muscle

1.2.1 Skeletal Muscle Formation

Skeletal muscle is formed during embryonic development by a process called myogenesis. Transcription factors such as MyoD, stimulate indeterminate stem cells to become determinate muscle cells (Berkes and Tapscott 2005). These determinate muscle cells undergo myogenesis in order to develop into mature muscle cells. Mature muscle cells develop into larger cells called myoblasts that fuse together forming myotubes. These myotubes will eventually develop into long strands of muscle fibers. Muscle fibers are arranged longitudinally and are bound together by connective tissue. It is these fibers that make up mature muscle.

1.2.2 Skeletal Muscle Structure and Function

Skeletal muscle fibers are made up of many myofibrils that are arranged longitudinally and run along the axis of each fiber. Each myofibril contains sarcomeres (see figure 1.1) that are made of two types of filaments, thick and thin filaments. Thin filaments are made up of two actin strands, which twist together to form an alpha helix, bound to this helix are the proteins tropomyosin and troponin. Tropomyosin lies in the grooves of the actin helix with one troponin complex associated with each tropomyosin molecule (Squire and Morris 1998). The troponin complex is made up of troponin C (TnC) that is the binding site for calcium ions (Ca^{2+}), troponin I (TnI) that inhibits actin-myosin binding and troponin T (TnT) that binds strongly to tropomyosin. Thick filaments are made up of myosin. A myosin molecule is composed of 6 polypeptides: 2 heavy chains (MHC) and 4 light chains (MLC) (2 regulatory and 2 alkali) (Clark et al. 2002). A regulatory and an alkali light chain are associated with each heavy chain. The MLCs make up the myosin heads of the thick filament and are called subfragment 1 (S1) and are connected to the alpha-helix tail made of MHCs. Thin filaments surround each thick filament and it is this arrangement that gives muscle cells its striated appearance. Muscle force is produced when projecting myosin heads on the myosin molecule interact with adjacent actin filaments.

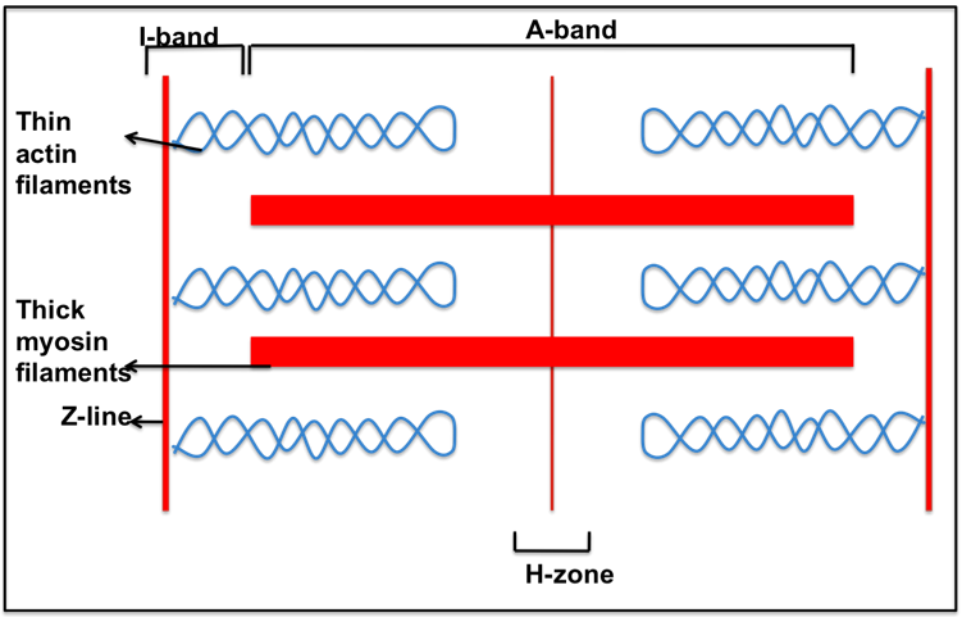

Figure 1.1 Sarcomere structure

Shown is the simplified structure of the sarcomere. The sarcomere is the single contractile unit of skeletal muscle. The Z line is made up of actinin and act to anchor the thin filaments. The A band is a condensed area at the centre of the sarcomere and consists of the thick filaments and overlapping areas of thin filaments. The I band consists of the non-overlapping portions of the thin filaments and the Z line. Adapted from Huxley (2004).

Skeletal muscle contraction begins at the motor cortex of the brain and travels through the somatic nervous system as an electrical signal. When this signal reaches a motor neuron that ends at a muscle fiber it comes to a neuromuscular junction (shown in Figure 1.2). At the neuromuscular junction the electrical signal is converted to a chemical one in the form of acetylcholine (ACh) in order to allow the signal to cross the gap (synapse) between the motor neuron and the muscle fiber. ACh is released from the terminus of the motor neuron, crosses the synapse and binds to post-synaptic acetylcholine receptors (AChR) located on the muscle membrane. Activation of AChR causes localized depolarization (Farley et al. 1977) resulting in the opening of sodium channels. As sodium ions (Na^+) enter the cytosol the sarcolemma becomes depolarized (Hodgkin et al. 1960) and an action potential is started. The action potential travels along the sarcolemma and enters into the transverse tubules (T-tubules), which are invaginations of the sarcolemma.

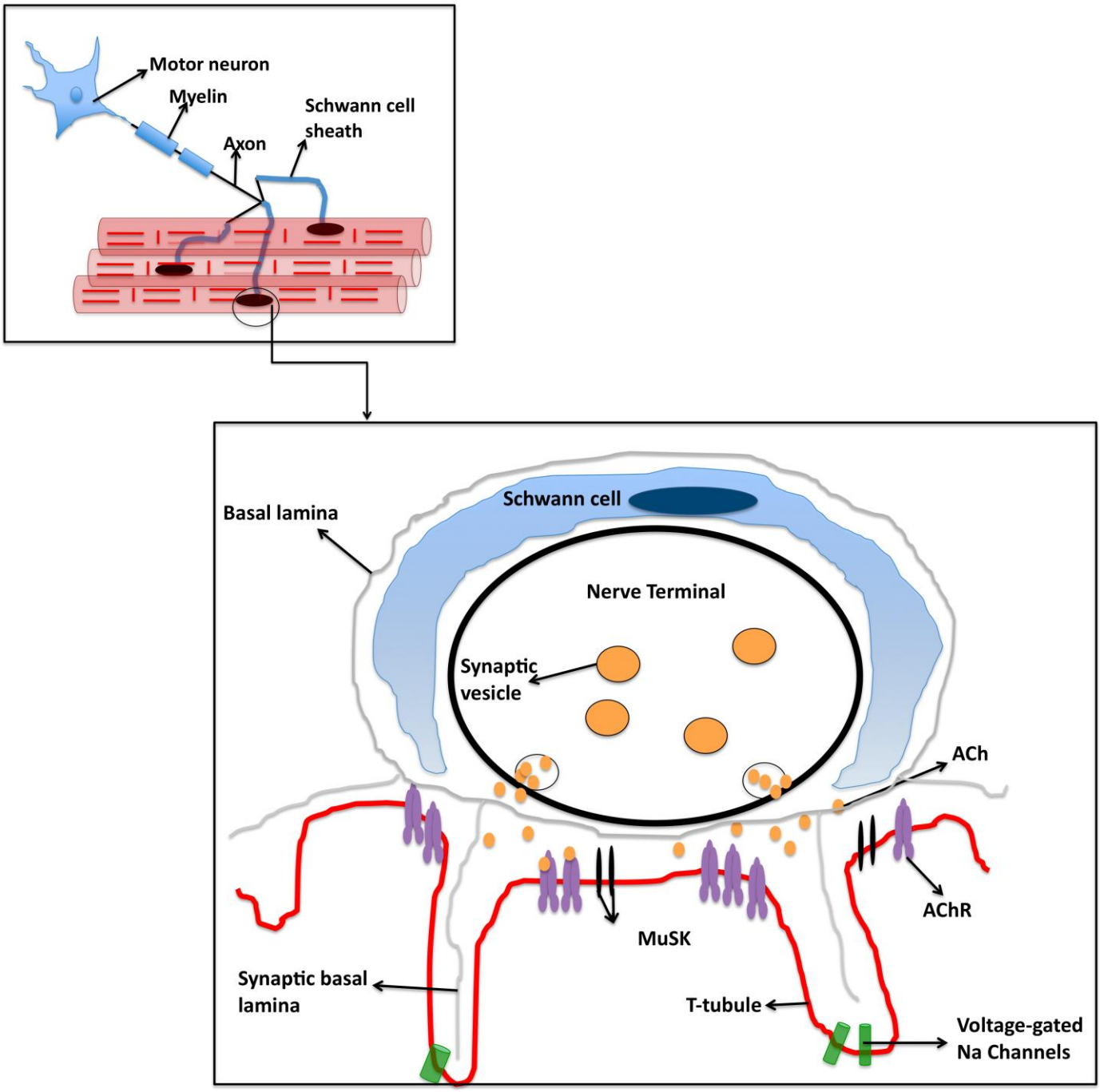

Figure 1.2 Structure and molecular architecture of the neuromuscular junction.
Shown is the progressive enlargement of the neuromuscular junction. The neurotransmitter acetylcholine (Ach) is released from the axon and diffuses across the synapse and binds to acetylcholine receptors (AChR) on the sarcolemma that results in the start of an action potential along the sarcolemma. Muscle thyrosine kinase (MuSK) functions to organize AchR clustering at the neuromuscular junction in order to maintain muscle function. Redrawn from Shigemoto et al. 2010.

Depolarization traveling in the T-tubules activates the voltage sensing alpha 1 subunit of the Dihydropyridine receptor (DHPR) resulting in a conformational change in the protein allowing its II-III loop domain to directly interact with the intracellular ryanodine receptor (RyR) (Proenza et al. 2002) of the sarcoplasmic reticulum (SR). This interaction allows RyR to open its calcium channels allowing the flux of calcium ions (Ca^{2+}) into the cytoplasm of the muscle cell. Cytosolic Ca^{2+} then binds to TnC (shown in Figure 1.3) resulting in a conformational change in the troponin complex. TnI no longer inhibits the actin-myosin binding. In the presence of ATP, the myosin head on the thick filament binds to the myosin binding site on the actin molecule, ATP is broken down to ADP and Pi, the myosin head releases and moves onward to the next actin molecule along the thin filament. Myosin heads of the thick filaments walk toward the ends of the thin filaments thus shortening the sarcomere. This process of movement, attach and release is called cross-bridge cycling (Huxley et al. 1954). This is repeated until there is a lack of Ca^{2+} or ATP. For muscle relaxation, chloride and potassium channels are activated by depolarization of the sarcolemma. Once activated chloride ions (Cl^-) flood into the cell and potassium ions (K^+) move out of the cell. The movement of Cl^- into the cell and K^+ out of the cell function to repolarise the sarcolemma. Membrane repolarisation results in the disassembly of the DHPR-RyR interaction leading to the energy-dependent re-uptake of Ca^{2+} into the lumen of the SR by the sarcoplasmic/endoplasmic reticulum ATPase (SERCA). The lack of cytoplasmic Ca^{2+} causes the calcium ions bound to troponin to be released and tropomyosin returns to its normal conformation, preventing any cross bridges from being formed, and the muscle relaxes.

It is critical that the myosin heads of the thick filament operate with low processitivity such that they are tightly bound to the actin of the thin filament for a short amount of time i.e. one cycle of ATPase so that they do not hold each other back. This rapid shortening of thousands of sarcomeres lying end-to-end in each myofibril results in skeletal muscles ability to contract rapidly and is called the sliding filament theory. It is important to note that since sarcomere shortening is due to each filament sliding past each other and not due to a change in length of the filament. Accessory proteins in the sarcomere enable uniformity in filament organization, length and spacing and thus play a huge role in muscle contraction.

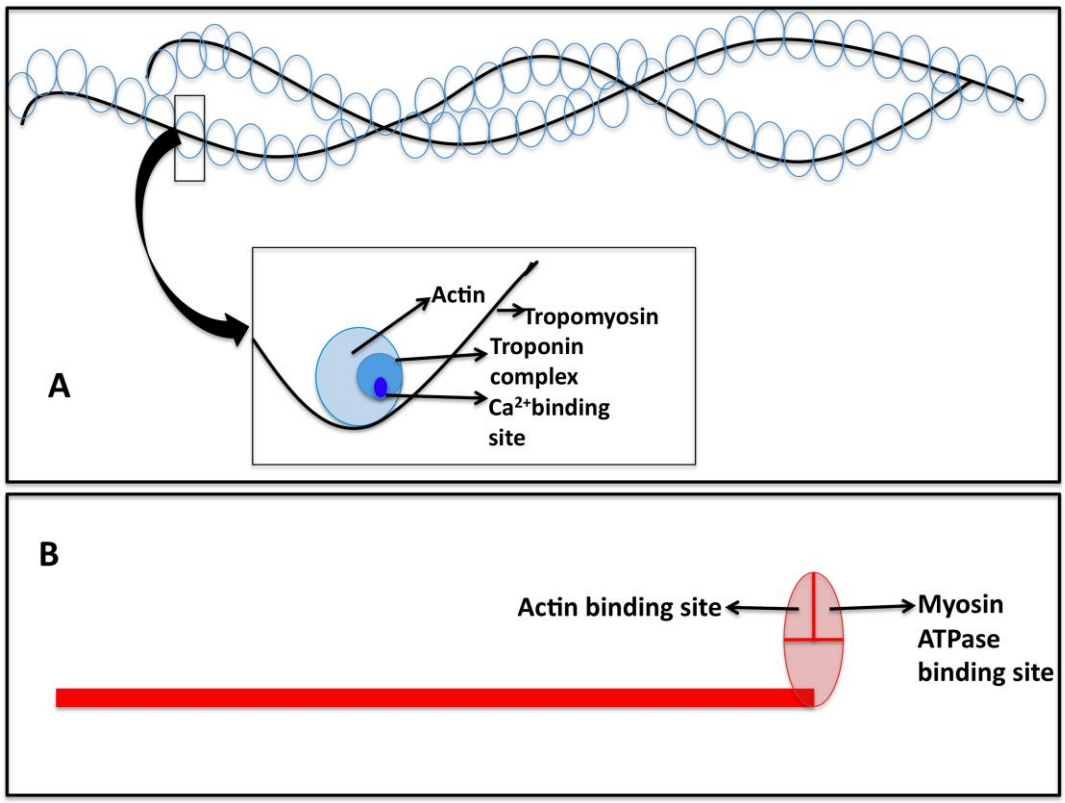

Figure 1.3 Structure of thin filament and thin filaments

Shown is the structure of the thin filaments (A) with actin and its regulatory proteins troponin and tropomyosin. The thick filament made of myosin molecule (B) is also shown. Adapted from Squire and Morris 1998.

1.2.3 Skeletal Muscle Fibers

Skeletal muscle is a complex, versatile tissue composed of a large variety of functionally diverse fiber types. The properties of individual muscles largely depend on the combination of the individual properties of their different fiber types and their proportions. The earliest classification of fiber types began when French anatomist Louis Antoine Ranvier in 1873 observed that some muscles of the rabbit were redder in color and contracted in a slower manner compared to paler muscles. This observation formed the basis for the classical terminology of red (slow-twitch) or type I fibers and white (fast-twitch) or type II fibers. In humans a further subdivision was made whereby fast-twitch fibers were either more aerobic using oxidative metabolism Type IIA or anaerobic using glycolytic metabolism Type IIB. This allowed muscle fibers to be classified in terms of their contractile and metabolic properties. Today muscle fibers are classified by three different methods: histochemical staining for myofibrillar ATPase (mATPase), myosin heavy chain (MHC) isoform identification and biochemical identification of metabolic enzymes (Staron and Pette 2000).

1.2.4 Fiber Classification

1.2.4.1 Fiber Metabolism

Muscle tissue requires pathways for energy metabolism that can provide energy during long periods of slightly increased energy consumption and short bursts of high-energy consumption. Energy is mainly consumed by the molecular motors during muscle contraction i.e. myosin heads and ion pumps (Westerblad et al. 2010). The energy required for muscle contraction depends on the type of contraction, whether it is short repeated contraction or long continuous contraction. In skeletal muscle, energy for contraction is supplied by adenosine triphosphate (ATP) via anaerobic glycolysis, the phosphocreatine shuttle and oxidative phosphorylation (Ohlendieck, 2010).

Glycogen breakdown is regulated by glycogen phosphorylase. Glycogen phosphorylase releases glucose residues from glycogen. Glucose enters the glycolysis pathway were it is ultimately converted to pyruvate with the production of ATP. Fast twitch fibers mainly use glycolysis for their energy metabolism (Peter et al. 1972). During intense exercise lactate dehydrogenase turns NADH $+H^+$ +pyruvate into lactate $+NAD^+$. This reaction occurs to regenerate NAD^+ that is consumed during glycolysis so that the muscle can maintain the glycolytic pathway (Katz et al. 1988).

Anaerobic metabolism is also dominated by degradation of phosphocreatine. The degradation of phosphocreatine (PCr) is catalyzed by the enzyme creatine kinase. Creatine kinase breaks down PCr + ADP to creatine + ATP.

Oxidative metabolism of carbohydrates and lipids are the dominating-ATP producing systems during aerobic metabolism. The major carbohydrate used for oxidative metabolism is glucose. In the presence of oxygen, glucose + oxygen are broken down to release carbon dioxide + water. This process takes place within the mitochondria through the Krebs cycle and oxidative phosphorylation. The substrate for lipid metabolism is free fatty acids obtained from triglyceride stored in muscle. Also amino acids can be an additional substrate for aerobic metabolism. Amino acids can be derived from muscle protein degradation. Slow-twitch fibers gain their energy needs mostly through oxidative metabolism.

1.2.4.2 Myosin Heavy Chain isoform

As previously stated myosin is a hexameric protein composed of heavy and light chains. One of the best ways to characterize muscle fibers types is based on myosin heavy chain (MHC) complement. A total of eleven MHC isoforms have been identified to date (Pette and Staron 2000). Some MHC isoforms are expressed in a specific manner; for example, MHC embryonic (MHC_{emb}) is only expressed in adult extraocular muscles (Pette and Staron 2000). Others are widely distributed throughout skeletal muscle. Skeletal muscle isoforms of MHC include: MHCI, MHCIIa, MHCIId and MHCIIb. Shown in Table 1.1 are the pure fibers that only express one MHC isoform and include slow type I, and three fast types type IIA, type IID and type IIB (Pette and Staron 2000). Muscles in humans and other large mammals do not express MHCIIb therefore fibers that were classified as type IIB in human muscle have been renamed type IIX and express MHCIIx. MHCIId and fiber type IID found in small mammals like the rat are considered to be equivalent to MHCIIx and fiber type IIX respectively in human muscle (Pette and Staron, 1990; Schiaffino and Reggiani, 1994, 1996). Co-expression of specific pairs of MHC isoforms results in the formation of hybrid fibers (shown in Table 1.1). Hybrid fibers bridge the gap between pure fibers in muscle tissue.

PURE FIBERS	MYOSIN ISOFORM	TISSUE
Slow type I	MHCIb	Soleus muscle
Fast type IIA	MHCIa	Diaphragm
Fast type IID/IIX	MHCIId/IIx	Tibialis Anterior
Fast type IIB	MHCIIb	EDL
HYBRID FIBERS		
Type I/IIA	MHCI>MHCIIa	Vastus Lateralis (women)
Type IIA/I	MHCIIa>MHCIb	Vastus Lateralis (men)
Type IIA/IID	MHCIIa>MHCIId	Tibialis Posterior
Type IID/IIA	MHCIId>MHCIIa	Tibialis Anterior
Type IID/IIB	MHCIId>MHCIIb	Gastrocnemius
Type IIB/IID	MHCIIb>MHCIId	EDL

Table 1.1 Muscle fiber types

Shown are the different MHC isoforms that make up both pure muscle fibers and hybrid muscle fibers along with examplar tissues. Slow fibers are found in postural muscle tissue e.g. soleus muscle where as fast fibers are found in muscle tissue that functions in phasic contraction. (Staron and Pette 2000).

1.2.4.3 Contractile Activity

Skeletal muscle fibers show characteristic mechanical properties including shortening velocities and ATPase activity. Correlations between contractile properties and myosin isoforms were initially demonstrated by the work of Bárány in 1967 (Bárány 1967). More refined experiments have shown correlations between MHC-based fiber types and maximum shortening velocities i.e. shortening of the sarcomere during contraction (Bottinelli et al. 1991). Velocity is lowest in type I fibers and fastest in type IIB. Histochemical staining for mATPase shows the differences in the pH stability of mATPase activity with fibers being separated based solely on staining intensities (Weiss et al. 1999). The slowest fiber type I stains light whereas the fastest fiber type IIB stain more (Staron 1997). As mATPase resides

in the heavy chain of myosin molecule in muscle (Weiss et al. 1999) histochemical staining of mATPase correlates with the type of MHC isoform expressed by the muscle fiber.

1.2.4.4 Other Proteins

As well as specific MHC isoform expression muscle fibers also have fiber type-specific programs of gene expression for many other muscle proteins. Fiber type-specific isoforms exist for the myosin light chain (MLC) of the myosin molecule, the three troponin units, tropomyosin, a-actinin and Ca^{2+}-regulatory proteins. Not only are there differences in isoform expression between muscle fibers, there exists certain proteins that are only expressed in certain muscle fibers. For example, in rodents the Ca^{2+}-binding protein parvalbumin is expressed in type II fibers but not in type I fibers (Celio and Heizmann 1982). Parvalbumin is a calcium binding protein and is thought to function in relaxation of fast-twitch fibers by acting as a temporary Ca^{2+} buffer (Racay et al. 2006). Chen and colleagues (2001) found parvalbumin deficiency in fast-twitch fibers results in the fibers becoming more resistant to fatigue with the ability to sustain muscle activity for prolonged periods indicative of slow-twitch fibers.

1.2.5 Fiber Type Transitions

Muscle fibers are dynamic structures that are capable of change under a variety of circumstances for example, altered neuromuscular activity, mechanical unloading or loading, altered hormonal profiles, systemic diseases or during aging. Fiber transitions generally follow a scheme of either fast-to-slow or slow-to-fast and are determined by changes in MHC isoform expression shown below:

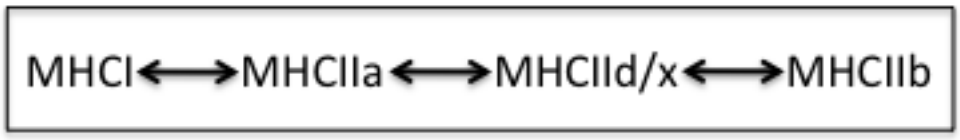

These MHC isoform transitions are related to energy cost of force production (Bottinelli et al. 1994a) and also differences in the ATP phosphorylations in fast and slow muscle fibers (Conjard et al. 1998). Extensive literature on muscle plasticity show fast-to-slow fiber transformation is evoked by increased motor nerve activity, cross-innervation, electrical pacing, or excercise. Slow-to-fast fiber transformation occurs as a consequence of decreased motor nerve activity, cross-innervation, certain diseased states, hypogravity, or physical inactivity (Neufer et al. 1996).

The importance of neuromuscular activity on muscle fiber phenotype has been demonstrated by numerous denervation experiments for example, by Jakubiec-Puka and colleagues (1990). In the absence of innervation slow muscles become faster and fast muscles become slower. Therefore denervation causes decreases in concentrations of slow MHC isoforms in slow muscles and a similar decrease of fast MHC isoforms in fast muscles (Jakubiec-Puka et al. 1990). In 1959 Buller and co-workers carried out a series of cross-reinnervation experiments, whereby fast muscles were reinnervated with a slow nerve and slow muscles were innervated with a fast nerve. The results showed that the fast muscles turned slow and the slow muscles turned fast. These experiments showed the important of innervation in the establishment of specific muscle phenotypes. The changes in phenotype followng cross-reinnervation are primarly due to specific neural impulses delivered to the muscle. Later two protocols for eletrostimulation elvolved to mimic the firing patterns delivered to muscle from fast and slow motor neurons. Salmons and Vrbová in 1969 used chronic low-frequency stimulation (CLFS) to mimic the impulse patterns of slow motor neuron and Lömo and co-workers in 1974 used

phasic high-frequency stimulation to mimic the pattern normally delivered to fast-twitch muscles by the fast motor neuron. CLFS mimics the impulse pattern by prolonging contraction and relaxation times of the fast twitch muscle (Pette 2001). CFLS of fast-twitch muscle induces a shift in MHC isoform from MHCIIb to MHCI. Up to a 60% increase in hybrid fibers is also seen during this muscle transformation (Pette 2001). Studies using CFLS have shown it affects all functional elements of the muscle fiber including the major myofibrillar proteins, mitochondrial and cytosolic enzymes involved in energy metabolism (Berchtold et al. 2000) and variuos proteins of the sarcoplasmic reticulum (Ohlendieck et al. 1999).

CFLS can also be applied to slow-twitch muscle but will have no effect unless the muscle is denervated whereby the slow phenotype will be maintained by direct low-frequency stimulation (Pette et al. 1975).

Phasic high-frequency stimulation of denervated slow muscles shows a slow-to-fast transition in myosin isoforms (Gorza et al. 1988). However the slow-to-fast transition is never complete even following days of stimulation whereby significant amounts of slow myosin still remain (Bacou et al. 1996).

Meachanical unloading of muscles has been studied using models of immobilisation, limb suspension and microgravity. Unloading of slow muscles via these methods induces a slow-to-fast transformation (Staron et al. 1998), whereas unloading of fast muscles induces less obvious changes (Jänkälä et al. 1997). Mechanical overloading is obtained by the method stretch overload whereby muscles are immobilised in a lengthened position. This has been shown to increase slow fibers in immobilised fast muscle (Pattullo et al. 1992). Functional overload has also been used in the compensatory hypertrophy model (Goldberg, 1967). Similar to stretch overload it showed an increase in slow fibers and increases in MHCI at the protein level and mRNA level (Gregory et al. 1986, 1990).

Thyroid hormones have an immense effect on muscle fiber phenotype. Generally hypothroidism causes fast-to-slow transitions (Fitts et al. 1980) whereas hypertyroidism causes a slow-to-fast transition (Pette and Staron 1997). Low levels of thyroid hormones cause a fast-to-slow transition in MHC isoform expression: MHCIIb-MHCIId-MHCIIa-MHCI, whereas high levels of thyroid hormones causes a slow-to-fast MHC isoform expression: MHCI-MHCIIa-MHCIId-MHCIIb (Caiozzo et al. 1992). Another hormone that can have a significant effect on fiber type is testosterone. Studies have shown that testosterone can effect the temporalis muscle in the guinea pig (Gutmann and Hanzlíková

1970) and the laryngeal muscle fibers of the frog (Catz et al. 1995). Expression of the largngeal specific MHC "LM" was shown to be decreased with the removal of testis from the male and incresed in females when subjected to exogenous androgen.

Muscle aging has severe effects on muscle mass. Numerous studies have shown that there is an age-related change in fiber type and MHC isoform expression. In skeletal muscles of the rat Gannon and colleagues (2009) have shown a drastic reduction in MHC fast expression in aged muscle. As extrinsic and intrinsic factors play a role in muscle aging it is difficult to say whether these changes are primary or secondary events in aging muscle.

1.2.6 Mechanisms of Fiber Transitions

As discussed muscle fiber transitions can occur under a variety of conditions and include changes in MHC isoforms, sarcoplasmic reticulum proteins and metabolic proteins. These changes in protein isoforms and their expression are controlled by transcription, translation and protein degradation. A change in gene transcription and translation effect gene expression and repression whereas proteolysis plays a role in the degradation of proteins. Skeletal muscle fiber phenotype is regulated by several independent signalling pathways. These include pathways involved in Ras/mitogen-activated protein kinase (MAPK), calcineurin, calcium/calmodulin-dependent protein kinase IV and the peroxisome proliferator g coactivator 1 (PGC-1).

The Ras pathway has been shown to control differentiation of muscle fiber types by nerve activity (Muriga et al. 2000). Muriga and coworkers (2000) showed that activated MAPK pathway is sufficient to drive a slow myosin gene programme in denervated regenerating soleus muscle. Also slow motor neurons cannot induce slow myosin when Ras/MAPK signalling is inhibited.

Calcineurin is a Ca^{2+}/calmodulin-acitvated phosphatase. Binding of Ca^{2+} to a calmodulin/calcineurin complex stimulates serine/threonine phospatase activity of calcineurin. The major substrate for calcineurin is a family of nuclear factor of activated t cells (NFAT) transcription factors. Dephosphorylation of NFATs by calcineurin promotes their translocation to the nucleus where they bind to DNA and stimulate transcription of target genes. Chin and coworkers in 1998 described how calcineurin relates motor neuron activity control programs of gene expression that define fast and slow subtypes of skeletal fibers. They investigated how tonic motor neuron activity characterisitc of those innervating slow muscles sustains Ca^{2+} concentration at sufficient levels to activate the calcineurin-NFAT

pathway. Whereas phasic firing of motor nerve activity characteristic of those innervating fast muscles are of insufficient duration to maintain calcineurin in the active state and so NFAT proteins remain phosphorylated and do not enter the nucleus (Chin et al. 1998). When NFAT proteins do not enter the nucleus the slow-specific program of proteins is down regulated and genes encoding the fast fiber-specific proteins are transcribed. McCullagh and coworkers in 2004 described how NFAT acts as a sensor selectively responsive to slow patterns of nerve electrical activity and NFAT controls the nerve activity-dependent induction of slow gene program during muscle regeneration and maintenance of the slow phenotype in adult skeletal muscle. These studies support the idea that calcineurin-dependent signalling is an important mechanism to muscle transformations.

PGC1 is a transcriptional co-activator of nuclear receptors involved in the regulation of a number of mitochondrial genes that are involved in oxidative metabolism (Lin et al. 2002). Increased expression of mitochondrial genes may be related to increased oxidative metabolism that is characteristic of slow-twitch fibers.

Peroxisome proliferator-activated receptor d (PPARd)-mediated transcriptional pathway is involved in the regulation of the skeletal muscle phenotype (Wang et al. 2004). Wang and coworkers found that mice with activated PPARd display an increase in oxidative enzymes and increased proportion of slow-type fibers.

Together these pathways form the basis of a signalling network that controls skeletal muscle fiber-type transformation and metabolic profiles.

1.3 Myotonia

Skeletal muscle contraction requires the participation of ion channels in the spreading of an excitatory signal from the endplate region along the surface membrane, and coupling this signal in T-tubules to the release of Ca^{2+} from the sarcoplasmic reticulum. Hyperexcitabilty of the sarcolemma due to muscle action potentials in response to a single input at the neuromuscular junction results in abnormally sustained muscle contraction and is termed Myotonia.

Myotonia is a symptom of myotonic disorders and is characterised as a muscle hyperexcitabiltiy or a delay in muscle relaxation. Myotonic disorders can be classified into two groups: myotonic dystrophies and nondystrophic myotonias. The myotonic dystrophies (DM) are dominantly inherited disorders (Mankodi 2008) and are classified into three groups: DM1, DM2 and DM3. Myotonia is the most common symptom but not the most serious complication of DM and it is unknown to what extent myotonia contributes to the dystrophic process (Wheeler 2008).

1.3.1 Non Dystrophic Myotonias

Non dystrophic myotonias are pure skeletal muscle disorders whereas dystrophic myotonias can effect multiple tissues. The pure skeletal muscle disorders can be subdivided into sodium channel myotonias and chloride channel myotonias. Both are due to mutations in voltage-gated sodium or chloride channel genes that are expressed exclusively in skeletal muscle. Mutations in the gene encoding the muscle N^{+}-channel are associated with paramyotonia congenita, potassium-sensitive myotonia and hyperkalemic periodic paralysis with myotonia. In contrast, nondystrophic chloride channelopathies are responsible for myotonia congenita, recessive Becker myotonia and dominant Thomsen myotonia. Mutations in these two different genes underlie hereditary pure myotonias (Pusch 2002). The non dystrophic myotonias can be dramatic and disabling with potential triggers including: emotional surprise, cold, potassium and exercise. The chloride channel (CLC-1) functions in reducing excitability and stabilising resting potential whereas the sodium channel renders the membrane excitabilty.

Chloride channel myotonias include: autosomal dominant myotonia congenita (Thomsen's disease), autosomal recessive myotonia congenita (Becker's disease), myotonia levior and fluctuating myotonia congential. The CLCN1 gene encodes 130kDa chloride channel (CLC-1) that is expressed exclusively in skeletal muscle. Gain-of-function and loss-of-function

mutations in CLCN1 cause two types of myotonia congentia, namely dominantly inherited Thomsen type and recessively inherited Becker type respectively. Thomsen type is very rare whereas Becker type is more common with 1:50'000 being affected each year (Rüdel 2000).

Thomsen type myotonia congentia has a dominant mode of inheritance pattern with symptoms begining during infancy or childhood. Clinical presentation includes generalised myotonia, muscle hypertrophy in extremities and facial muscles and painless muscle stiffness on muscle activation after rest with this stiffness reducing after continued activity termed the "warm-up" phenomenon (Mankodi 2008). Emotional surprises, cold and pregnancy can worsen myotonia. Muscle strength is normal in Thomsen type myotonia congenita.

Becker type myotonia congenita has an autosomal recessive mode of inheritance with clinical presentation of generalised myotonia and muscle hypertrophy of lower extremities, shoulders and sometimes seen in forearms, hands and anterior neck. Similar to Thomsen type myotonia it is exacerbated by cold, prolonged muscle strain, pregnancy and emotional tension. Unlike Thomsen type, Beckers type symptoms have an insidious onset and occur later during childhood. The symptoms in Becker type are slowly progessive and can stabilise in the third decade. Hypertrophy of the lower extremities can become pronounced. Current treatments for Thomsen and Beckers type myotonia congenita are activity adjustment and avoidance of triggers.

1.3.2 The Chloride Channel

Chloride channels regulate the anion flow by switching on or off in response to stimuli e.g. ligand-binding, changes in voltage and changes in Ca^{2+} intracellular concentration. They are present in the plasma membrane and in the membrane of intracellular organelles and are involved in a wide variety of functions including: cell volume regulation, transepithelial transport, endocytotic trafficking and stabilisation of the membrane potential. The voltage-gated chloride channel ClC-1 found exclusively in skeletal muscle will now be discussed in detail based on function and structure.

1.3.2.1 Function

All living cells have charge differences across their membrane and this charge difference arises due to differences in ionic composition of intracellular and extracellular fluids and the selective permeabiltiy of the plasma membrane. Intracellular and extracellular fluids contain a variety of electrically charged ions. The principal positively charged ions (cations) outside the cell are sodium ions (Na^+) with some potassium ions (K^+). Inside the cell the situation is reversed with K^+ the principal cation and Na^+ is in lower concentration. Outside the cell the principal negatively charged ion (anion) is chloride (Cl^-). Ion channels are pores that allow the movement of ions across the plasma membrane. Internal anions are predominantly large organic molecules that cannot pass the plasma membrane they are a constant pool of internal negative charge, therefore inside the cell is more negatively charged than outside the cell. This difference in charge across the cellular membrane causes an eletrical gradient or voltage across the membrane and is called the membrane potential. Muscle cells and neurons have the ability to generate active changes in their membrane potential and are called excitable cells. When an excitable cell recieves a signal one or more gated ion channels open resulting in Na^+ ions moving into the cell bringing a more postive charge. As Na^+ builds up inside the cell the membrane potential will become less negative reducing the electrical gradient, this process is called depolarisation. Repolarisation of the membrane occurs by rapid Na^+-channel inactivation and opening of K^+-channels that mediate the outward K^+ current. (Jurkat-Rott et al. 2002). Compared with other excitable cells skeletal muscle has an usually high chloride conductance accounting for up to 85% of resting membrane conductance (Bryant et al 1971). The high chloride conductance is important due to the large size of muscle fibers that require the T-tubule system to propagate an action potential into depth of the cell to initiate synchronised contraction of the fiber (Matthews et al. 2010). Chloride conductance plays a vital role in maintaining normal muscle excitability and is thought to do this by reducing both the accumulation of K^+ and its depolarising effect in the T-tubule system (Dutka et al. 2008). Without the high chloride conductance K^+ accumulation in the small space of the T-tubule system during prolonged muscle activity would increase the normally low intratubular K^+ concentration thereby shifting the K^+ equilbrium potential and depolarising the membrane leading to generation of new action potentials. The high Cl^- conductance in skeletal muscle helps to alleviate this problem. The concentration of Cl^- within the extracellular fluid is more than an order of magnitude greater than that of K^+ therefore any effect of Cl^- movement out of the extracellular fluid and into the cell on the total Cl^- concentration in the extracellular fluid

and the Cl^- equilibrium potential is negligible and the Cl^- conductance is able to negate the depolarising effect of K^+ accumulation (Waldegger and Jentsch 2000). Therefore the hyperexcitability seen in myotonia is due to a permanent reduction of the resting chloride conductance of the muscle fiber membranes.

1.3.2.2 Structure

Strucutral analysis of chloride channels began by Jentsch and co workers in 1990 with the cloning of the Torpedo electric organ Cl^- channel ClC-0. ClC-0 was shown to have a "double-barrelled" structure with two identical pores that gate independently from each other "fast gates" also these can be gated simultaneously by another common gate "slow gate". This homodimeric structure where each pore is formed by a single CLC-0 protein was proposed for CLC-1 the skeletal muscle Cl^- channel by Saviane and co-workers in 1999 and later confirmed by X-ray crystallography (Dutzler et al. 2002). The ClC-1 channel is composed of 18 transmembrane domains with intracellular localisation of the N- and C-termini of the protein (Dutzler et al. 2002) and can be seen in figure 1.3. CLC channel proteins share a common structural feature: a tandem repeat of cystathionine-b synthase (CBS) domains in the carboxy terminus (Schmidt-Rose and Jentsch 1997). The function of the CBS domains are unknown although work by Waldegger and Jentsch (2000) whereby deletion of CBS-2 in CLC-1 resulted in consistent channel function indicating there is no requirement for this domian. Both fast and common gates are activated by depolarisation and deactivated by hyperpolarisation (Fahlke and Rüdel, 1995). It is important to note that deactivation by hyperpolarisation is not complete and results in a steady-state current therefore the channel has an open probability even at very negative voltages (Jentsch 2002). ClC-1 is primarly located in the sarcolemmal membrane of skeletal muscle (Gurnett et al 1995; Mankodi et al. 2002) which is unusual as physiological investigations revealed that muscle Cl^- conductance is mainly found in the T-tubule system (Mankodi et al. 2002). It is suggested that either a distinctly different Cl^- conducting channel or a splice varient of CLC-1 may be present in the T-tubule system (Gurnett et al. 1995). ClC-1 is blocked by 9-anthracene-carboxylic acid and 4-chloro-phenoxy-acetic acid (Jentsch et al. 2005).

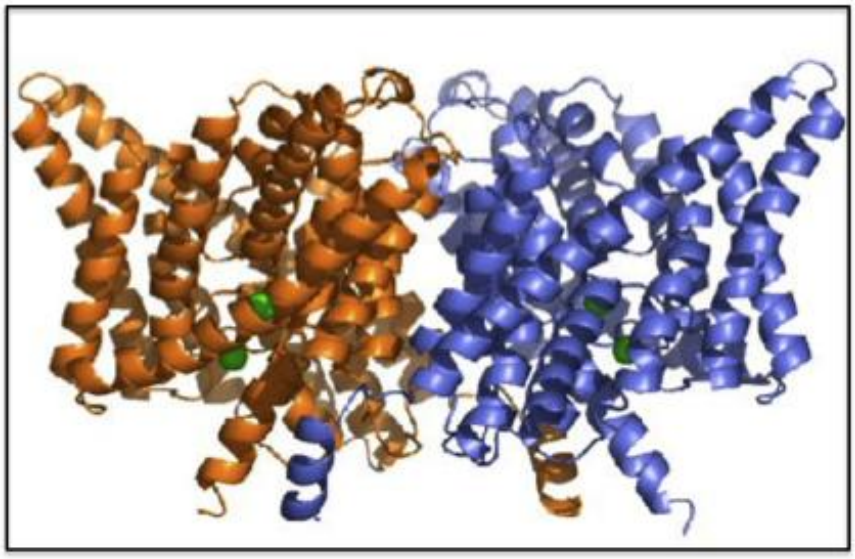

Figure 1.3 CLC-1 Chloride Channel

Shown is the skeletal muscle chloride channel CLC-1 as a double-barreled channel with each protein forming a channel. Green spheres are chloride ions. Obtained from chemistry.umeche.maine.edu/.../1ofs-1.jpg

1.3.3 Mutations of CLC-1

In both dominant myotonia congenita (Thomsen type) and recessive generalised myotonia (Becker type), mutations in the gene encoding the major skeletal muscle chloride channel CLCN1 result in reduced sarcolemmal Cl^- conductance (Adrian and Bryant 1974). This abnormal membrane property leads to membrane hyperexcitability, repetitive firing of muscle action potentials and clinical myotonia that is characterised by muscle stiffness upon sudden forceful movement. Mutations in CLC-1 was first described in the myotonic "arrested development of righting response" ADR mouse by Steinmeyer and colleagues in 1991. Then in 1993 similar mutations in CLC-1 were identified in human myotonia (Koch et al. 1993). Today 80 mutations have been identified in the CLCN1 gene causing myotonia (Pusch 2002) with 40 of these identified in patients with dominant or recessive myotonia (Lehmann-Horn and Jurkat-Rott 1999). These mutations include: missense and nonsense mutations, splice-site mutations and frame shift mutations (Jentsch 2002). Most mutations lead to recessive myotonia congenita where both alleles are mutated and can result in the total loss of CLC-1 channel function. Dominant myotonia can be explained by mutant subunits which can inhibit the function of dimers that are formed with wild type (WT) subunits encoded by the other allele. Therefore with dominant Thomsen type myotonia it is expected that heterzygous patients will have 25% fully funcional WT/WT channels. This is shown as myotonia is clinically less severe in dominant compared with recessive forms. The first reported mutation discovered in Thomsen type myotonia causes the substitution of a glycine residue by glutamic acid located between transmembrane segments 4 and 10 in human CLC-1 (George et al. 1993). Fahlke and colleagues in 1997 looked at another dominant mutation in CLCN1 which was found to affect the pore properties of the CLC-1 channel. There also exists single mutations that in some families exhibit a dominant phenotype, whereas in other families the recessive phenotype is observed. The fs793X mutation shows dual modes of inheritance (Kuo et al. 2006).

1.3.4 Myotonia Treatment

Many myotonia congenita patients manage their disease without medication. If necessary myotonic treatments include drugs that reduce the increased excitability of the cell membrane by interfering with the sodium channels of muscle membrane. Mexiletine has been tested and can be administered orally and is the drug of choice for the treatment of myotonia (Matthews et al. 2010).

1.4 Animal Models of Myotonia

The use of myotonic mouse models has allowed the research of the pathogenesis and the molecular basis of myotonia.

In 1984 Watkins and Watts described a mouse mutant with abnormal motor behaviour. The spontaneous mutation showed recessive autosomal mode of inheritance and was termed "arrested development of righting response" (ADR) as the affected mice had difficulty righting themselves when placed surpine. Early analysis showed repetitive action potentials in ADR muscle leading to the suggestion that the ADR phenotype was caused by muscle membrane abnormality (Mehrke et al. 1986;1988). Steinmeyer and colleagues in 1991 confirmed that the membrane abnormality was due to an insertional mutation in the CLC-1 gene.

A similar spontaneous mutation was observed by Heller and co-workers in 1982 sharing the same physiological features as ADR mutants and was termed "myotonia" (MTO) mutant. Both diseased mice were recognised by typical stiffening response to a sudden challenge like being turned on their backs. The disease affects first the hind quaters and then forelimbs and results in a reduced life span, weight loss and brittleness of bones in both mutant mice. Then in 1988 Jockusch and co-workers showed that both independent, spontaneous mutations MTO and ADR were allelic. The ADR myotonic mouse (phenotype ADR, genotype *adr/adr*) is caused by an insertional (allele *adr*) mutation at gene locus Clc1 on chromosome 6 of muscle chloride channel CLC-1. In MTO mice myotonia is due to a nonsense mutation (allele *mto*) at the same locus. Myotonic ADR and MTO mice are both genocopies of human congenital myotonia. They display a more pronounced phenotype, making them ideal model systems for studying secondary effects of myotonia on skeletal muscle.

A new allele mto*5j at the Clc1 locus carries a base insertion in codon 75 which causes a frameshift in the reading frame of the gene resulting in a stop codon in position 93. MTO*5j mice were discovered at Jackson Laboratory in 2000 and allelism has been shown with MTO

mice. MTO*5J mice are midly affected, show less reduced body weights and have a near normal life span. The physiological and histochemical properties of MTO*5J muscles are intermediate between those of ADR and WT control muscles (Staunton et al. 2011). This milder phenotype is clinically closer to human congenital myotonia.

All three alleles are null mutations that do not produce CLC-1 protein. The reasons for the mild response to a complete CLC-1 deficiency in MTO*5J mutants is not known.

1.5 Motorneuron disease

Motorneuron diseases represent a class of progressive, neurodegenerative disorders which result in the loss of motor neurons. They are characterised by selective and progressive loss of lower and/or upper motor neurons. There are many types of motor neuron disease, such as; progressive muscular atrophy, primary lateral sclerosis and amyotrophic lateral sclerosis (ALS) (Wijesekera and Leigh, 2009). ALS accounts for the majority of the motor neuron diseases and is characterised by the degeneration of motor neurons in the brain and spinal cord, resulting in loss of muscle function (Goodall and Morison, 2006). Today, ALS is an incurable disease leading to death within three to five years from onset of symptoms. Approximately 20% of patients can survive more than five years and only about 10% more than ten years (Kuzma-Kozakiewicz and Kwiecinski, 2011). Patients generally die from respiratory failure due to loss of function of repiratory muscles. ALS has an incidence of on average 1.89 per 100,000/ year (Wijesekera and Leigh, 2009). Approximately two thirds of patients with ALS have spinal form of the disease (limb onset) and present muscle weakness and wasting. These symptoms may start either distally or proximally in upper or lower limbs. Patients may have noticed fasciculations or cramps preceding onset of weakness or wasting for some months. Muscle weakness has gradual onset with other limbs developing weakness and wasting eventually patients go on to develop bulbar symptoms. Late stages of the disease patients can develop bladder dysfunction, sensory symptoms or cognitive symptoms (Wijesekera and Leigh, 2009). In contrast bulbar onset ALS patients present with dysarthria of speech which during early stages of the disease may only occur after the ingestion of small amounts of alcohol. Patients develop dysphagia of solids and liquids. Limb symptoms develop simultaineously with bulbar and eventually develop sialorrhoea due to difficulty swallowing and mild facial weakness (Wijesekera and Leigh, 2009). The rate of disease progression varies greatly amoung patients and clinical observations suggest the rate of progession of ALS in most patients is not explained by age or site of onset (Beghi et al. 2007). Therefore the process of motor neuron degeneration in ALS is complex and mulifactorial.

In 10% of cases ALS is familial and there is a family history of the disease and so are termed familial ALS (FALS). In the majority of ALS cases there is no known cause of the disease and are termed sporadic ALS (SALS) (Valentine et al. 2005). The clinical and pathological characteristics of FALS and SALS are indistinguishable (Baghi et al. 2007).

The molecular pathway causing motor neuron degeneration in ALS is unknown and is thought to be due to a multiple of pathogenic cellular mechanisms including: (i) genetic factors, (ii) excitotoxicity, (iii) mitochondrial dysfunction, (iv) impaired axonal transport, (v) protein aggregation and (vi) oxidative stress.

To date mutations in six genes have been discovered to be associated with ALS (Beghi et al. 2007). Mutations in the Copper-Zinc superoxide dismutase (Cu/Zn SOD) protein encoded by the sod1 gene was first described by Rosen and collegues in 1993 as a cause of autosomal dominant FALS. Since then 140 mutations in sod1 have been identified they account for 20% of all FALS cases and 2% of SALS cases (Rosen et al. 1993). Cu/Zn SOD is an ubiquitously expressed anti-oxidant enzyme. Mutations in the gene are thought to cause disease through a toxic gain-of-function rather than causing impairment to the antioxidant function of the enzyme (Shaw, 2005). Mutations found in ALSIN is the cause of a rare autosomal recessive form of ALS characterised by juvenile onset and slowly generalised spasticity (Beghi et al., 2007). The physiological role of ASLIN and the mechanism by which its mutation causes motor neuron degeneration is unclear. It is thought that ASLIN may have a role in axon transport (Kunita et al. 2004). A mutation that has been found to affect axonal transport is that in dynactin. Dynactin is the largest polypeptide of the dynactin complex and functions in retrograde axonal transport of vesicles and organelles along microtubules (Holzbaur and Tokito 1996). Other mutations have been found in senataxin and vesicle associated protein B (VAPB). Recently a mutation in TARDBP gene have been linked to both FALS and SALS (Wijesekera and Leigh 2009).

The term excitotoxicity is used to describe neuronal injury induced by excessive glutamate induced by stimulation of postsynaptic glutamate receptors (Wijesekera and Leigh 2009). Over stimulation of glutamate receptors is thought to result in massive calcium influx into neurons leading to increased nitric oxide formation and thereby neuronal death. Glutamate levels in the cerebral spinal fluid (CSF) have been shown to be elevated in some patients with ALS (Shaw et al. 1995). This elevation has been attributed to loss of astroglial glutamate transporter (EAAT2) protein found in affected regions of ALS patients (Rothstein and Kunel 1995). The loss of EAAT2 could be an indirect consequence of neuronal death as expression of glial glutamate transporters is regulated by neuronal activity (Beghi et al. 2007). It is unclear if the alteration in glutamate metabolism in ALS patients are a consequence or cause of disease.

The first suggestion of a role for mitochondrial dysfunction in ALS came from the obseration of abnormal mitochondrial morphology in tissues of ALS patients. Mitochondria from transgenic sod1 mice show elevated calcium levels and decreased activity of respiratory chain complexes I and IV implicating defective energy metabolism (Barber and Shaw 2010).

Neurofilaments are major components of the motor neuron's cytoskeleton and function in the regulation of axonal transport. Accumulation of neurofilaments in motor neurons and their axons is a hallmark of ALS (Kuzma-Kozakiewicz and Kwiecinski 2011) but it is unknown if this accumulation is a primary or secondary effect in neurodegeneration.

Intraneuronal aggregates such as bunina bodies, ubiquitinated skein-like inclusions and neurofilament rich hyaline conglomerate inclusions have been found in motor neurons and are hallmarks of ALS. The formation of these protein aggregates may be due to impaired degradation of misfolded mutant proteins e.g Cu/Zn SOD or dysfunction in the ubiquitin-proteasome pathway (UPP).

Oxidative stress has long been linked to neurodegeneration and it is known that accumulation of reative oxygen species (ROS) cause cell death. This thought is backed by the fact mutations in sod1 gene cause FALS.

1.5.1 Treatment of ALS

Numerous compounds have been tested as potential disease modifying therapies for ALS yet only the drug riluzole has been licensed for this purpose (Miller et al. 2007). Riluzole exerts its protective effect in ALS patients by acting as an antiexcitotoxic agent (Lacomblez et al. 1996). Riluzole acts by blocking different processes including the release of glutamate from presynaptic neurons and therefore can inhibit the glutamate-mediated overstimulation of postsynaptic glutamate receptors (Pratt et al. 1992). Clinical trials using riluzole prolonged ALS survival in patients by 3-6 months (Lacomblez et al. 1996). The effect of riluzole enforces the idea of glutamate-induced excitotoxicity in ALS.

Other drugs that have recieved attention are the tetracycline derivative minocycline. Minocycline is a multifunctional drug that affects different molecular pathways involved in ALS. One function of minocycline is that it inhibits cytochrome C release from the mitochondria and has been shown to delay the disease onset and also extend survival in sod1 transgenic mice (Zhu et al. 2002).

Olesoxime is a steroidal oxime which binds to the mitochondrial permeability pore and shows potential efficacy in preclinical models of ALS and spinal muscular atrophy (Bordet et

al. 2007). Also dexpramipexole and pramipexole are both drugs that have shown neuroprotective properties by reducing ROS production.

The wide array of drugs that have been tested for the treatment of ALS only confirm the idea that ALS is a multifactorial disease with a multitude of cellular mechanisms that lead to motor neuron death.

1.5.2 The Wobbler Mouse

The Wobbler mouse suffers an autosomal recessive mutation producing severe motorneuron degeneration and astrogliosis in the spinal cord. It is considered a suitable animal model for motor neuron disease such as ALS. The mutation arose as a spontaneous mutation in the Institute of Animal Genetics, University of Edinburgh, Edinburgh, Scotland. The name "Wobbler" is due to the fine tremor of the head mice experience by week four. Homozygous (*wr/wr*) mice show no clinical abnormality during the first three weeks, by the fourth week they are smaller than their littermates and remain so, they also experience a high stepping, unsteady gait along with tremor of the head. From week four to week five weakness of the muscles become apparent and is most obvious in forelimbs. By week twelve there is progressive weakness of the head, neck and forlimbs with hindlimbs less affected. In advanced stages of the disease mice have difficulty using forelimbs for climbing and walking. By the third or fourth month the disease seems to slow down in progression in some whereas in others the disease is fatal by the third or fourth month. Motor neuron degeneration in the Wobbler mouse is confined to the cervical spinal cord region, with the lumbar spinal cord remaining unaffected (Bastone et al. 2009). The Wobbler mouse also shows defective spermiogenesis in males (Pérez-Victoria et al. 2010).

A missense mutation whereby leucine 967 is changed to glutamine near the C-terminus of the vescile sorting protein 54 (Vsp54) is responsible for the wobbler phenotype (Schmitt-John et al. 2005). VSP 54 is a subunit of the Golgi-associated retrograde protein (GARP) complex and is responsible for the transport of vesicles to the trans-Golgi network (Schmitt-John et al. 2005). The GARP complex is a herterotetrameric complex composed of four subunits; Vsp51, Vsp52, Vsp53 and Vsp54. Pérez-Victoria and co-workers (2010) looked at the structural consequence of the wr mutation and found that leucine967 is critical for domain stability and folding and therefore the wobbler phenotype results from the destabilisation of Vsp54 and thus reduced levels of Vsp54 and addtionally the GARP complex. Meisler and colleagues (2008) found no direct link between Vsp54 mutation and human ALS. However, the Wobbler

mouse is considered a suitable model for neurodegenerative disease due to the similarities between clinical features of motor neuron degeneration in wobbler mice and in humans, thus suggesting the possibility of common pathways in both.

Studies on the wobbler mouse have focused on the spinal cord (Bastone et al. 2009) and motor neurons (Meyer et al. 2010) in order to gain a greater understanding of the pathogenesis of motor dengeneration in the mouse. In contrast, very little is known of the secondary effects of motor neuron degeneration on skeletal muscle. Previous studies have looked at the proportions of MHC in affected muscles (Agbulut et al. 2004) whereby a shift to the fast MHCIIB was found in wobbler tibialis anterior muscles. Analysis at the mRNA level has also been looked at in the skeletal muscle of the wobbler mouse (Sedehizade et al. 1997). Sedehizade and colleagues looked at the mRNA levels of myogenic factors myogenin and MyoD that function in gene transcription and the Ca^{2+}-binding protein parvalbumin. Myogenin mRNA was elevated in wobbler skeletal tissue whereas parvalbumin mRNA was decreased (Sedehizade et al. 1997). In order to understand fully understand the secondary effects of the loss of motor innervation has on the skeletal muscle proteome, it is neccessay to gain a wider picture of the changes in the protein complement of the wobbler skeletal tissue.

1.6 Proteomics

The complement of proteins expressed by a cell is referred to as its proteome. The skeletal muscle proteome is highly dynamic, and differs from fiber to fiber. Proteomics is the study of the proteins expressed by a cell. There are two main fields in proteomics; expression proteomics and functional proteomics. Expression proteomics involves the denaturation of proteins, and using subsequent analysis to determine quantitative changes in the abundance of proteins under different condition. In contrast, functional proteomics involves maintaining the proteins native structure and gaining functional information on that protein. It is important to note that translation of the nucleotide sequence has been shown not to match fully with the proteins produced in the cell (Anderson and Seilhamer 1997). This is because the proteome is subjected to environmental influences that can act to apply post translational modifications (PTM) to adapt to a change in situation. For example, altered neuromuscular activity leads to increased cytosolic Ca^{2+} resulting in decreased expression of transcription factors resulting in a changed transcription pattern in the muscle cell. This has been shown at the mRNA level whereby denervation due to motor neuron disease results in a decrease of the transcription factor myogenin mRNA in skeletal tissue from the wobbler mouse (Sedehizade et al. 1997). A decrease of transcription factors may play a role in the fiber type transformation seen in wobbler skeletal muscle whereby there is a shift to faster MHCIIB expression in wobbler muscle tissue (Agbulut et al. 2004).

Expression proteomics begins with the solubilisation of the sample of proteins. Denaturing buffers are used for this process and contain a combination of chemicals to solubilise the maximum amount and variety of proteins. They are usually composed of 7-9M Urea to disrupt hydrogen bonds, along with detergents such as CHAPs and reducing agent such as DTT. There is no standard solubilisation buffer as they must be tailored to the sample to achieve optimum solubilisation.

1.6.1 Two Dimensional Gel Electrophoresis

Many proteomic techniques exist to separate and analyse proteins. One of the most powerful techniques for separating entire proteomes is the use of two-dimensional gel electrophoresis (2-D GE). This technique was first developed by O'Farrell in 1975 and involves the separation of proteins in two dimensions. In the first dimension proteins are separated on thin strips of polyacrylamide gel containing an immobilised pH gradient (IPG). These IPG strips are purchased as precast dehydrated gels supported by backing plastic. In the first dimension

proteins must enter the gel before they are separated. This can be done by a number of methods, firstly the strips are rehydrated using rehydration buffer. Protein sample can be added to the rehydration buffer and can enter the gel passively, or after rehydration during isoelectric focusing (IEF). As an electric current is applied to the IPG strip during IEF proteins move through the gel until they reach a pH where they no longer have a net charge. In this dimension a number of different pH gradients can be used. Narrow pH ranges can be used to give better separation of proteins and allow an increased nmber of proteins to be visualised. In the second dimension the IPG strip is placed horizontally along the top of a large polyacrylamide gel. An electric current is passed through the gel and forces the proteins through pores in the gel, smaller proteins will move faster through the gel than larger proteins. Therefore in the second dimension proteins are separated based on their molecular weight.

There are a number of limitations to this technique for example IPG strips have a limited capacity for the amount of protein they can hold and proteins above a certain size cannot enter the gel matrix of the IPG strip. Proteins of a very low molecular weight may run too quickly through a 2-D gel, and so become lost. Also insoluble proteins such as those found in the sarcolemma or membrane proteins are notoriously hydrophobic and will not go into solution easily and do not like the aqueous environment of the second dimension.

1.6.2 Visualising Proteins

After 2-DE, the separated proteins have to be visualised by staining techniques. The concentration of individual proteins in a cell differ between 6-7 orders of magnitude ranging from millions of copies for highly abundant proteins such as contractile proteins in muscle cells to a few copies for low abundant proteins. This is a major challenge for almost all protein detection methods available today. Important properites of protein visualisation methods include; (i) high sensitivity, (ii) high linear dynamic range, (iii) reproducabilty and (iv) compatability with protein identification methods. Today current stains that are widely used in proteomic studies are staining with anionic dye e.g. Coomassie blue, silver staining and fluorescence staining.

Coomassie brilliant blue (CBB) is used for the widespread detection of proteins due to its low price, ease of use and compatibility with protein identification methods. The limitations with CBB is its insufficient sensitivity as it cannot detect low abundance proteins.

Silver staining is alot more sensitive than CBB staining and only requires 100 mg of protein per gel for detection. Unlike CBB, silver staining is not reproducable due to its subjective

end-point of the staining procedure and so makes silver staining less suitable for quantitative analysis.

Better and more confident results in terms of sensitivity and linear dynamic range of detection are obtained by protein detection relying on fluorescent compounds. Fluorescent detection of proteins can be done in two ways; firstly by the covalent derivatisation of proteins with fluorophores prior to separation techniques or secondly by post-electrophoretic protein staining. Pre-electrophoretic protein staining can be carried out using fluorescent labels e.g. cyanine-based dyes, that react with the lysyl residues of proteins. Proteins can also be stained with a fluorescent dye molecule after electrophoretic separation. The cost efficient ruthenium II tris (bathophenanthroline disulfonate) developed by Rabilloud and co-workers in 2001 is now widely used due to its ease of use and compatability with protein detection methods.

1.6.3 Protein Identification

The Identification of proteins after 2-D gel electrophoresis is carried out using mass spectrometry. Sample preparation for mass spectrometry begins with desalting and destaining of samples to remove contaminants. The samples are then enzymatically digested e.g using trypsin which cleaves proteins at lysine and arginine amino acid residues. When applied to the mass spectrometer samples go through several processes including; ionisation, analysis and detection.

1.6.3.1 Mass Spectrometry

By definition a mass spectrometer (MS) consists of an ion source, a mass analyser that measures the mass-to-charge ratio (m/z) of the ionised analytes and a detector that regisiters the number of ions at each m/z value (Abersold and Mann 2003). Throughout this project an ion trap LC/MS has been used for protein identification.

The ion source used was electrospray ionisation (ESI) whereby peptides are dissolved in a polar solution then pumped through a narrow capillary tube. The sample travels through the tube and on exiting the tip of the tube it has a high voltage applied to it. This causes the sample to form an aerosol which is directed towards the mass spectrometer by a gas usually nitrogen. The warm nitrogen gas causes the solvent to evaporate allowing free ions to enter the mass spectrometer (Yamashita and Fenn 1983).

Ions then enter the ion trap where they are captured or "trapped" for a certain amount of time and then subjected to MS/MS analysis. Ion traps are often used as they are robust and relatively inexpensive.

Fragment ions are produced by bombardment with an inert gas. The ions are first analysed in normal mode, then parent ions are fragmented again by collision induced dissociation resulting in MS/MS spectra. The spectra of peptide ions produce several masses and are then searched in protein data bases such as MASCOT to identify the protein of interest.

1.7 Membrane proteomics

Membrane proteins are proteins that integrate into the phospholipid bilayer of membranes and play important role in cell-to-cell interactions, signal transduction and molecular transport (Groen and Lilley 2010). Two main challenges are imposed by proteomic analysis of membrane proteins; firstly they are extremely hydrophobic and secondly they are present in low abundance and therefore can be underrepresented in proteomic analysis. A multitude of methods have been developed in order to over come these challenges from solubilisation methods such as the use of Triton X-114 whereby proteins are separated into aqueous and detergent phases (Staunton et al. 2010). One method that has been sucessfull in overcoming problems incountered with 2-DE proteomics is the digestion of proteins on nitrocellulose membranes.

1.7.1 Digestion on nitrocellulose membrane

The digestion of proteins with trypsin from nitrocellulose membranes was first described by Abersold in 1987. This method overcame problems incountered with 2-DE proteomics as it is easier for large membrane proteins to enter large gradient gels. Proteins are transferred to the membrane via electrostatic interactions and hydrophobic binding. The membrane bound proteins can be directly digested thus reducing the loss of peptides that can occur during wash steps.

1.8 Aims of the project

The purpose of this study was to carry out proteomic profiling of skeletal muscle from mouse mutants affected by myotonia and motor neuron disease. Myotonia congenita is a skeletal muscle disorder and is classified as a muscle hyperexcitability or a delay in muscle relaxation. In order to fully understand the effects of hyperexcitability on the skeletal muscle we have carried out proteomic profiling of skeletal muscle from three mouse mutants: ADR, MTO and MTO*5J. As the MTO*5J mutant shows a less severe phenotype we can assess the changes comparatively between the MTO*5J and more severly affected ADR and MTO mice. In contrast to myotonia motor neuron disease results in the loss of motor neurons and so a loss of muscle innervation. In this study we have carried out proteomic profiling of skeletal muscle from the wobbler mouse mutant an animal model for the motor neuron disease ALS. By looking at the secondary effects of muscle denervation due to motor neuron loss we can potentially establish biomarkers for the disease. By using 2-D gel electrophoresis we can establish the changes in the global protein expression pattern in skeletal muscle effected by these muscle diseases.

2. Materials and Methods

2.1 Materials

2.1.1 General chemicals and reagents

General reagents and chemicals were purchased from Sigma Chemical Company (Dorset, UK) and were of reagent/electrophoresis grade, unless otherwise stated. Distilled H_2O was purified using a Millipore Milli-Q apparatus to obtain milli-Q water. The bradford reagent for protein quantification was purchased from Biorad (Bio-Rad Labs., Hemel0Hempstead, Herts., UK). Protease inhibitors were from Roche Diagnostics (Manheim, Germany).

2.1.2 1-D and 2-D electrophoresis

Ultrapure Protogel acrylamide stock and 4X Protogel Resolving Buffer stock solutions were obtained from National Diagnostics (Atlanta, GA, USA). Isoelectric focusing pH Gradient (IPG) drystrips for 2-D electrophoresis, ampholytes and cover fluid were purchased from Amersham Bioscience/GE Healthcare (Little Chalfont, Bucks, UK). Protein molecular weight ladders and laemmli buffer were purchased from Biorad Laboratories (Hemel-Hempstead, Herts., UK).

2.1.3 Staining

Coomassie Blue R-350 tablets were purchased from Amersham Biosciences/GE Healthcare (Little Chalfont, Bucks, U.K). Bathophenanthrolinedisulfonic acid and disodium salt hydrate for RuBPs dye were purchased from Reagecon Diagnostic Limited (Shannon, Ireland). Sodium Ascorbate for RuBPs was purchased from Sigma Chemical Company (Dorset, U.K). DIGE dyes were purchased from GE Healthcare (Little Chalfont, Bucks., UK).

2.1.4 Mass Spectrometry

All solvents used for Mass Spectrometry analysis were of Mass Spectrometry grade and purchased from Sigma Chemical Company (Dorset, UK). Acetonitrile was obtained from Amersham Biosciences/GE Healthcare (Little Chalfont, Bucks., UK) Sequencing grade modified trypsin was purchased from Promega (Madison, WI, USA). LC-MS Chromaslv water and formic acid were from Fluka (Dorset, UK). Model 6340 Ion Trap LC/MS, LC/MS

vials, LC/MS vial caps and ProtlD-Chip-150 II 300A C18 150nm col were obtained from Agilent Technologies Ireland Ltd. (Santa Clara, CA, USA).

2.1.5 Western Blotting

Nitrocelulose membrane was obtained from Millipore (Bedford, MA, USA). Chemiluminscence substrate was purchased from Roche Diagnostics (Manheim, Germany). X-ray film was purchased from Fuji Photo Film Co. Ltd. (Tokyo, Japan). GBX Developer/Replenisher, GBX Fixer/Replenisher and Ponceau S-Red Staining Solution were obtained from Sigma Chemical Company (Dorset, UK). Memcode reversible stain was purchased from Thermo Scientific (MA, USA). All secondary antibodies used were obtaned from Chemicon International (Temecula, CA., USA). All commerically available antibodies used in this research were purchased from the companies detailed see Table 2.1. For antibodies used and dilutions see Table 2.2.

Table 2.1 Antibody Suppliers

Company	Address
Abcam	Abcam Plc (cambridge, UK)
ABR	Affinity Bioreagents (Golden, CO., USA)
Santa Cruz Biotechnology	Santa Cruz, CA, USA.
Sigma	Dorset, UK
Upstate Biotechnology	Lake Placid, NY.

Table 2.2 Antibodies

List of antibodies used for this project including the dilutions used for each primary and secondary antibody, host species (species) and ordering information.

Antibody	1^o Ab dilution	Species	2^o Ab dilution	1^o order no.	Company
Adenylate Kinase	1:1000	Ms	1:1000	Ab54824	Abcam
Aldolase	1:1000	Rb	1:1000	Ab6910	Abcam
Alpha dystroglycan	1:1000	Ms	1:1000	05-298	Upstate
Calsequestrin	1:1000	Rb	1:1000	MA3-913	ABR
Creatine Kinase	1:500	Rb	1:1000	Ab38178	Abcam
Cu/Zn SOD	1:500	Rb	1:1000	Ab13498	Abcam
Desmin	1:1000	Rb	1:1000	Ab8592	Abcam
GAPDH	1:1000	Gt	1:1000	Ab34492	Abcam
MHC-fast	1:1000	Ms	1:1000	Ab51263	Abcam
MHC-slow	1:1000	Ms	1:1000	Ab11083	Abcam
MLC-2	1:1000	Rb	1:1000	Ab48003	Abcam
MLC-phospho20	1:1000	Rb	1:1000	Ab2480	Abcam
MYBP	1:1000	Ms	1:1000	Ab55559	Abcam
Myoglobin	1:500	Rb	1:1000	M-8648	Sigma
Parvalbumin	1:1000	Rb	1:1000	Ab11427	Abcam
Ryanodine receptor	1:500	Ms	1:1000	MA3-925	ABR
Sarcalumenin	1:1000	Ms	1:1000	Sc-58845	Santa Cruz
SERCA1	1:1000	Ms	1:1000	MA3-912	ABR
SERCA2	1:1000	Ms	1:1000	MA3-919	ABR
Triosephosphate isomerase	1:1000	Gt	1:1000	Ab28760	Abcam
Tropomyosin	1:1000	Ms	1:1000	Ab7785	Abcam
Troponin T	1:1000	Gt	1:1000	Ab30807	Abcam

2.2 Methods

2.2.1 Animals and Dissections

Tissue from C57 BL6 control mice and age-matched myotonic and wobbler mice were obtained from the Animal House of the University of Bielefeld. Animals were kept under standard conditions and all procedures were performed in accordance with German guidelines on the use of animals for scientific experiments. The gastrocnemius muscle from ADR, MTO, MTO*5J, and control mice were dissected, snap frozen in liquid nitrogen and stored at -70^{o}C. Similarly the gastrocnemius, tibialis anterior and vastus lateralis were dissected from wobbler and control mice, snap frozen in liquid nitrogen and stored at -70^{o}C.

2.2.2 Extraction of Total Muscle Protein Complement

Muscle tissue samples were kept frozen in liquid nitrogen while being ground into a fine powder using a motar and pestle. Equal quantities of 100mg wet weight of muscle were used for both control and diseased samples. The powder was placed into 1 ml of lysis buffer (7M Urea, 2M Thiourea, 2M (3-[3-Cholamidopropyl)-Dimethylammonio]-1-Propane sulfonate) (CHAPS), 100mM dithiothretiol (DTT), 5% (v/v) ampholytes and 5tabs protease inhibitor cocktail containing 1mM leupeptin, 1.4 mM pepstatin, 0.15mM soybean trypsin inhibitor, 0.2 mM prefabloc, 0.3 mM E-64, and 1mM EDTA. Samples were homogenised for 10 s each with a plytron hand held homogeniser (Polytron PT, 1200, Kinematica AG, Switzerland). DNA was removed by the addtion of 10ml of DNAase-1 per 1ml lysis buffer. Samples were then incubated at room temperature for 2.3 h on a rotatory shaker and vortexing every 20 min for 10 s. The suspension was spun at 14,000 x *g* for 20 min at 4^{0} C using Eppendorf 5417 R centrifuge (Eppendorf, Hamburg, Germany). The resulting pellet and top layer was discarded with the middle layer of supernant being retained and stored at -70^{o}C.

2.2.3 Acetone Precipitation

Samples were first precipitated by adding 100% of ice cold acetone at a dilution of 1:4 with protein sample and vortexing briefly. The mixture was incubated for 1 h at -70^{o}C. The sample was then centrifuged for 15 min at 5,000 x *g* in Eppendorf 5417 R centrifuge (Ependorf, Hamburg, Germany) and the supernatant was discarded. The pellet was then resuspended in four times the equal volume of the original sample of 80% ice cold acetone and left in -70^{o}C for 1 h, this proceedure was repeated three times before being resuspended in an appropriate

volume of lysis buffer. Resuspension of the sample was aided by vortexing or sonication with a sonoplus HD 2200, Bandelin (Berlin, Germany).

2.2.4 Protein Quantification

Proteins were quantified using a Bradford assay. A standard curve was prepared by dilutng a stock solution of 5mg/ml BSA with milli-Q water in the range of 0-100mg BSA. Standards were diluted with different dilutions of milli-Q water and 0.1 M HCL. 5 ml of sample/5ml of lysis buffer were also diluted with 80ml of milli-Q water and 0.1 M HCL. To both samples and standards 3.5 ml of working bradford reagent (1 part bradford reagent dye: 3 parts distilled water) was added, mixed and incubated at room temperature for 10 min. Absorbance was read for the standards and samples at 595 nm and protein concentration was obtained by comparing unknown samples to the standard curve (Bradford, 1976).

2.2.5 1-D Gel Electrophoresis

One dimensional SDS polyacrylamide gel electrophoresis was performed according to Laemmli (1970), using a Bio-Rad Mini-Protean III gel system (Bio-Rad Labs., Hemel-Hempstead, Herts., UK). Ten percent resolving gel was made of 10% (w/v) acrylamide from protogel acrylamide stock, 4X Protogel resolving buffer, 0.438 M SDS, 0.69 M APS and 0.1% (v/v) N, N, N', N'-tetramethylethylenendiamine (TEMED). The stacking gel was made of 5% (w/v) acrylamide, 0.5M Tris-PO_4 pH6.7, 0.438 M SDS, 0.69 M APS and 0.1% (v/v) TEMED. Resolving gel was poured first and allowed to polymerise and stacking gel was layered over the resolving gel. Samples were boiled for 10 min in Laemmli buffer with 350 mM DTT in a 1:1 dilution before loading onto the gel. 5- 10mg of protein was loaded per well. Electrophoresis was carried out using running buffer (0.0125 M Tris, 0.69 M Glycine, 0.1% (w/v) SDS) and at 50 volts until the tracking dye ran off the end of the gel.

2.2.6 2-D Gel Electrophoresis

IPG strips for isoelectric focusing were firstly rehydrated for 12 h in rehydration buffer (7 M urea, 2 M thiourea, 4% CHAPS, 2% (v/v)ampholytes, 2% (v/v) DTT and 0.05% (w/v) bromophenol blue as tracking dye) and sample in a re-swelling tray from Amersham Biosciences/GE Healthcare (Little Chalfont, Bucks., UK). Different volumes were used according to the IPG strip length and amount of sample required depending on staining technique. For 24 cm IPG strips a total volume (rehydration buffer and sample) of 450ml was used, for 18 cm IPG strips a total volume of 350ml was used. After re-swelling, the IPG strips were loaded gel side up in an Amersham Ettan IPGphor manifold and covered with 108 ml of coverfluid. The following running conditions were used for pH3.0-10.0 and pH 4.0-7.0 24 cm strips, and 18 cm pH6.0-11.0 strips: 120min at 100V (step and hold), 90min at 500V(step and hold), 60min at 1000V(step and hold), 60min at 2000V(step and hold), 60min at 4000V(step and hold), 120min at 6000V(step and hold), 240min at 8000V(step and hold), 180min at 500V(step and hold) and 240min at 8000V(step and Hold) for a total of 70'000 Vh. Following first-dimension separation, gel strips were equilibrated for 30min. For the first 20min gel strips were washed in equilibration buffer containing 100mM dithiothreitol followed by 10min of equilibration buffer containing 0.25M ideoacetamide. Using the Ettan Dalt-Tweleve system from GE Healthcare (Little Chalfont, Bucks., UK), the gel electrophoretic separation of muscle proteins in the second dimension was performed with standard 12.5%(w/v) slab gels that were made in the lab and used following 12h of polymerization. Following washing in SDS running buffer, isoelectric focusing strips were placed on the top of the second dimension gel and held in place with a 1%(w/v) agarose sealing gel. Twelve slab gels were run in parallel at 0.5W/gel for 60 min and then 15W/gel until the blue dye front had disappeared from the bottom of the gel.

2.2.7 1-D gel electrophoresis for susequent digestion

Sodium dodecyl sulfate polyacrylamide gel electrophoresis was carried out with 3-12% gradient (1.5 mm thickness; 16 cm length) at a constant setting of 200 V until the blue dye front had disappeared from the bottom of the gel. Electrophoretic transfer to nitrocellulose sheets was performed for 90 min at 100 V. The reversible staining of membrane sheets was carried out with Ponceau Red or MemCode dye to visualise and evaluate the successful electrophoretic transfer of SR proteins.

2.2.8 DIGE Labelling

Cy3 and Cy5 dyes were reconstituted as a stock solution of 1mM in fresh DMF (Dimethylformamide) and then diluted to a 0.2mM solution prior to use. Protein samples were suspended in 1ml of DIGE lysis buffer (9.5M urea, 4% w/v CHAPS, 30mM Tris-Cl, pH8.5). Labelling was performed with 200pmols of Cy3 fluor dye per 50mg protein. A 50mg protein sample was labelled for each of the protein samples being studied, normal extracts and wobbler extracts were each labelled with Cy3 dye and the pooled internal standard with Cy5 dye. The labelling reaction was carried out for 30min on ice and in the dark, and then quenched by incubation with 10mM lysine for 10min on ice. The labelled protein extracts were pooled and immediately used for electrophoresis. An equal volume of 2X buffer (9.5M urea, 4%CHAPS, 2%IPG buffer pH3.0-10.0 and 100mM DTT) was added and this suspension was left on ice for 10min prior to electrophoresis separation.

2.2.9 DIGE Image Acquisition and Analysis

Labelled proteins were visualised using the Typhoon Trio vaiable mode imager from Amersham Biosciences/GE Healthcare (Little Chalfont, Bucks., UK) at a scanning wavelength of l=550nm for Cy3 and l=650nm for Cy5 labelled proteins. The PMT values for gels analysed were between 500V and 700V and the maximum pixel volume was between 85,000 and 95,000. Scanning was performed at 50mm resolution for DIGE gels and 100mm resolution for RUBPs stained gels. The gel images were then analysed using Progenesis Same Spots software version 3.2.3 from NonLinear Dynamics (Newcastle Upon Tyne, UK). All gels in an experiment were alligned to a reference gel. Spots were then detected and filtered. After filtering, images were then separated in to groups (control verus disease) and spots were then analysed to detect changes in abundance. A list was formed of spots with changed abundance. An power score was given to each spot above 0.8 and any below 0.8 were excluded from consideration. Similarly, spots with a P value less than 0.05 were taken and those greater than 0.05 were excluded from the experiment. An anova score was determined using the one way anova test. Any spot with Anova score above 0.5 were excluded from consideration. Any spots that met all criteria were susequently identified by Liquid Chromatography-Mass Spectrometry.

2.2.10 Protein Staining

2.2.10.1 Collodial Coomassie Staining

Colloidal Coomassie staining was carried out according to Neuhoff and co-workers (1988). After electrophoresis gels were washed twice with dH_2O and placed into Colloidal Coomassie staining solution (1 Part Stock Solution A(5% (w/v) Coomassie Brilliant Blue G250), 40 parts Stock Solution B(10% (w/v) ammonium sulfate, 2% (v/v) phosphoric acid), 10 parts methanol) and incubated overnight. The gels were washed with neutralisation buffer (0.1M Tris-PO_4 adjusted to pH6.5) for 1-3 min. The background was reduced by washing with 25% methanol for 1 min and the dye was fixed overnight in fixation solution (20% (w/v) ammonium sulphate). The procedure is repeated 3-4 times until sufficient protein pattern is visualised.

2.2.10.2 Silver Staining

Silver staining was carried out according to Chevallet and collegues (2006). After electrophoresis gels were fixed in 30% ethanol, 10% acetic acid for a minimum of 30min. The gels were then rinsed twice using 20% ethanol for 10 min and then twice with milli-Q for 10 min. The proteins were then sensitised by placing the gel in sensitising solution (0.8 mM sodium thiosulfate) for 1 min. The gels were then rinsed twice with milli-Q for 10 min. The proteins were then stained with 2 mM silver nitrate for a minimum of 20 min to 2 h. The gels were then rinsed with milli-Q for 10 s and then developed with 3% sodium carbonate, 250 ml formalin, 125 ml 10% sodium thiosulfate made up to 1L with milli-Q. In order to stop development gels were placed into stopping solution (40g Tris, 20 ml acetic acid /1L milli-Q). Gels were scanned using a Umax Image Scanner from Amersham Biosciences/GE Healthcare (Little Chalfont, Bucks., UK). Gels were then stored in a 5% acetic acid solution.

2.2.10.3 RuBPs Stain Preparation

Ruthenium II Bathophenathroline Disulfonate Chelate 20 mM stock solution was prepared according to Rabilloud and co workers (2001). Potassium pentachloro aquo ruthenate (0.2g) was dissolved in 20 ml of boiling dH_2O and kept under reflux having a deep red-brown colour. Bathophenanthroline disulfonate (3 M) was then added and kept under reflux for 20 min giving the solution a greenish-brown colour. Five milliliters of a 500mM sodium ascorbate solution was then added and kept under reflux for another 20 min until the solution turned a deep orange-brown colour. The solution was allowed to cool and was then adjusted

to pH 7.0 with sodium hydroxide. The final volume was adjusted to 26 ml with dH_2O. The stain was stored at 4°C and kept for several months.

2.2.10.4 RuBPs staining

Following electrophoresis gels were placed in 30% ethanol, 10% acetic acid overnight in order to fix proteins in the gel. The gels were then washed three times in 20% ethanol for 30 min. The gels were then stained for 6 h in 20% (v/v) ethanol containing 200 nM of ruthenium chelate. Following staining gels were destained for 15 h in 40% ethanol, 10% acetic acid. Gels were then re-equilibrated twice for 10 min in dH_2O. Gels were scanned using Typhoon Trio vaiable mode image from Amersham Biosciences/GE Healthcare (Little Chalfont, Bucks., UK) at a scanning wavelength of l=650nm. The PMT values for gels analysed were between 500V and 700V and the maximum pixel volume was between 85,000 and 95,000. Scanning was performed at 100mm resolution for RuBPs stained gels.

2.2.10.5 Hot Coomassie Staining

The staining solution (0.025% (w/v) PhastGel Coomassie Blue R-350 blue tablet and 10% (w/v) acetic acid) was heated to 90°C and poured over gel to be stained. The gel was placed on shaker for 1 h. To destain gels were placed in 10% (w/v) acetic acid with knot of tissue to soak up excess coomassie dye. Gels were scanned using a Umax Image Scanner from Amersham Biosciences/GE Healthcare (Little Chalfont, Bucks., UK). Gels were then stored in a 1% acetic acid solution.

2.2.11 Liquid Chromatography-Mass Spectrometry

The mass spectrometric analysis of peptides was carried out on a 6340 Model Ion Trap LC/MS apparatus from Agilent Technologies (Santa Clara, CA). Excision, washing, destaining and treatment with trypsin was performed by an optimised method (Doran et al. 2004). Trypsin-generated peptides were obtained by removing supernatants from digested gel plugs. Further recovery was achieved by adding 30%acetonitrile/ 0.2%trifluoroacetic acid to the gel plugs for 10min at 37°c with gentle agitation. Resulting supernatants were pooled with the initially recovered cohort of peptides following trypsin digestion. Further peptide recovery was achieved through the addition of 60% acetonitrile/0.2% trifluoroacetic acid to each plug for 10min at 37°c with gentle agitation. Supernatants were added to the peptide pool. The sample was dried through vacuum centrifugation and concentrated peptide fractions were then

suspended in mass spectrometry-grade distilled water and 0.1% formic and spun down through spin filter and added to LC-MS viles for identification by ion trap LC-MS analysis. Separation of peptides was performed with a nanoflow Agilent 1200 series system (Agilent Technologies). Mobile phases used were A: 0.1% formic acid, B: 50% acetonitrile and 0.1% formic acid. Five microliters of sample were loaded into the enrichment at a capillary flow rate set to 2ul/min with a mix of 0.1% formic acid and 50%acetonitrile and formic acid at a ratio of 19:1. The cappilary voltage was set to 1800V. Tryptic peptides were eluted with a linear gradient of 10-90% solvent B over 15min with a constant nano pump flow of 0.60ml/min. A five min post time of solvent A was used to remove any sample carryover. Database searches were carried out with Mascot MS/MS Ion search(Matrix Science, London, UK) under the following parameters: (i) two missed cleavages by trypsin, (ii) mass tolerance of precursor ions± 2.5 Da and product ions ± 0.7 Da, (iii) carboxymethylated cysteins fixed modification and (iv)oxidation of methionine as variable modification. Searches used "musculus" as taxonomic categorgy unless otherwise stated and used the NCBInr database release: 20100212. Identification of protein of interest was accepted when Mascot score > 49 was obtained with 2 or more peptides matched and molecular weight and p*I* matched the master gel. By choosing a score of greater than 49 we are 95% confident our match is correct.

2.2.11.1 Liquid Chromatography-Mass Spectrometry of on-membrane digestion.

Recovered peptides were analyzed on an Agilent 6340 LC-MS instrument (Agilent Technologies, Santa Clara, CA, USA) on a gradient of 5 to 100% acetonitrile/0.1% formic acid for 142min. Separation of peptides was performed with a nanoflow Agilent 1200 series system equipped with a Zorbax 300SB C18 analytical reversed phase column (5mm, 43mmx75mm) using high-performance liquid chromatography (HPLC)-chip technology. Mobile phases used were A(0.1%formic acid) and B(90%acetonitrile/0.1% formic acid). Samples(5ml) were loaded into the enrichment at a capillary flow rate set to 4ml/min with a mix of A and B at a ratio 19:1. Tryptic peptides were eluted with a gradient of 5 to 34% solvent B over 1min, 34 to 36%solvent B over 40min, 36 to 38% over 1min, 38 to 40%over 80min, 40 to 90% over 5min, 90 to 100% for 5min and 100 to 5% over 5min with a constant nano pump flow of 0.60ml/min. A 5min post time of solvent A was used to remove any carry over. The capillary voltage was set to 2000V. The flow and temperature of the drying gas were 4L/min and 300^{o} respectively. Identified peptides were used to determine the protein species present in the distinct protein bands. Database searches were carried out with Mascot

tandem mass spectrometry (MS/MS) ion search (Matrix Science, London, UK, NCBI database) with the same parameters as discussed in section 2.2.11 with "mammailia" as taxonomic categorgy.

2.2.12 On-membrane digestion

Protein bands were excised from membranes, placed in small eppendorf tubes, destained, and washed five times with distilled water. Nitrocellulose bands were then blocked with 0.5% polyvinylpyrrolidone (PVP-40) at 37^{o}C for 37min with gentle shaking. Nitrocellulose bands were susequently washed five times with distilled water. Treatment with trypsin was performed by an optimised method (Doran et al. 2004). Membrane bands were digested overnight at 37^{o}C in 100ml of working trypsin solution. Trypsin-generated peptides were obtained by removing supernatants from digested nitrocellulose bands. Further recovery was achieved by adding 30%acetonitrile/0.2%trifluoroacetic acid to the gel plugs for 10min at 37^{o}c with gentle agitation. Resulting supernatants were pooled with the initially recovered cohort of peptides following trypsin digestion. Further peptide recovery was achieved through the addition of 60%acetonitrile/0.2%trifluoroacetic acid to each plug for 10min at 37^{o}c with gentle agitation. Supernatants were added to the peptide pool. The sample was dried through vacuum centrifugation and concentrated peptide fractions were then suspended in mass spectrometry-grade distilled water and 0.1% formic and spun down through 22-mm cellulose spin filter tubes to remove any membrane particles, and then aliquoted to LC-MS viles for identification by ion trap LC-MS analysis.

2.2.13 Western Blotting

Gel electrophoresis and transfer was carried out with a Mini-Protean II electrophoresis and transfer system from Bio-Rad Laboratories (Hemel-Hempstead). Muscle proteins were transfered to nitrocellulose membranes for 70 min at 100 V at 4^{o}C in transfer buffer (28.28g Glycine, 6.56g Tris, 1600 ml dH_2O and 400 ml Methanol). Efficiency of transfer was evaluated by Ponsceau S-Red staining of membranes, followed by de-staining with phosphate buffered saline (PBS) (50mM sodium phosphate, 0.9% (w/v) NaCl, pH7.4). Membranes were placed in blocking sloution (5% (w/v) fat free milk powder in PBS) for 60 min at room temperature. Membranes were then incubated with primary antibody appropriately diluted (see table 2.2) with blocking solution for 3 h at room temperature. Membranes were then washed 4X 10 min washes: 2 X 10 minutes in blocking solution and 2 X 10 min in PBS.

Membranes were then incubated with appropriate dilution peroxidase-conjugated secondary antibody for 60 min at room temperature. The membranes were then washed with 4 X 10 min washes: 2 X 10 min with blocking solution and 2 X 10 min in PBS. Immuno-decorated bands were visualised by the enhanced chemiluminescence method using chemiluminescence substrate from Roche Diagnostics (Mannheim, Germany).

2.2.14 Statistical Analysis

Statistical analysis of densitometry results from immunoblots was performed using ImageJ (NIH, Bethesda, Maryland, USA). Statistical analysis of densitometric results from immunoblots were carried out using Graphpad prism statistical software (Graphpad software Inc.). Throughout this project a probability value of 0.05 was used within student's t-test. By choosing this our data is significant with 95% confidence.

3. RuPBs analysis of Gastrocnemius muscle proteome of the myotonic animal model: MTO*5J

3.1 Introduction

Myotonia is a symptom of various genetic and aquired skeletal muscle disorders and is characterised by hyperexcitability of muscle sarcolemma. Skeletal muscle hyperexcitability is caused by either lowered Cl^- conducatance (myotonias) or prolonged activity of Na^+ channels (paramyotonia). Both disorders belong to a distinct group of skeletal muscle disorders called ion channelopathies. Ion channelopathies are characterised by recurrent patterns of mutation in ion channels including: Cl^-, Na^+, K^+ and Ca^{2+}-channels. Myotonias can be classified as dystrophic, where multiple tissues are affected, or non-dystrophic where it is only skeletal muscle that is affected. Nondystrophic myotonias are closely related to ion channel dysfunction, and are classified as channelopathies affecting muscle-specific Cl^-- or Na^+-channels (Planells-Cases et al. 2009). Mutations in the gene encoding the muscle Na^+-channel are associated with paramyotonia congenita, potassium-sensitive myotonia and hyperkalemic periodic paralysis with myotonia. In contrast, nondystrophic chloride channelopathies are responsible for myotonia congenita, recessive Becker myotonia and dominant Thomsen myotonia (Fahlke, 2000).

Genetic animal models of neuromuscular diseases are widely used for studying the molecular pathogenesis and secondary effects of disease. For this study gastrocnemius muscle from MTO*5J mice was used to represent myotonic muscle. The characterization of the new allele MTO*5J at Clc1 locus of mice allows longer survival of homozygous animals as compared to other myotonic mouse mutants ADR and MTO. The affected mice do not produce immunologically demonstrable CLC-1 protein and they display central nuclei in their muscle fibers indicating ongoing regeneration.

This chapter attempted broad proteomics-based analysis to determine changes caused by single mutation by means of a changed physiological activity of the organ in which this gene is expressed, skeletal muscle. Protein extracts were obtained from gastrocnemius muscle from 4 control mice and from 4 MTO*5J mice. Protein extracts were separated in the first dimension by their isoelectric point and in the second dimension based on their molecular weight. Separated proteins were then visualized using the fluorescent dye RuPBs (ruthenium II tris[bathophenanthroline disulfonate]) was used. RuBPs is a ruthenium-based metal chelate stain and was first described as an in gel protein stain by Rabilloud in 2001.

3.2 Results

3.2.1. 2-D gel electrophoretic analysis of gastrocnemius muscle proteome of myotonic animal model: MTO*5J

Crude soluble protein extracts were obtained from 11-week old control and MTO*5J mouse gastrocnemius muscle and were separated first by one-dimensional gel electrophoresis to check equal loading (see Figure 3.1). From Figure 3.1 it is difficult to determine changes in protein expression of one particular protein therefore in order to gain better separation protein extracts were separated by standard 2-D gel electrophoresis. Isoelectric focusing was performed in the pH ranges of pH4.0-7.0 and pH6.0-11.0 and was followed by SDS-PAGE electrophoresis covering a molecular mass range of approximately 10kDa to 220kDa. RuPBs stained protein gels are shown in Figure 3.2. Progenesis Same Spots software version 3.2.3 from NonLinear Dynamics (Newcastle Upon Tyne, UK) was employed for the statistical evaluation of changes in individual protein spots in diseased versus control. Protein spots with altered expression were then identified by mass spectrometry.

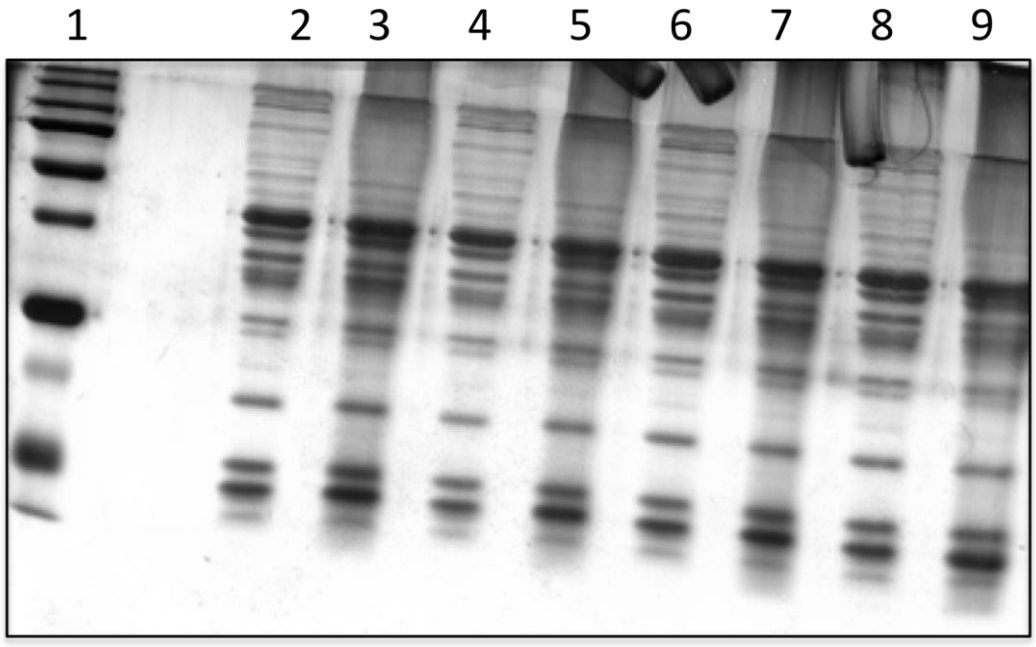

Figure 3.1 Silver stained 1-Dimensional gel

Shown is silver stained 1-D gel electrophorectically separated total gastrocnemius muscle extracts from control (lanes 2,4,6 and 8) and MTO*5J (lanes 3,5,7 and 9). A total of 10mg of protein is loaded in each lane and 5ml molecular weight standard (lane 1).

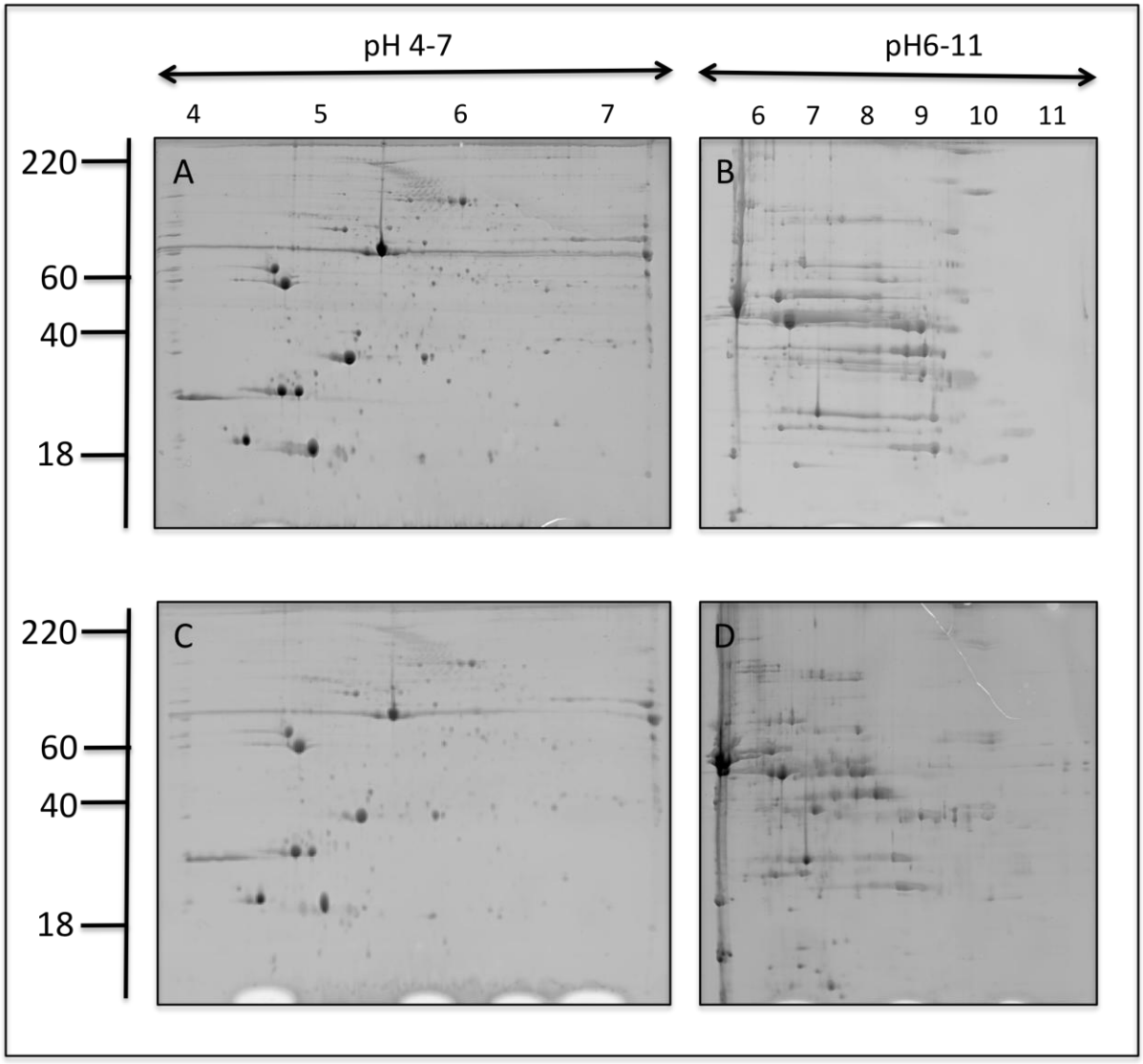

Figure 3.2 2-D gel electrophoretic analysis of normal versus myotonic gastrocnemius muscle

Shown are 2-D gels electrophoretically separated total crude soluable extracts in both pH ranges from control (A;pH4-7,B;pH6-11) and myotonic (C;pH4-7,D;6-11) from MTO*5J mice. 2-D gels were stained with RuBPs stain. The pH values of the first dimension and molecular mass standards of the second dimension are indicated on the top and on the left of the panels respectively.

3.2.2 Differential protein expression pattern in myotonic animal model MTO*5J

Two-dimensionial spot patterns were compared across 8 slab gels using Progenesis Same Spot software. In total 950 clearly separated protein spots were identified by RuPBs staining. A total of 12 protein spots with changed abundance were identified in the MTO*5J mouse model of mild myotonia. The proteins with changed abundance ranged in pI from 4.8 (myosin light chain fast MLC2f) to 9.2 (F1-ATPase synthase) and ranged in molecular mass from 19 kDa (myosin light chain) to 61 kDa (heat shock protein Hsp60). Table 3.1 summarizes information gained from proteomic profiling of MTO*5J mouse model. It gives information on protein name and number so that it can be correlated to the numbering in the 2-D MTO*5J master gel shown in figure 3.3. Table 3.1 shows fold changes, percentage coverage, isoelectric point and molecular weights of identified proteins. Table 3.1 lists 4 proteins being decreased and 8 proteins being increased in MTO*5J samples. While myosin heavy chain MHC1 (spot 1), myosin light chain MLC2f (spot 2), T complex protein 1 (spot 3) and heat shock protein Hsp60 (spot 4) were shown to be reduced, protein spots representing troponin TnTf (spots 6 and 12), triosephosphate isomerase (spot 11), desmin (spot 10), F1-ATP synthase (spot 9), NADH dehydrogenase (spot 8), heat shock protein Hsp27 (spot 7) and superoxide dismutase (spot 5) were found to be increased in MTO*5J specimens.

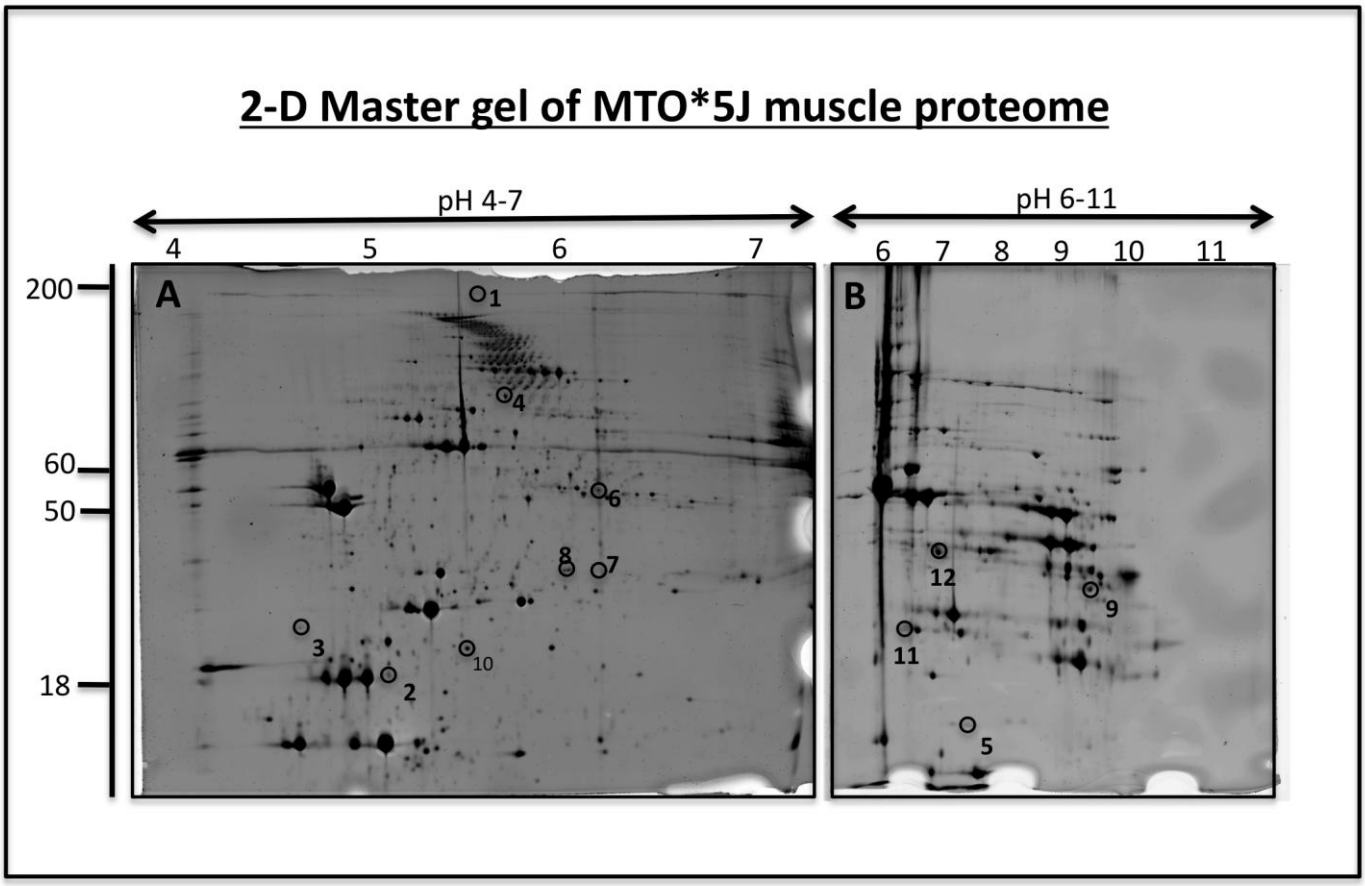

Figure 3.3 2-D Master gel of MTO*5J mouse model of mild myotonia

Shown is a 2-D master gel of the MTO*5J gastrocnemius muscle proteome separated in the pI ranges pH4-7 (A) and pH6-11 (B). Proteins with a drastically altered expression that have been identified by LC/MS are numbered 1-12. A total of 8 protein changes were identified in the pH 4-7 (A) range and 4 changes in the pH 6-11 (B) range. Table 3.1 shows details of fold changes in myosin heavy chain (pI 5.61; 22 kDa), myosin light chain phosphorylatable, fast (pI 4.82; 19 kDa), T complex protein 1 (pI 5.82; 60 kDa), Hsp 60 (pI 6.07; 61 kDa), superoxide dismutase SOD2 (pI 8.67; 24 kDa), troponin T, fast (pI 5.98; 30 kDa), Hsp 27 (pI 6.45; 23 kDa), NADH (pI 6.67; 30 kDa), F1-ATPase synthase (pI 9.16; 28 kDa), desmin (pI 5.21; 53 kDa), triosephosphate isomerase (pI 5.62; 22 kDa) and troponin T, fast (pI 6.18, 30 kDa). The pH values of the first dimension and molecular mass standards of the second dimension are indicted on the top and on the left of the panel respectively.

Table 3.1: List of proteins that exhibit a changed abundance in myotonic MTO*5J versus normal gastrocnemius muscle.

Spot no.	**Name of identified protein**	**Protein accession no.***	**p*I***	**Molecular mass (kDa)**	**Sequence coverage (%)**	**Mascot score ****	**Peptides matched**	**Fold change *****	**Anova**
1	Myosin, heavy chain, MHC1, skeletal muscle	gi|187956263|	5.61	224136	33	476	22	-5.8	1.50E-02
2	Myosin light chain MLC2f, phosphorylatable, fast muscle	gi|7949078|	4.82	19059	5	100	34	-3.6	5.00E-03
3	T complex protein 1	gi|228954|	5.82	60960	16	368	41	-3.6	1.40E-02
4	Heat shock protein Hsp60	gi|51766670|	6.07	61190	23	461	43	-1.4	3.00E-03
5	Superoxide dismutase SOD2, mitochondrial	gi|17390379|	8.67	24244	5	177	24	2.4	9.00E-03
6	Troponin TnT, fast	gi|2340064|	5.98	30691	4	98	28	2.5	1.10E-02
7	Heat shock protein Hsp27	gi|424143|	6.45	22945	10	152	49	2.9	1.30E-02
8	NADH dehydrogenase FeS protein 3, mitochondrial	gi|58037117|	6.67	30305	12	315	36	2.9	3.85E-04

9	ATP synthase, mitochondrial F1 complex	gi|122889678|	9.16	2864	11	520	36	3.0	2.00E-03
10	Desmin	gi|33563250|	5.21	53523	27	582	59	3.4	1.00E-02
11	Triosephosphate isomerase	gi|1864018|	5.62	22720	12	531	76	3.7	1.40E-02
12	Troponin TnT, fast	gi|2340068|	6.18	30297	9	347	30	6.0	1.20E-02

*NCBInr Database, release 20100212

** The mascot score has a 95% confidence level if >49.

*** Myotonic versus normal muscle tissue

3.2.3 Immunoblot analysis of potential biomarkers of Myotonia

In order to verify alterations in abundance of skeletal muscle proteins and to confirm our proteomic profiling of myotonic muscle several proteins were selected for immunoblotting studies. As shown in Figure 3.4 A-C, the decrease in triosephosphate isomerase (TPI), myosin light chain phosphorylatable (MLC-phospho) and myosin light chain 2 (MLC-2) can be seen. Although the statistical analysis of immuno-decorated bands showed no significance the analysis showed a slight decrease of the proteins in myotonic muscle. As shown in Figure 3.5 the decrease in myosin heavy chain fast in myotonic muscle was clearly confirmed by immunoblot analysis. This statistically significant difference in expression correlates with the proteomic findings listed in Table 3.1. As previous studies on more pronounced myotonic muscle has described a variety of expression changes in MHC isoforms (Agbulut et al. 2004), it was therefore interesting to see was this change similar in our new allele *mto*5j*. The decrease of myosin heavy chain fast isoform in MTO*5J myotonic muscle is shown in Figure 3.5 (A). The immunoblotting of fiber type-specific markers of regulatory elements of muscle relaxation Ca^{2+} isoforms SERCA1 and SERCA2 is shown in Figure 3.6. The immunoblotting of the slow isoform SERCA2 (B;F) showed a significant increase in myotonic muscle whereas the fast isoform SERCA1 (A;E) showed a decrease in expression although the statistical analysis was not significant. As shown in Figure 3.6 (C, G) immunoblotting analysis was also carried out on the myoglobin protein and showed a slight increase in the myotonic muscle. Similarly in Figure 3.6 (D, H) immunoblotting was carried out on the high-affinity Ca^{2+}-binding protein parvalbumin. Previously published immunoblot work on more pronounced myotonic muscle showed a decrease in parvalbumin (Jockusch et al. 1988) and so it was of interest to see did the mto*5j allele show a similar decrease in parvalbumin. As illustrated in Figure 3.6 (D, H) parvalbumin was marginally decreased in MTO*5J myotonic muscle. Figure 3.7 shows immunoblotting of alpha-dystroglcan as a loading control. The data presented here clearly verifies alterations in abundance of some of proteins from our proteomic profiling of myotonic muscle.

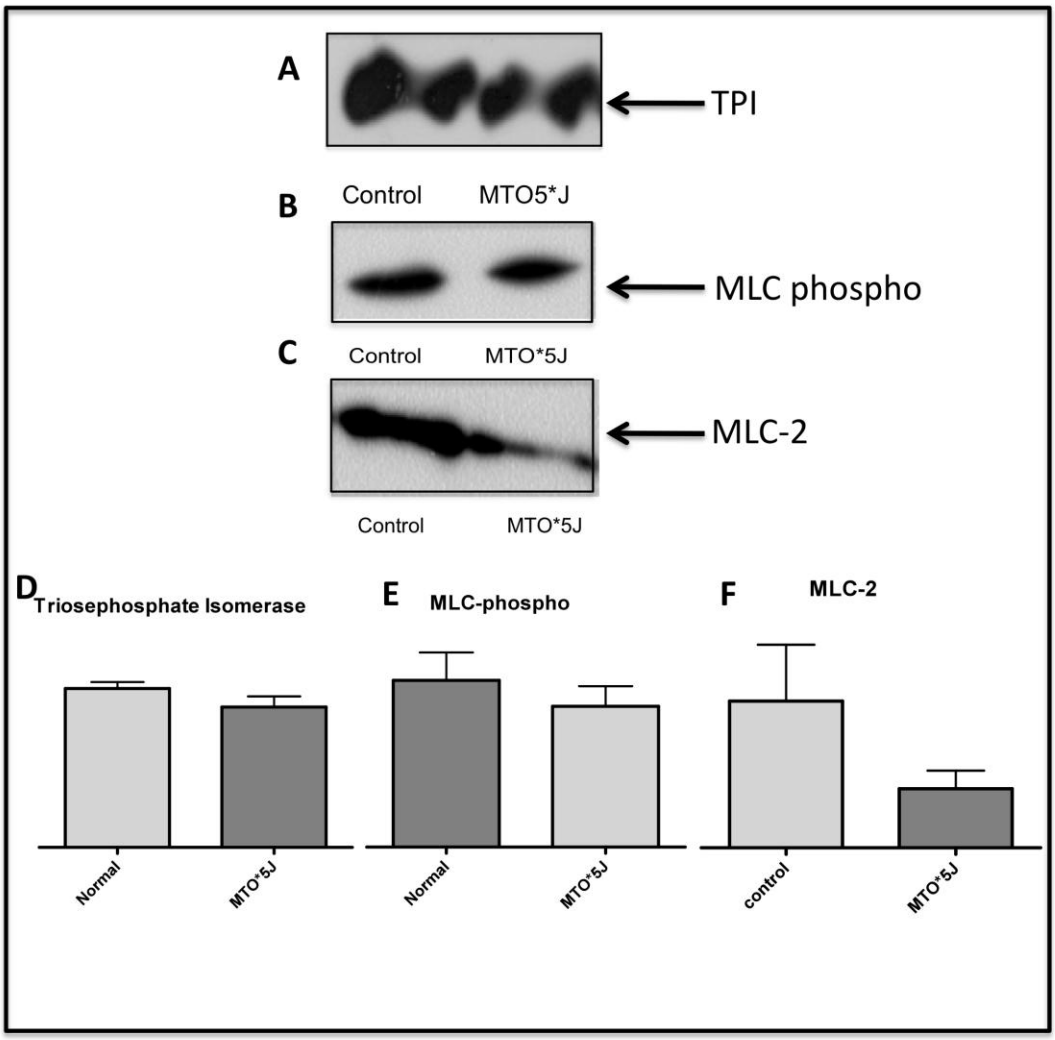

Figure 3.4 Immunoblot analysis of triosephosphate isomerase, myosin light chain phosphorylatable and myosin light chain-2 in myotonic muscle.

Shown are the imuno-decoration bands of nitrocellulose replicas of 1-D gels. Antibodies were directed against triosephosphate isomerase (A), myosin light chain phosphorylatable (B) and myosin light chain-2 (C). The immuno-decorated bands from normal and myotonic muscle were statistically evaluated using unpaired Student's t-test ($n=4; p^*<0.05$) and is graphically shown in panels (D), (E) and (F).

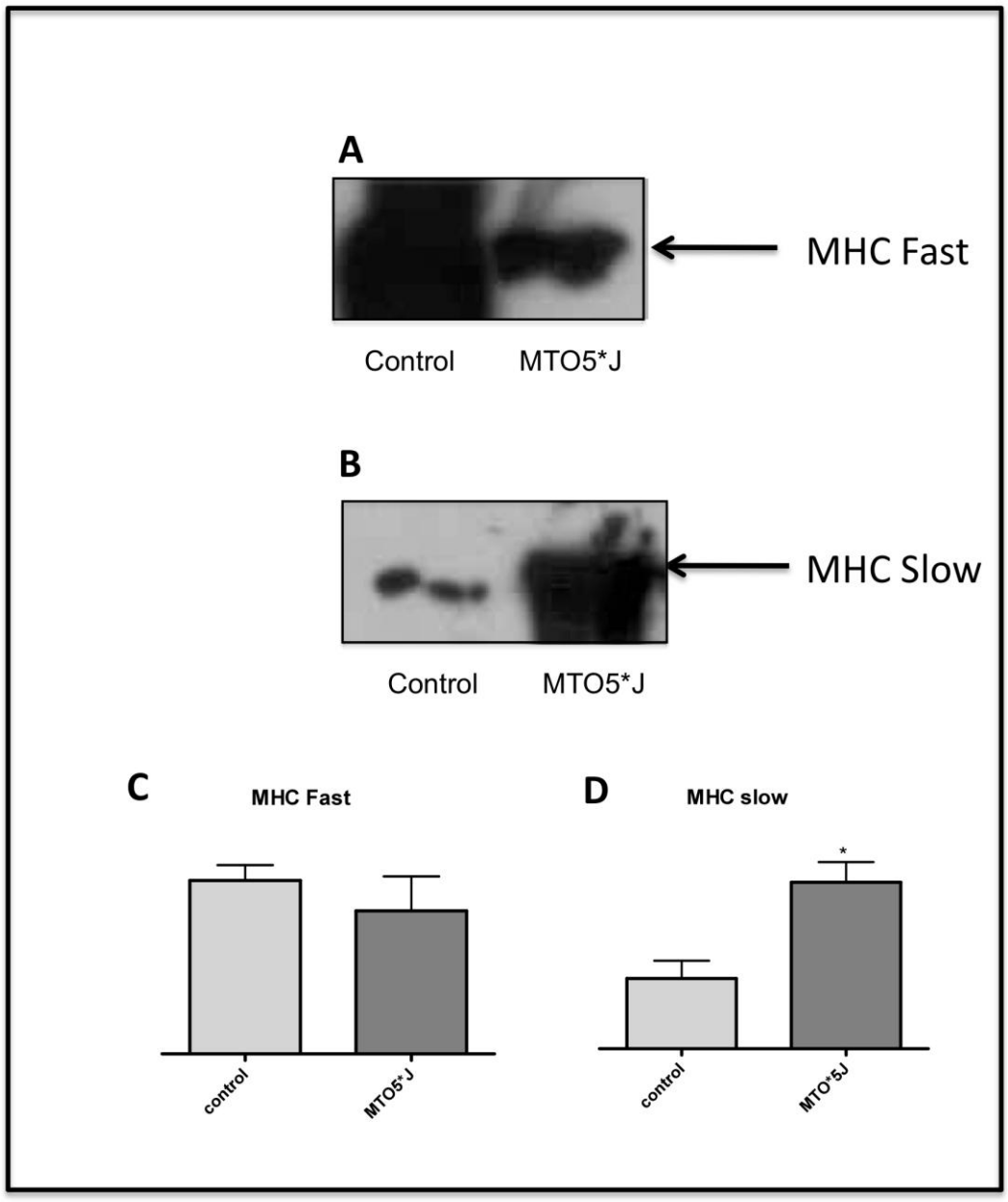

Figure 3.5 immunoblot analysis of myosin heavy chain fast and myosin heavy chain slow
Shown is the immuno-decoration of nitrocellulose bands of 1-D gels. Antibodies were directed against myosin heavy chain fast (A) and myosin heavy chain slow (B). The comparative immuno-decorated bands were statistically evaluated using an unpaired Student's t-test (n=4;*p<0.05) and are shown graphically in panels (C) and (D).

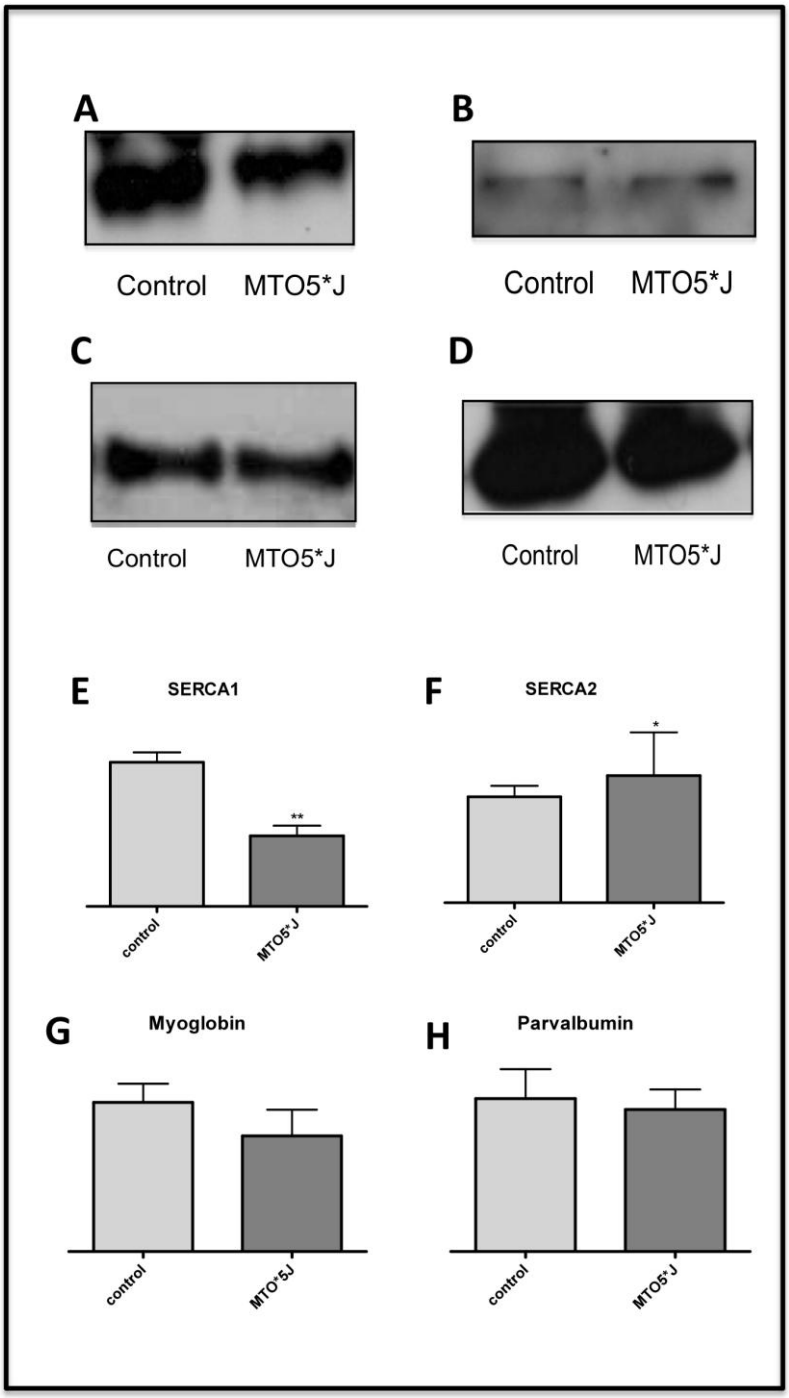

Figure 3.6 Immunoblot of SERCA1, SERCA2, Myoglobin and parvalbumin in myotonic muscle.

Shown is the immuno-decoration of nitrocellulose bands from 1-D gel. Antibodies were directed against SERCA1 (A), SERCA2 (B), myoglobin (C) and parvalbumin (D). Comparative immuno-decorated bands were statistically evaluated using unpaired Student's t-test (n=4;*p,0.05) and are graphically shown in panels (E), (F), (G) and (H).

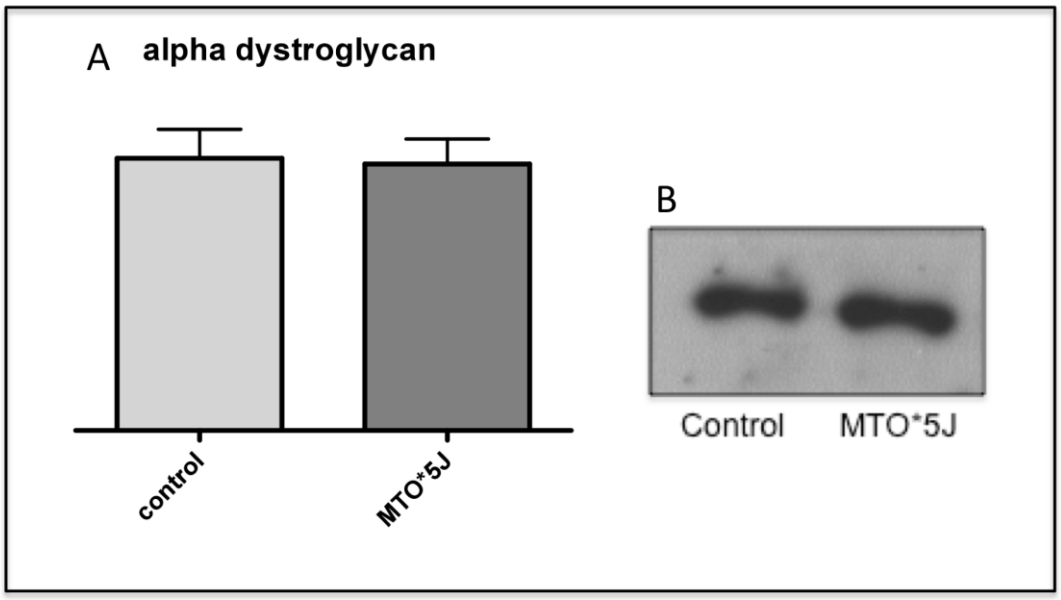

Figure 3.7 Immunoblot of alpha dystroglycan in myotonic muscle.

Shown is the immuno-decorated nitrocellulose bands from 1-D gel. Antibodies were directed against alpha dystroglycan (B). Comparative immuno-decorated bands were statisically evaluated using unpaired Student's t-test (n=4) and is graphically shown in panel (A).

3.3 Discussion

Two dimensional gel electrophoresis with RuPBs staining revealed 12 protein spots with altered expression in MTO*5J myotonic muscle. Of these 12 spots 4 showed decrease in expression and 8 with an increase in expression. These 12 proteins were identified by Liquid chromatography mass spectrometry and are involved in multiple functions in the muscle cell ranging from muscle contraction to muscle metabolism. These proteins will now be discussed in detail.

3.3.1 Contractile proteins

The contractile units of skeletal muscle are composed of thick and thin filaments. Skeletal muscle myosin forms a hexameric structure consisting of 2 myosin heavy chains (MHCs) and 2 myosin light chains (MLCs) and make up thick filaments (Clark et al. 2002). Thin filaments are composed of actin and accessory proteins troponin and tropomyosin. Molecular coupling between the myosin head structure and actin filaments, in the prescence of ATP causes sliding of the thin filaments past thick filaments resulting in sarcomeric shortening and muscle contraction. In this study two contractile proteins were found to have a decreased abundance in MTO*5J gastrocnemius muscle, myosin heavy chain MHC1 (spot 1) and myosin light chain MLC2f (spot 2). MHC1 was found to have a 5.8 fold decrease in MTO*5J gastrocnemius tissue. MHC1 is part of the MHCs isoforms found in fast muscle fibers. MLC2f was shown to have a 3.6 fold decrease in MTO*5J gastrocnemius tissue compared to control tissue. MLC2f is the regulatory light chain found in skeletal muscle it is associated with the MHC neck region of the myosin molecule.

Previous work on the more profoundly affected ADR mouse showed a drastic reduction in MHC IIB (Agbulut et al. 2004) which supported the idea that the shift in MHC fast observed in ADR mice was caused by the hyperexcitability of muscle. Agbulut and colleagues (2004) concluded that the hyperexcitability of the myotonic muscle leads to unschelduled episodes of trains of action potentials. Immunoblotting of MTO*5J gastrocnemius muscle agrees with this previous work as seen in Figure 3.5. MHC fast showed a significant decrease in MTO*5J muscle whereas MHC slow showed a significant increase. Similarly previous proteomic studies have shown that isoform changes in MLCs represent reliable markers of muscle transformation (Reininghaus et al. 1988). Donoghue and co-workers (2007) carried out chronic low-frequency stimulation of fast rabbit muscle and showed it triggers a significant decrease in various MLCf molecules and an increase in slower counterparts. Immunoblotting

shown in Figure 3.4 agrees with a significant decrease in MLC2 isoform. Although the statistical analysis of Western blotting showed no significant difference in the abundance of MLC2f between MTO*5J and control gastrocnemius muscle the overall analysis indicated a trend towards increased expression of slower MHC isoforms and a decrease in fast isoforms of MHC and MLC2. The effect of repetitive firing of action potentials seen in myotonic muscle seems to mirror the effect of chonic low-frequency stimulation on fast muscle i.e. muscle transformation from fast isoforms to their slower counterparts.

Troponin I (spot 3) was found to be decreased in MTO*5J muscle with a 3.6 fold change. The troponin compex is a set of three regulatory proteins of muscle contraction (Tobacman 1996). As described previously it is a component of the thin filaments along with actin and tropomyosin. Troponin I binds actin to hold the troponin-tropomyosin complex in place. A decrease abundance of troponin could affect the integrity of the contractile apparatus in myotonic muscle.

The changes seen in contractile proteins in MTO*5J gastrocnemius tissue mirror those seen during electrostimulation-induced muscle transformation. Changes in the accessory protein may indicate contractile apparatus remodeling due to myotonia.

3.3.2 Metabolic enzymes

Metabolism is responsible for the production of energy in the form of ATP. Glycolysis is the process used to convert glucose into pyruvate, with the generation of energy in form of NADH and ATP along the pathway. It is an anerobic process and is main metabolic pathway in fast-twitch fibers (Peter et al. 1972). Respiration is carried out in the mitochondrion through the electron transport chain and the Krebs cycle. In this study four enzymes involved in metabolism have shown altered abundance in MTO*5J gastrocnemius muscle. Triosephosphate isomerase (TPI, spot 11) was found to have a 3.7 fold increase in MTO*5J muscle. Figure 3.4 shows a slight decrease in TPI however statistical analysis showed no significant difference. TPI rapidly interconverts dihydroxyacetone phosphate and D-glyceraldehyde-3-phosphate (Trentham et al. 1969). D-glyceraldehyde-3-phosphate is further used in the glycolysis pathway. There are five complexs altogether that result in the production of ATP in respiration. NADH dehydrogenase (spot 8) showed a 2.9 fold increase in MTO*5J muscle. NADH dehydrogenase (complex I) is an enzyme located in the inner membrane of mitochondria. It is responsible for the entry of electrons into the electron transport chain by moving electrons from NADH to quinone. Succinate dehydrogenase

(SDHA) is part of complex II and functions in oxidative phosphorylation chain but also in the citric acid cycle. Ubiquinol-cytochrome c reductase core protein 1 is a subunit of complex III and is responsible for the movement of electrons from quinone to cytochrome c. Together the above complexes pass electrons along the electron transport chain and are also responsible for the export of protons into the intermembrane space creating a proton gradient. H^+ transporting ATP synthase (complex V) pumps electrons in the opposite direction allowing the formation of ATP a cellular store of energy. The increased abundance of NADH in myotonic muscle might result in a higher rate of ATP production by oxidative metabolism. The use of oxidative metabolism for ATP production is indicative of a slower fiber population.

The 3-fold increase in mitochondrial ATP synthase (spot 9) in MTO*5J muscle also agrees with the suggestion that there is a reduction in the utilization of glucose and increase in mitochondrial metabolism. This increase in mitochondrial metabolism increases oxidative stress as mitochondria are the biggest producers of free radicals. Evidence of this increase in oxidative stress in myotonic muscle is see by the 2.4 fold increase in superoxide dismutase (SOD, spot 5). SOD destroys radicals which are normally produced by the mitochondria. Similar evidence of mitochondrial metabolism is seen in the striking red colour of myotonic muscle which was first described by Watkins and Watts (1984). Immunoblotting for the oxygen carrying protein myoglobin showed a slight increase in the MTO*5J gastrocnemius muscle. It is interesting that the increase in myoglobin has also been reported to occur in fast muscle following chronic electro-stimulation (Donoghue et al. 2007). This finding agrees with the idea that myotonic runs mirror the effect that electro stimulation has on fast muscle tissue.

3.3.3 Muscle transformation

Differences in muscle protein isoforms reflect distinct biological adaptations to specific functional demands. Antibody labeling shown in Figure 3.6 confirmed a switch from the SERCA1 isoform of the sarcoplasmic reticulum Ca^{2+}-pump to its SERCA2 form. Relaxation of skeletal muscle is assisted by the action of SERCA where calcium is pumped back into the SR. There are five primary SERCA isoforms that are encoded by three separate genes (Rossi et al. 2006). The ATP2A1 gene encodes the SERCA 1 isoform, this gene can be spliced into adult SERCA 1a and neonatal SERCA 1, similarly ATP2A2 can be spliced to form adult SERCA 2a and neonatal SERCA 2b (Rossi et al. 2006). SERCA 1a is the principal isoform found in fast-twitch skeletal muscle whereas SERCA 2a is the principal isoform found in slow-twitch skeletal muscle. The tissue specific expression pattern of each different SERCA isoform indicates the functionally distinct properties of skeletal muscle fibers. Immunoblot analysis (Figure 3.6) showed a significant increase in the slow SERCA 2 isoform however analysis of the fast SERCA 1 isoform showed no significant difference in MTO*5J gastrocnemius muscle. Increases in SERCA 2 agree with fiber transformation to a slower population due to myotonia.

3.3.4 Other proteins

As well as proteins involved in muscle contraction, metabolism and calcium uptake a number of other proteins were found to have an altered abundance in MTO*5J gastrocnemius muscle. Of these heat shock porteins Hsp 60 (spot4) and Hsp 27 (spot 7) were found to be decreased and increased in myotonic muscle by 1.4 and 2.9 fold change respectively. Heat shock proteins are a set of highly conserved proteins that are sythesised in response to certain environmental and physiological conditions (Locke and Noble 1995). They function in protein folding, import and translocation. Hsp 60 is localised in the mitochondria and facilitates the folding and assembly of proteins as they enter the mitochondrion and stabilises preexisting proteins under stress (Lui and Steinacker 2001). Hsp 27 is localised in the cytosol under unstressed conditions and translocates inside the nucleus during stress. The major functions of Hsp27 include stabilisation of microfilaments and cytokine signal transduction (Lui and Steinacker 2001). Increases in these proteins not only agrees with muscle transformation in myotonic muscle but also suggests MTO*5J muscle is under cellular stress from hyperexcitabilty of the plasma membrane that causes muscle stiffness. Perhaps the

increase in Hsp27 in myotonic muscle functions to aid in the stabilisation of contracted muscle filaments.

An increase was also seen in the intermediate filament protein desmin. Intermediate filament proteins are important for the structural integrity of the muscle cell they help provide elasticity within the contractile fibers. The increase in expression of desmin maybe due to the sustained contraction in myotonic muscle after voluntary contraction.

Previous studies on the more profoundly effected ADR mouse by Jockusch and colleagues (1988) demonstrated a reduction in the Ca^{2+}-binding protein parvalbumin. A considerably less pronounced reduction of parvalbumin was observed in the mild MTO8*5J phenotype (Figure 3.6).

3.4 Conclusion

In this study we have analysed the myotonic mouse MTO*5J using fluorescent 2D gel electrophoresis and mass spectrometry to identify novel protein markers of the myotonia-related changes. Mild myotonia appears to trigger changes in contractile apparatus, cellular processes and muscle energy metabolism. Altered protein expression in MTO*5J were comparable with changes in fast skeletal muscle following chronic electro-stimulation. An overall shift from fast-to-slow isoforms in MHC and SERCA and an increase in mitochondrial metabolism markers such as mitochondrial ATPase and superoxide dismutase suggest that myotonia triggers a glycolytic-to-oxidative transformation process in myotonic fast muscle.

4. Comparative analysis of altered protein expression in myotonic animal models: ADR versus MTO.

4.1 Introduction

Genetic animal models of neuromuscular disorders are widely used for studying the molecular pathogenesis of inherited disorders, evaluating effects of drug treatment on disease progression and testing novel therapeutic stategies. In the case of myotonia research manifestation and molecular basis of the disease has been clarified by analysis of well established myotonic mouse mutants' arrested development of righting response (ADR) and myotonia (MTO). The ADR mutant is caused by insertional mutation (allele *adr*) whereas the MTO mutant is due to a nonsense mutation in the chloride channel gene locus *Clc1* on chromosome 6. ADR and MTO mice are both genocopies and phenocopies of human congenital myotonia. In human myotonia both recessive (Becker type) and dominant (Thomsen type) mutations at gene locus *CLCN1* on chromosome 7 have been identified. In contrast to the MTO*5J animial, ADR and MTO show a more pronounced phenotype displaying more severe symptoms, weight loss and reduced life span. Similar to the mto*5j mutation, adr and mto mutations are null mutations and result in complete deletion of the CLC-1 protein. Previous histochemical work on the ADR animal model show a variety of biochemical changes in affected muscles (Jockusch et al. 1988). Many of these biochemical changes were reminiscent of those observed in chronic low-frequency stimulated fast muscle which involves a fiber type shift from fast-glycolytic white muscle to fast-oxidative red muscle (Pette and Staron 2000). In long-term electrostimulated fast rabbit muscles, fiber transitions eventually result in a slow-oxidative muscle phenotype that is reflected by extensive fast-to-slow switches in protein isoforms (Donoghue et al. 2007). In myotonic muscles, transformations are well documented by the alterations in the isoform expression pattern of slow and heavy chains of muscle myosins. For example, hyperexcitability triggers a reduced phosphorylation of the fast myosin light chain MLC2f (Jockusch et al. 1988). A lower concentration of myosin heavy chain isoform MyHC-IIB has also been shown in myotonic fast muscles (Agbulut et al. 2004).

In this chapter we carried out a comparative proteomic survey of ADR versus MTO muscle preparations. Similar to MTO*5J myotonic gastrocnemius muscle analysis, gastrocnemius muscle from the hind leg from four ADR mice and four MTO mice versus gastrocnemius from four control mice was used in this study. Crude soluble protein extracts were separated

first by one dimensional gel electrophoresis in order to confirm equal loading (see Figure 4.1). As seen in Figure 4.1 separation by one dimensional gel electrophoresis it is difficult to determine changes in single protein species, therefore crude protein extracts were separated by 2-DE in the pH ranges of pH4.0-7.0 24cm strips and pH6.0-11.0 18cm strips in the first dimension and then separated in the second dimension based on their molecular weights. Separated proteins were visualized using the fluorescent RuPBs stain.

4.2 Results

4.2.1 1-D gel electrophoresis of gastrocnemius muscle proteome of ADR and MTO

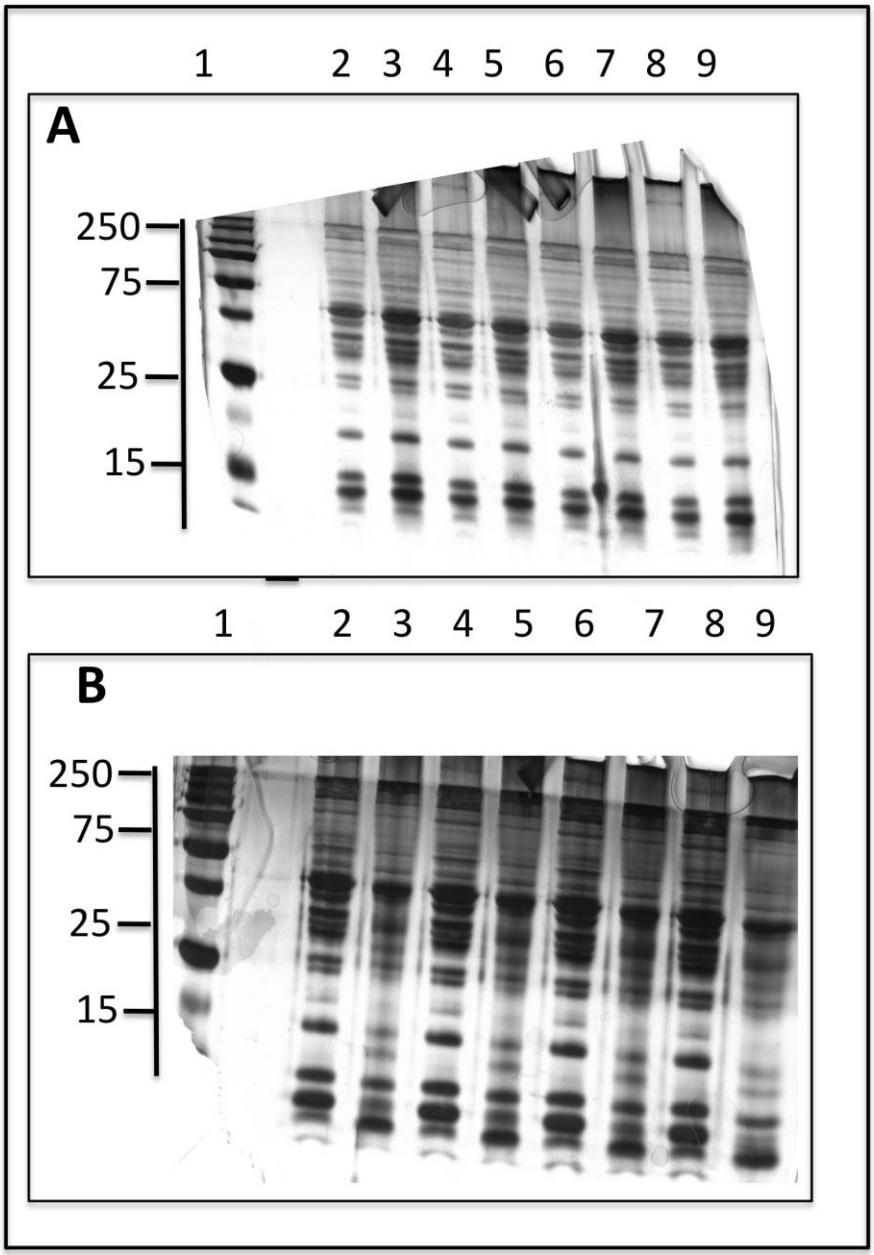

Figure 4.1 Silver stained 1-Dimensional gels

Shown are silver stained 1-D gels of ADR (A) gastrocnemius muscle (lanes 3,5,7 and 9) and control gastrocnemius muscle (lanes 2,4,6 and 8). The 1-D gel of MTO (B) gastrocnemius muscle (lanes 3,5,7 and 9) and control (lanes 2,4,6 and 8). A total of 5mg of protein was loaded per lane and 5ml of molecular weight marker is shown in gels A and B (lane 1).

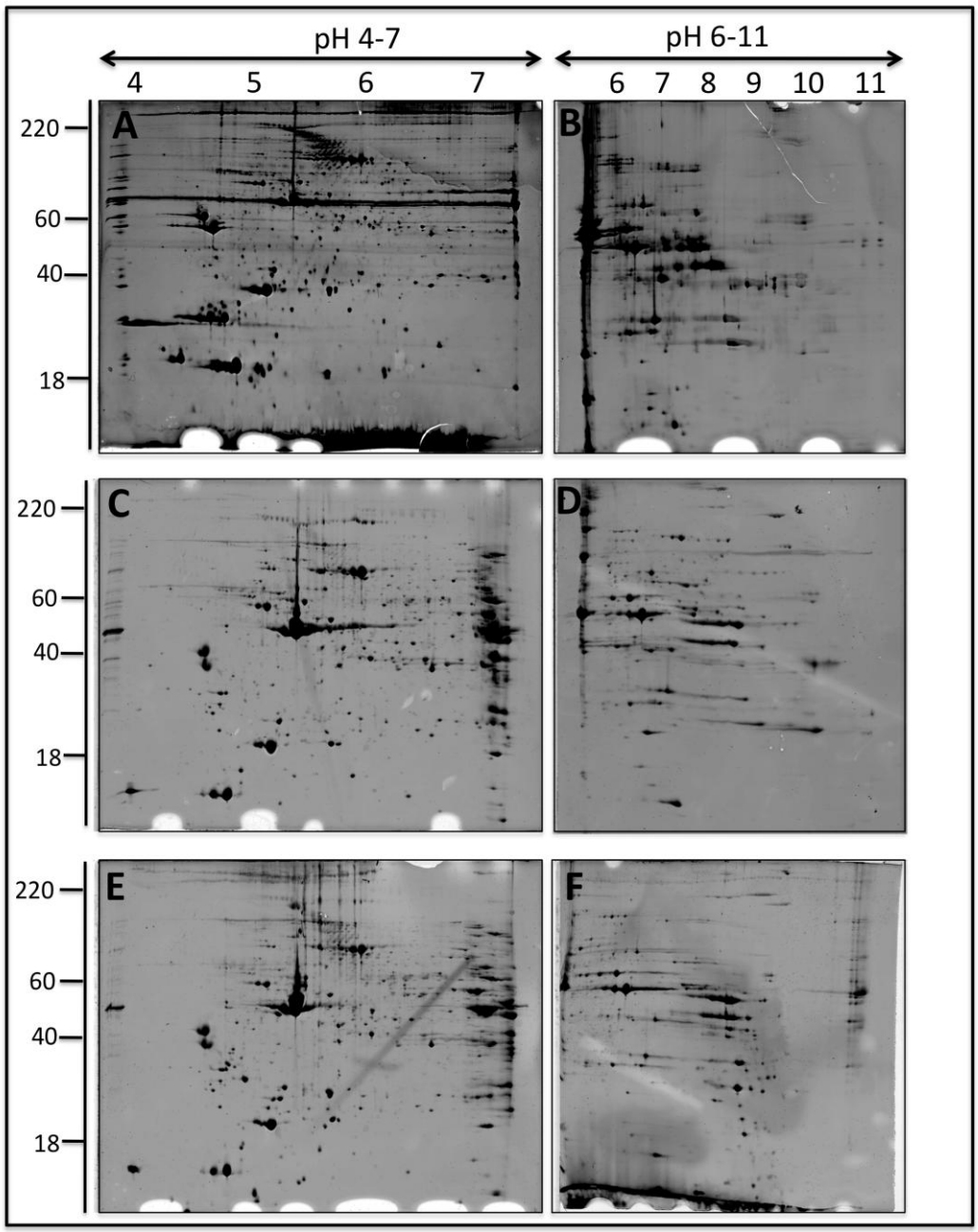

Figure 4.2 Two-Dimensional gel electrophoresis analysis of myotonic muscle versus control muscle

Shown are 2-D gel electrophoretically separated gastrocnemuis muscle extracts of control pH4-7(A) and pH6-11(B), MTO pH4-7 (C) and pH6-11 (D) and ADR pH4-7 (E) and pH6-11 (F) stained with RuPBs stain. The pH-values and molecular weight standards (kDa) are indicated at the top and left of the panels respectively.

4.2.2 Differential protein expression pattern in myotonic animal model MTO

Two-dimensional gel electrophoresis resulted in the identification of 42 muscle protein spots with a changed abundance in the MTO mouse. A representative master gel with electrophoretically separated gastrocnemius muscle proteins is shown in Figure 4.3. Muscle proteins with a changed concentration covered a p*I*-range from approximately 4.6 (tropomyosin) to 7.6 (cofilin) and ranged in molecular mass from apparent 19 kDa (myosin light chain) to 84 kDa (heat shock protein Hsp90). Table 4.1 summarizes the results of the mass spectrometric identification of the 42 protein species from MTO muscle tissue and combines data from both pH 4.0-7.0 and pH 6.0-11.0 gels. The majority of identified proteins in MTO preparations were shown to be constituents of major metabolic reactions, the contractile machinery, the cellular stress response and cell signaling pathways. An increased concentration was shown for 16 muscle proteins and 26 proteins were found to be decreased in MTO muscle. The protein species with the strongest reduction was the phosphorylatable fast MLC2f isoform of myosin light chain. Decreased proteins were identified as MLC2f (spots 1, 7, 8, 10, 14, 17, 20, 24), DJ-1 protein (spot 2), heat shock protein beta-7 (spot 3), myosin-binding protein H (spot 4), T Complex protein 1 (spot 5), myosin light chain MLCs (spot 6), creatine kinase (spot 9), ribonuclease/angiogenin inhibitor (spot 11), glycogenin 9spot 12), tropomyosin (13), heat shock protein Hsp-2 9spot 15), myosin light chain MLC3 (spot 16), glyceraldehydes-3-phosphate dehydrogenase (spot 18), F-actin capping protein (spot 19), triosephosphate isomerase (spot 21), protein disulfide isomerase (spot 22), pyruvate kinase (spot s 23 and 25) and sepiapterin reductase (spot 26). In contrast, phosphoglucomutase (spot 42) was shown to be the enzyme with the highest fold increase in MTO muscle. In addition, succinate dehydrogenase (spot 42), Actg2 protein (spot 40), cofilin (spot 39), troponin TnTf (spot 38), alpha actin (spots 36 and 37), mitochondrial NADH dehydrogenase (spot 35), heat shock protein Hsp90 (spot 34), albumin (spot 33), cytosolic malate dehydrogenase (spot 32), 14-3-3 protein (spot 31), tubulin (spot 30), UTP-glucose-1-phosphate uridyltransferase (spot 29), one specific subspecies of MLC2f (spot 28) and dihydrolipoamide-S-acetyltransferase (spot 27) were increased in MTO gastrocnemius muscle.

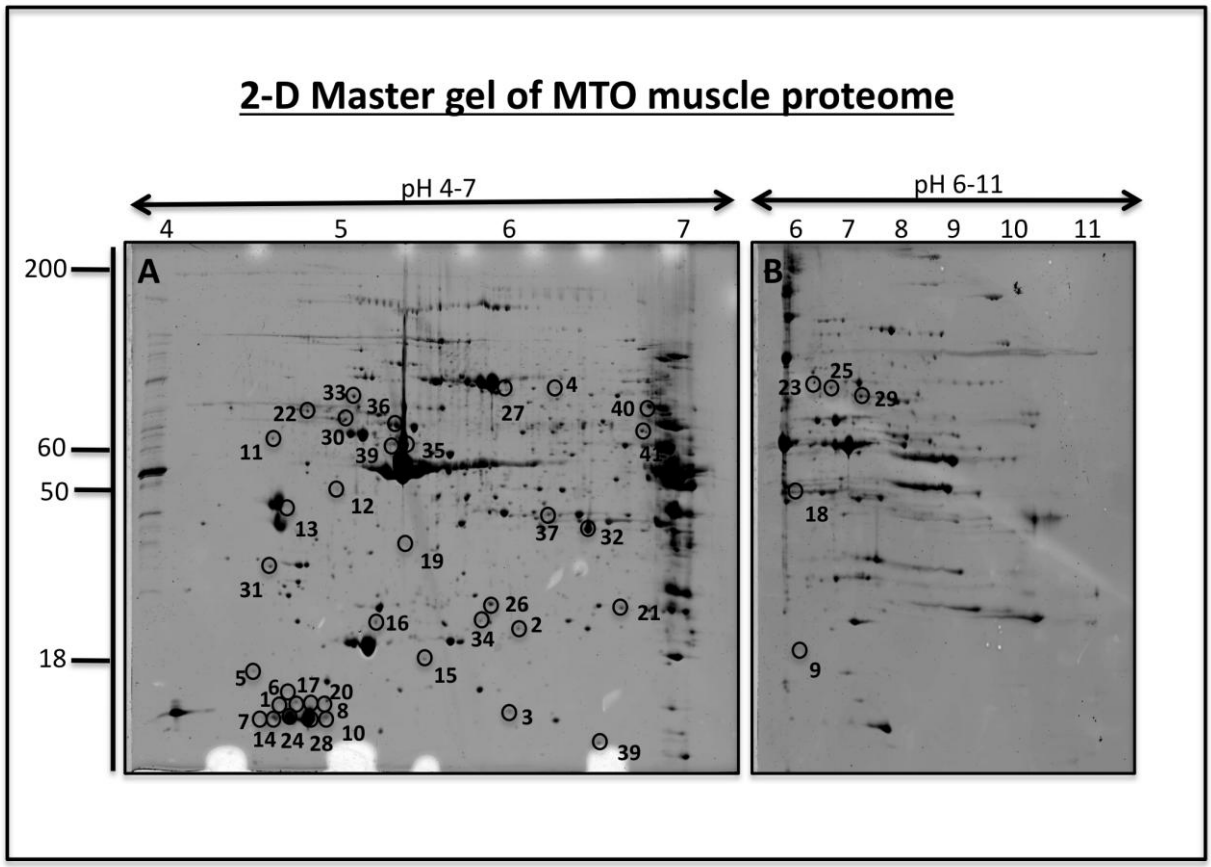

Figure 4.3 2-D master gel of the MTO myotonic muscle proteome

Shown are the 2-D master gels of the myotonic gastrocnemius muscle proteome of the MTO animal model. Proteins were separated in the p*I* ranges of pH4-7 (A) and pH6-11 (B). Proteins with an altered abundance and have been identified by LC/MS are numbered 1-42. A total of 37 proteins with changed abundance were identified in the pH 4-7 (A) range and 5 protein changes were identified in the pH 6-11 (B) range.

Table 4.1 List of identified protein species that exhibit a drastic change in MTO gastrocenmius myotonic muscle versus normal gastrocnemius muscle.

Spot no.	**Name of identified protein**	**Accession no.***	**p*I***	**Molecular mass (kDa)**	**Peptides matched**	**Mascot score****	**Coverage (%)**	**Fold change*****	**Anova**
1	Myosin light chain MLC2f, phosphorylatable, fast muscle	gi|7949078|	4.82	19059	7	129	48	-18.7	2.30E-04
2	DJ-1 protein	gi|55741460|	6.32	20240	14	191	76	-17.7	3.50E-04
3	Heat shock protein beta-7	gi|31542970|	5.95	18681	11	218	78	-17.2	1.00E-03
4	Myosin-binding protein H	gi|56676318|	5.75	53073	10	150	34	-10.6	1.00E-03
5	T complex protein 1	gi|228954|	5.82	60960	16	368	41	-10.3	2.19E-04
6	Myosin light chain MLC2, cardiac/slow	gi|153791853|	4.86	18852	10	113	66	-9.8	2.00E-03
7	Myosin light chain MLC2f, phosphorylatable, fast muscle	gi|7949078|	4.82	19059	7	126	48	-9.8	9.00E-03
8	Myosin light chain MLC2	gi|199985|	4.71	18870	14	216	87	-9.3	5.00E-03
9	Muscle creatine kinase	gi|6671762|	6.58	43250	12	393	34	-8.8	9.00E-03
10	Myosin light chain MLC2f,	gi|7949078|	4.82	19059	9	157	53	-8.0	3.00E-03

	phosphorylatable, fast muscle								
11	Ribonuclease/angiogenin inhibitor 1	gi|31981748|	4.69	51524	6	93	17	-7.8	1.62E-04
12	Glycogenin-1	gi|7305121|	5.06	37610	6	114	24	-6.5	6.08E-04
13	Tropomyosin, beta chain	gi|11875203|	4.66	32933	12	235	34	-6.2	2.00E-03
14	Myosin light chain MLC2f, phosphorylatable, fast muscle	gi|7949078|	4.82	19059	4	49	18	-6.1	2.68E-04
15	Heat shock protein Hsp 2	gi|39850111|	5.16	20425	4	123	34	-5.8	1.40E-02
16	Myosin light chain, MLC3	gi|33563264|	5.03	22523	15	404	77	-5.2	6.00E-03
17	Myosin light chain MLC2f, phosphorylatable, fast muscle	gi|7949078|	4.82	19059	10	182	47	-4.8	8.28E-04
18	Glyceraldehyde-3-phosphate dehydrogenase	gi|55153885|	7.59	36099	9	320	34	-4.5	4.00E-03
19	F-actin-capping protein, subunit beta isoform a	gi|83649737|	5.47	31616	8	142	27	-4.3	2.00E-03
20	Myosin light chain, MLC2	gi|199985|	4.71	18870	17	235	84	-4.2	2.00E-03
21	Triosephosphate isomerase	gi|54855|	6.9	27027	2	62	10	-4.1	1.49E-04

22	Protein disulfide isomerase	gi|129729|	4.79	57514	11	165	26	-3.2	5.00E-03
23	Pyruvate kinase	gi|31981562|	7.18	58388	18	936	39	-2.7	8.00E-03
24	Myosin light chain MLC2f, phosphorylatable, fast muscle	gi|7949078|	4.82	19059	14	236	75	-2.7	1.00E-02
25	Pyruvate kinase	gi|1405933|	7.18	58458	15	787	32	-2.6	6.00E-03
26	Sepiapterin reductase	gi|2498952|	5.58	28213	5	176	24	-2.3	4.00E-03
27	Dihydrolipoamide S-acetyltransferase	gi|16580128|	5.71	59395	18	390	48	1.5	1.00E-02
28	Myosin light chain MLC2f, fast muscle	gi|7949078|	4.82	19059	12	574	77	2.4	3.00E-03
29	UTP-glucose-1-phosphate uridylyltransferase	gi|21314832|	7.18	57118	23	837	54	2.7	6.00E-03
30	Tubulin, beta-3 chain	gi|12963615|	4.82	50850	11	238	31	2.9	4.00E-03
31	14-3-3 Protein gamma	gi|3065929|	4.8	28519	8	231	40	3.1	1.30E-02
32	Malate dehydrogenase, cytosolic	gi|387129|	6.16	36628	15	245	50	3.4	1.84E-05
33	Albumin	gi|899334|	7.82	8825	2	37	30	4.6	3.30E-04
34	Heat shock protein Hsp90-beta	gi|40556608|	4.97	83577	11	188	16	5.2	5.00E-03

35	NADH dehydrogenase (ubiquinone) Fe-S protein 2, mitochondrial	gi|20071222|	6.4	30361	6	211	28	5.5	5.61E-04
36	Actin, alpha	gi|4501881|	5.23	42372	17	209		5.6	1.20E-02
37	Actin, alpha	gi|4501883|	5.23	42388	7	110	19	5.7	1.30E-02
38	Troponin T, TnT fast	gi|2340068|	6.18	30297	3	141	14	6.5	6.00E-03
39	Cofilin-2	gi|6671746|	7.66	18814	6	207	39	9.3	1.40E-02
40	Actg2 protein	gi|29437296|	5.32	22615	8	91	58	16.0	6.00E-03
41	Succinate dehydrogenase	gi|15030102|	7.11	73382	17	306	30	16.6	8.56E-04
42	Phosphoglucomutase 2	gi|33416468|	6.02	63705	25	384	53	17.8	2.00E-03

*NCBInr Database, release 20100212

** The mascot score has a 95% confidence level if >49.

*** Myotonic versus normal muscle tissue

4.2.3 Differential protein expression pattern in myotonic animal model ADR.

Large-scale and high-resolution 2D gel electrophoresis lead to the identification of 51 muscle-associated protein spots with a considerable change in concentration levels in the ADR mouse model of severe myotonia. A representative master gel with electrophoretically separated gastrocnemius muscle proteins is shown for the pH 4-7 and pH 6-11 range in Figure 4.4 A and B respectively. Muscle proteins with a myotonia-related alteration in abundance ranged in molecular mass from apparent 19 kDa (myosin light chain) to 98 kDa (glycogen phosphorylase) and covered a p*I*-range from approximately 4.8 (protein disulfide isomerase) to 9.4 (troponin). The results of the mass spectrometric identification of the 51 protein species are summarized in Table 4.2, which combines data from both pH 4-7 and pH 6-11 gels. The majority of identified proteins were shown to be constituents of the contractile apparatus, major metabolic pathways, the cellular stress response and various cellular signaling mechanisms. A reduced concentration was found for 37 muscle proteins and 13 proteins were shown to be increased in their density. The muscle protein species with the highest fold decrease was identified as the phosphorylatable fast MLC2f isoform of myosin light chain. In addition to the contractile protein MLC2f (spots 1, 12, 14-17, 20), triosephosphate isomerase (spots 2, 3), 40 kDa protein (spot 4), aminoacylase (spots 5, 13), fast troponin TnI-2 (spots 6, 19), alpha-3 chain of tropomyosin (spots 7, 9), alpha and beta subunits of actin (spots 8, 18, 22), troponin TnT (spots 10, 23, 26, 27), beta subunit of trifunctional enzyme (spot 11), otubain (spot 21), aldolase (spot 24), glycogen phosphorylase (spot 25), myosin-binding protein H (spot 28), four-and-a-half-LIM- domains-1 protein (spot 29), kappa-B motif-binding proteins (spot 30), growth factor receptor bound protein 2 (spot 31), isocitrate dehydrogenase (spot 32), prosome (spot 33), carbonic anhydrase (spot 34), haloacid dehalogenase-like hydrolase (spot 35), myosin light chain isoform MLC3 (spot 36) and F-actin capping protein (spot 37) were found to be decreased in myotonic ADR muscle. In contrast, the muscle protein species with the highest fold increase was identified as the enzyme protein disulfide isomerase (spot 51). Other increased muscle proteins were represented by serpin (spot 50), heat shock protein Hsp70 (spot 49), alpha subunit of trifunctional enzyme (spot 48), mitochondrial ATP synthase (spot 47), alpha action (spots 44 and 46), slow MLC1s isoform of myosin light chain (spot 45), albumin (spot 43), cytochrome b-c1 complex (spots 38 and 42), dihydrolipoamide S-acetyltransferase (spot 41), troponin TnI-2f (spot 40) and ATP- specific succinyl-CoA synthetase (spot 39).

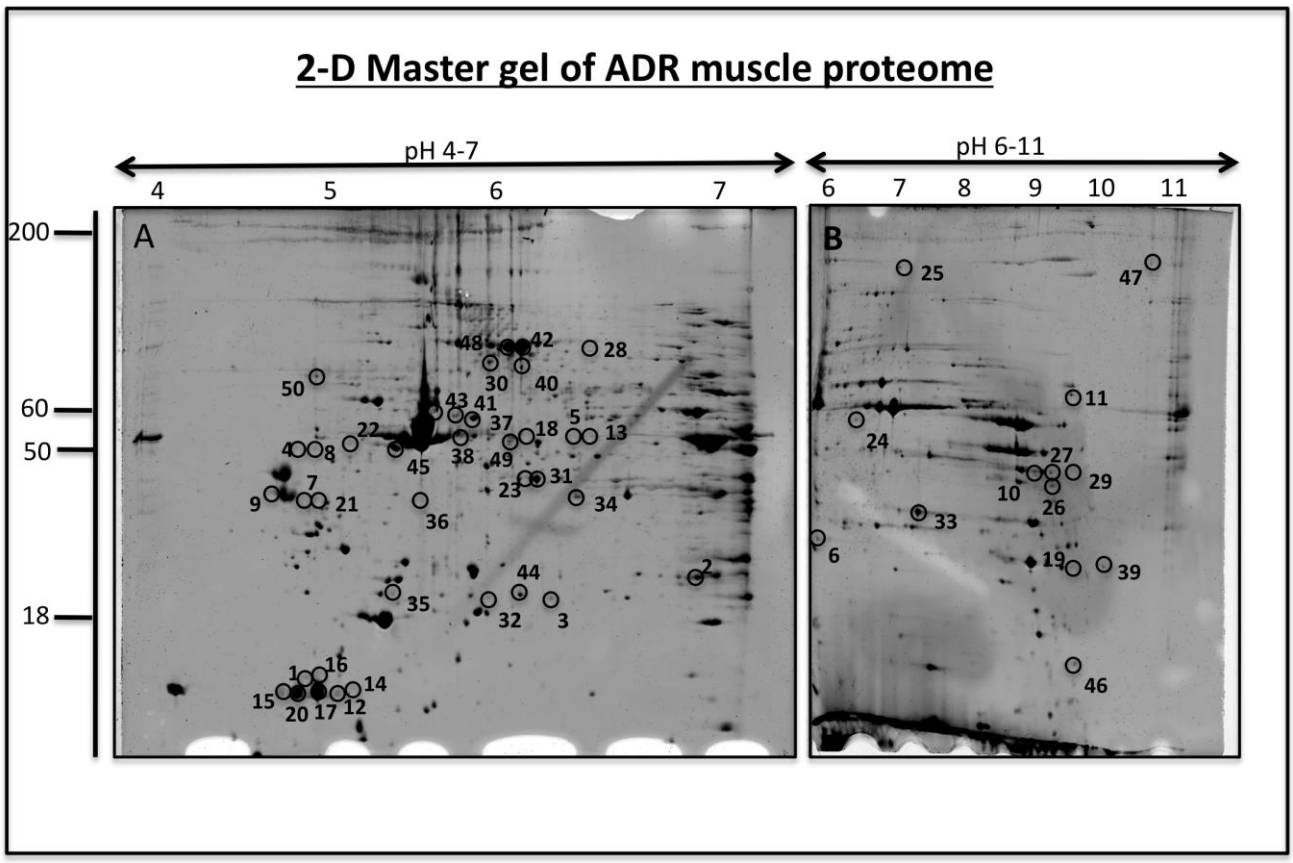

Figure 4.4 2-D Master gel of the ADR myotonic muscle proteome.

Shown is a 2-D master gel of the ADR gastrocnemius muscle proteme separated in the p*I* ranges pH4-7 (A) and pH6-11 (B). Proteins with altered abundance that have been identified by LC/MS are numbered 1-51 and are shown in table 4.2. A total of 38 proteins were identified with changed abundance on the pH 4-7 (A) range and 13 protein changes were identified in the pH 6-11 (B) range.

Table 4.2 List of identified protein species that exhibit a change in abundance in ADR gastrocnemius muscle versus Normal gastrocnemius musce.

Spot no.	**Name of Identified protein**	**Accession no.***	**p*I***	**Molecular mass (kDa)**	**Peptides matched**	**Mascot score****	**Coverage (%)**	**Fold change*****	**Anova**
1	Myosin light chain MLC2f, phosphorylatable, fast muscle	gi|7949078|	4.82	19059	11	206	56	-23	2.42E-06
2	Triosephosphate isomerase	gi|2851390|	6.9	27044	12	310	64	-14.0	8.00E-03
3	Triosephosphate isomerase	gi|1864018|	5.62	22724	9	165	66	-14.0	4.39E-04
4	40 kDa Protein	gi|226005|	4.8	32848	5	119	25	-14.0	7.81E-05
5	Aminoacylase 1	gi|13384746|	5.81	45998	10	121	29	-14.0	3.00E-03
6	Troponin I, fast TnI-2	gi|6678391|	8.65	21518	4	236	17	-14.0	1.36E-05
7	Tropomyosin, alpha-3 chain	gi|20178336|	4.68	32901	18	176	60	-13.0	9.65E-04
8	Actin, beta-like 2	gi|30425250|	5.3	42325	5	55	14	-13.0	3.24E-04
9	Tropomyosin, alpha-3 chain	gi|20178336|	4.68	32901	13	103	29	-13.0	4.00E-03
10	Troponin T	gi|2340048|	9.35	28318	13	500	43	-11.0	3.34E-04
11	Trifunctional enzyme, subunit beta	gi|21704100|	9.43	51353	12	556	24	-10.0	4.00E-03
12	Myosin light chain MLC2f, phosphorylatable, fast muscle	gi|7949078|	4.82	19059	11	174	61	-9.5	6.61E-04

13	Aminoacylase 1	gi|13384746|	5.81	45998	12	134	37	-8.9	2.00E-03
14	Myosin light chain MLC2f, phosphorylatable, fast muscle	gi|29789016|	4.98	20697	12	214	63	-8.3	1.00E-03
15	Myosin light chain MLC2f, phosphorylatable, fast muscle	gi|7949078|	4.82	19059	11	151	56	-8.3	3.00E-03
16	Myosin light chain MLC2f, phosphorylatable, fast muscle	gi|7949078|	4.82	19059	12	221	68	-7.2	2.54E-04
17	Myosin light chain MLC2f, phosphorylatable, fast muscle	gi|7949078|	4.82	19059	12	182	69	-7.1	1.50E-04
18	Actin, alpha	gi|49864|	5.45	38020	9	107	34	-7.1	3.00E-03
19	Troponin I, fast TnI-2	gi|123242975|	8.74	15725	4	134	22	-7.0	1.30E-02
20	Myosin light chain MLC2f, phosphorylatable, fast muscle	gi|7949078|	4.82	19059	13	188	60	-7.0	9.66E-04
21	Otubain 1 (OTU domain, ubiquitin aldehyde binding1)	gi|19527388|	4.85	31482	7	186	29	-6.5	1.40E-02
22	Actin, alpha	gi|49868|	5.78	39451	12	106	34	-6.4	1.77E-04
23	Troponin TnT	gi|3449358|	6.34	29992	2	64	10	-5.9	5.00E-03
24	Aldolase A	gi|151180645|	6.61	45895	12	556	31	-5.9	1.50E-02
25	Glycogen phosphorylase	gi|6755256|	6.65	97689	26	970	34	-5.6	1.00E-02
26	Troponin TnT	gi|2340048|	9.35	28318	13	499	38	-5.5	1.00E-03

27	Troponin TnT	gi|2340050|	9.36	28320	6	227	18	-5.2	5.00E-03
28	Myosin-binding protein H	gi|56676318|	5.75	53073	10	150	34	-5.1	2.00E-03
29	Four and a half LIM domains 1	gi|123122184|	8.83	35056	3	70	10	-4.4	6.00E-03
30	Kappa-B motif-binding phosphoprotein	gi|1083569|	5.19	51300	10	132	26	-4.3	9.00E-03
31	Growth factor receptor bound protein 2	gi|123228035|	6.31	23689	3	35	14	-3.8	5.00E-03
32	Isocitrate dehydrogenase 3	gi|148693873|	6.11	40988	13	318	42	-3.8	1.20E-02
33	Proteasome beta 4 subunit (prosome, macropain)	gi|14198355|	5.47	29229	6	161	30	-3.7	4.00E-03
34	Carbonic anhydrase CA3	gi|31982861|	6.89	29638	11	446	46	-3.1	1.40E-02
35	Haloacid dehalogenase-like hydrolase domain-containing protein 2 isoform 1	gi|21313310|	5.7	28886	6	143	30	-3.0	1.00E-03
36	Myosin light chain, MLC3	gi|33563264|	5.03	22523	6	127	39	-2.9	1.00E-03
37	F-actin-capping protein, subunit beta isoform a	gi|83649737|	5.47	31616	8	82	26	-2.8	8.00E-03
38	Cytochrome b-c1 complex, subunit 1, mitochondrial	gi|14548301|	5.75	53431	14	344	35	2.4	7.00E-03
39	ATP-specific succinyl-CoA	gi|3766201|	5.65	46563	21	273	46	2.4	3.00E-03

	synthetase, beta subunit								
40	Troponin I, TnI-2f	gi|148686202|	9.15	20957	6	314	24	2.8	8.00E-03
41	Dihydrolipoamide S-acetyltransferase	gi|16580128|	5.71	59395	11	157	25	2.8	1.30E-02
42	Cytochrome b-c1 complex, subunit 1	gi|14548301|	5.75	53431	8	136	20	2.9	2.00E-03
43	Albumin	gi|899334|	7.82	8825	4	66	64	3.5	2.00E-03
44	Actin, alpha	gi|33563240|	5.23	42372	13	141	50	3.5	4.18E-06
45	Myosin light chain MLC1s, slow muscle	gi|26986555|	5.41	22851	17	247	77	4.0	1.00E-02
46	Actin, alpha	gi|49864|	5.45	38020	9	152	36	4.7	3.00E-03
47	ATP synthase, mitochondrial	gi|20070412|	10	23407	9	374	53	5.1	3.00E-03
48	Trifunctional enzyme, subunit alpha,mitochondrial	gi|33859811|	9.24	82617	12	596	19	5.3	9.00E-03
49	Heat shock protein Hsp70	gi|14917005|	5.91	73773	23	476	47	6.4	3.37E-06
50	Serpin, B6 isoform	gi|6678097|	5.53	42919	15	279	47	6.5	1.00E-03
51	Protein disulfide isomerase	gi|129729|	4.79	57514	12	142	25	13.6	6.00E-03

*NCBInr Database, release 20100212

** The mascot score has a 95% confidence level if >49.

*** Myotonic versus normal muscle tissue

4.2.4 Immunoblot analysis of potential biomarkers of myotonia in animal models MTO and ADR

In order to verify key findings from our proteomic data of myotonic muscle four proteins with changed abundance were investigated by immunoblotting. Shown in Figure 4.10 anibodies directed against alpha dystroglycan in MTO and ADR muscle versus control muscle showed no significant differences and shows all lanes were equally loaded. As illustrated in Figure 4.5 slow MLC2 isoform and MLC phosphorylatable were greatly reduced in MTO and ADR muscle tissue. The statistical significant differences Figure 4.5 (E,F,G and H) correlated well with our proteomic data listed in Table 4.1 and 4.2. Thus there is a reduced abundance of these contractile elements in severely myotonic muscle. The immunoblotting of tropomyosin shown in Figure 4.6 (A ,B) confirms a reduction in myotonic muscle. Similarly in Figure 4.6 (C,D) shows a decrease in the abundance of the glycolytic enzyme triosephosphate isomerase. This reduction was also seen in the MTO*5J model with the more severe myotonic muscle ADR and MTO showing a greater reduction. As with our MTO*5J model immunoblotting of fiber-specific markers was carried out on both MTO and ADR muscle tissue as shown in Figure 4.7 and Figure 4.8. The decreased abundance of fast isoforms of MHC and increase in slow isoforms of MHC shown in Figure 4.7. Similarly the increased abundance of the slow isoform SERCA2 Figure 4.8 correlates with previously published work suggesting a glycolytic-to-oxidative transformation process.

Figure 4.9 (C) and (D) shows a drastic reduction of parvalbumin in MTO and ADR gastrocnemius muscle respectively. This agrees with previously published work carried out by Jockusch and co workers (1988). An increase in myoglobin is also shown in Figure 4.9 (A) and (B) for MTO and ADR respectively.

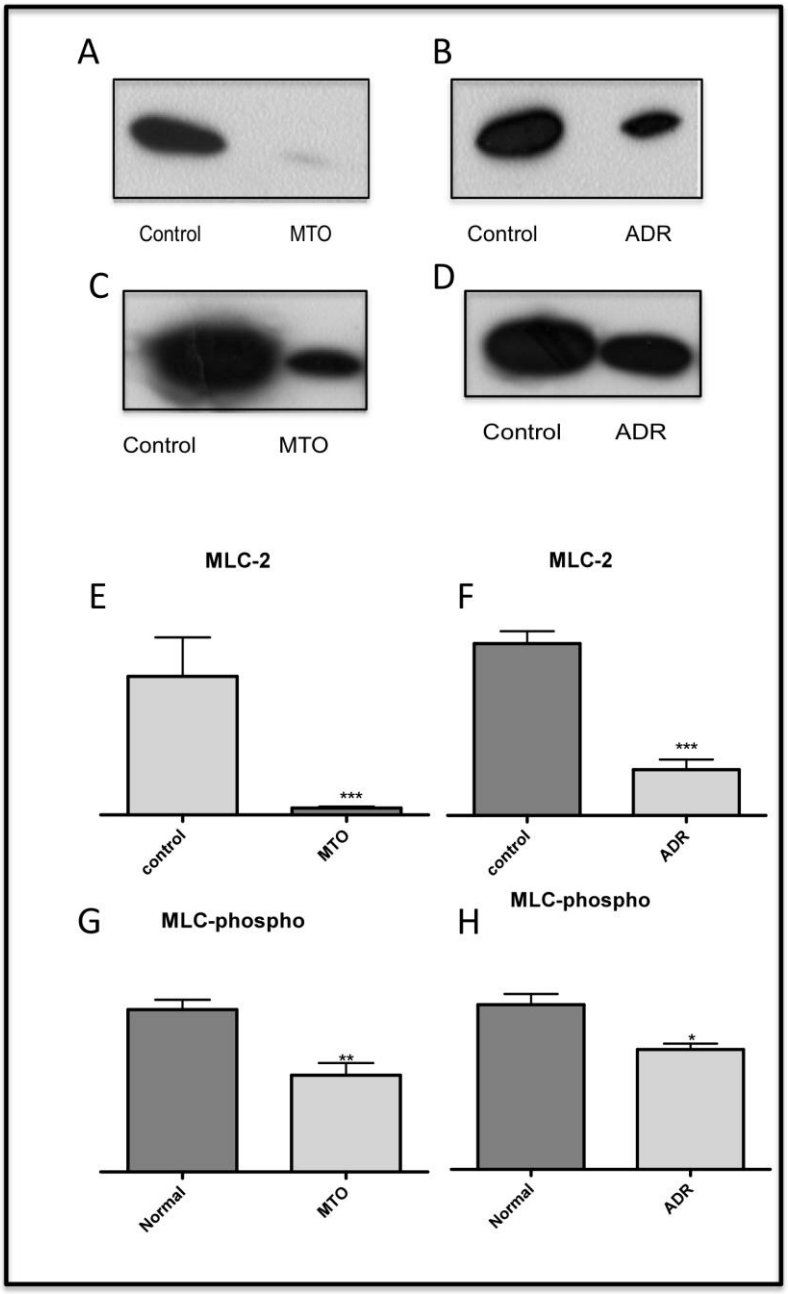

Figure 4.5 1-D immunoblot analysis of MLC2 and MLC-phospho 20 in myotonic muscle
Shown is the immuno-decorated nitrocellulose bands. Antibodies were directed against MLC2 in MTO muscle (A) and ADR muscle (B), and against MLC-phospho 20 in MTO muscle (C) and ADR muscle (D). The comparative immunoblotting with MTO muscle and ADR muscle versus normal was statistically evaluated using unpaired Student's t-test (n=4;*p<0.05,**p<0.01,***p,0.001) and is graphically shown in panels (E) and (F) for MLC2 and (G) and (H) for MLC-phospho 20.

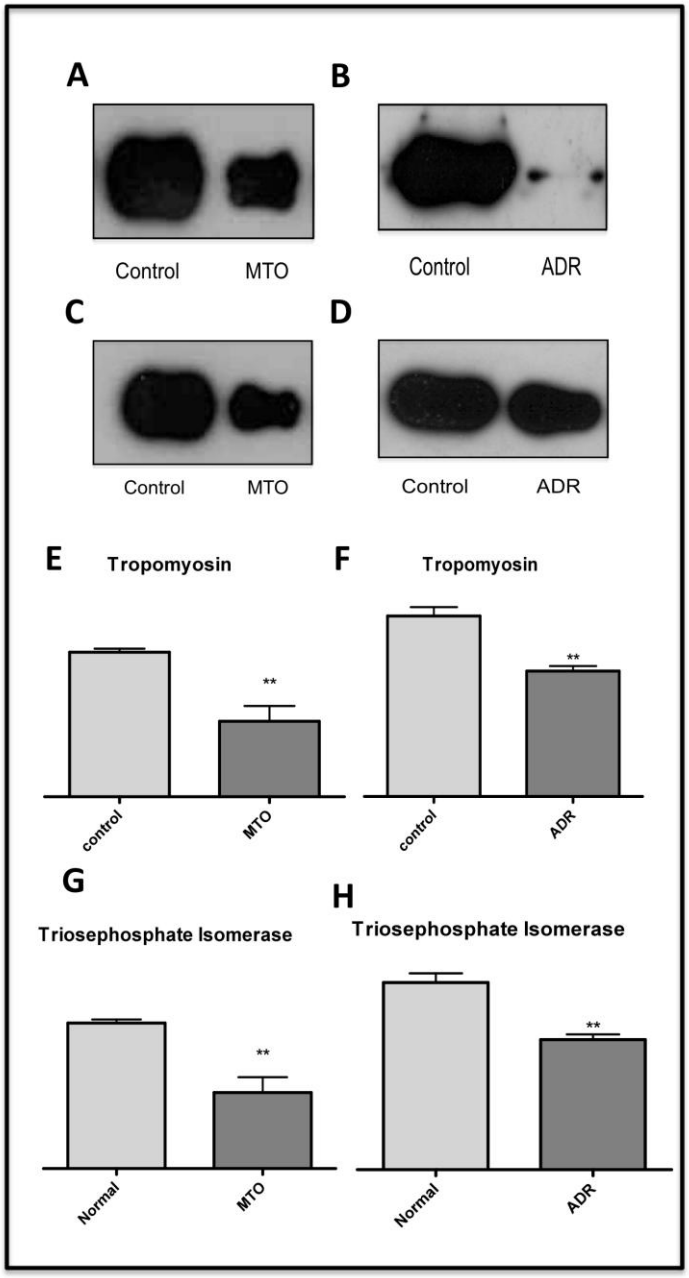

Figure 4.6 1-D immunoblot analysis of Tropomyosin and triosephosphate isomerase in myotonic muscle

Shown is the immuno-decorated nitrocellulose bands. Antibodies were directed against tropomyosin in MTO muscle (A) and ADR muscle (B), and against triosephosphate isomerase in MTO muscle (E) and ADR muscle (F). The comparative immunoblotting with MTO muscle and ADR muscle versus normal was statistically evaluated using unpaired Student's t-test (n=4;*p<0.05,**p<0.01,***p,0.001) and is graphically shown in panels (C) and (D) for tropomyosin and (G) and (H) for triosephosphate isomerase.

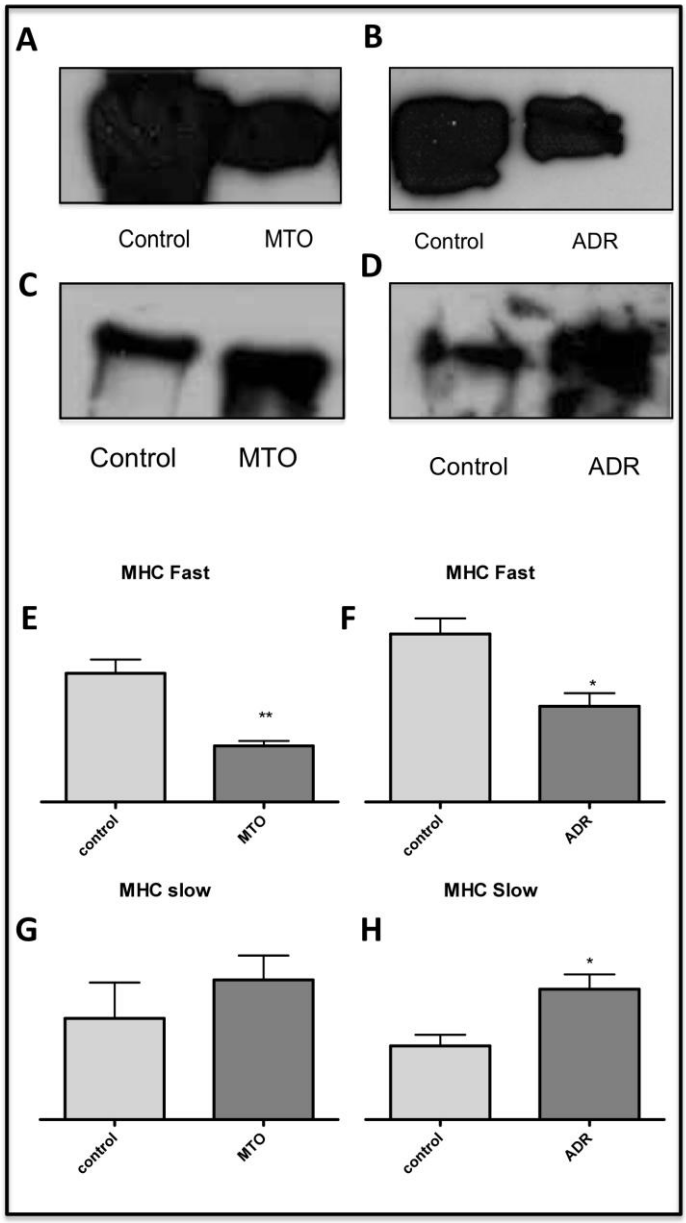

Figure 4.7 1-D immunoblot analysis of MHC fast and MHC slow in both MTO myotonic muscle and ADR myotonic muscle

Shown is the immuno-decoration of nitrocellulose bands. Antibodies were directed against MHC fast in MTO muscle (A) and in ADR muscle (B), MHC slow in MTO muscle (C) and ADR muscle (D). Comparative immunoblotting of myotonic muscle versus normal muscle was statistically evaluated using an unpaired Student's t-test ($n=4$,$^{*}p<0.05$,$^{**}p<0.01$) and is grapically shown in panels (E) and (F) for MHC fast MTO and ADR respectively, panels (G) and (H) for MHC slow MTO and ADR respectively.

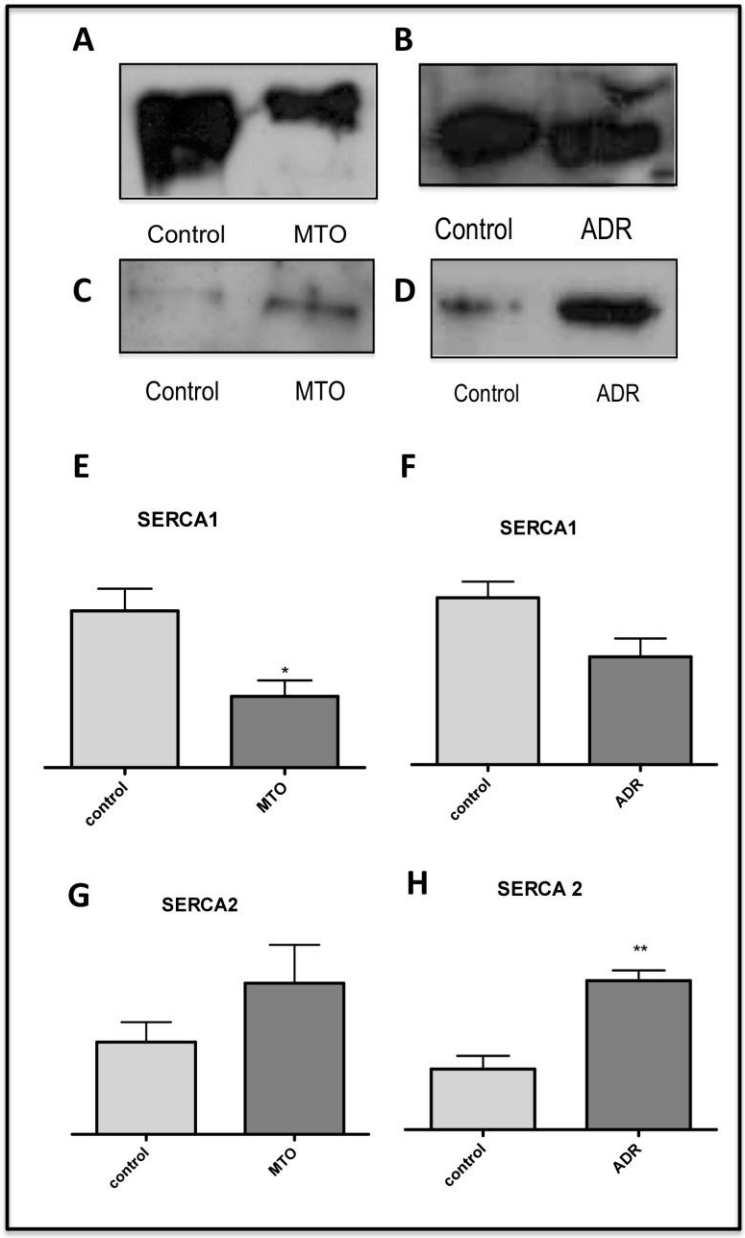

Figure 4.8 1-D immunoblot analysis of SERCA 1 and SERCA 2 in both MTO myotonic muscle and ADR myotonic muscle

Shown is the immuno-decoration of nitrocellulose bands. Antibodies were directed against SERCA 1 in MTO muscle (A) and in ADR muscle (B), SERCA 2 in MTO muscle (C) and ADR muscle (D). Comparative immunoblotting of myotonic muscle versus normal muscle was statistically evaluated using an unpaired Student's t-test ($n=4$,$^{*}p<0.05$,$^{**}p<0.01$) and is grapically shown in panels (E) and (F) for SERCA 1 MTO and ADR respectively, panels (G) and (H) for SERCA 2 MTO and ADR respectively.

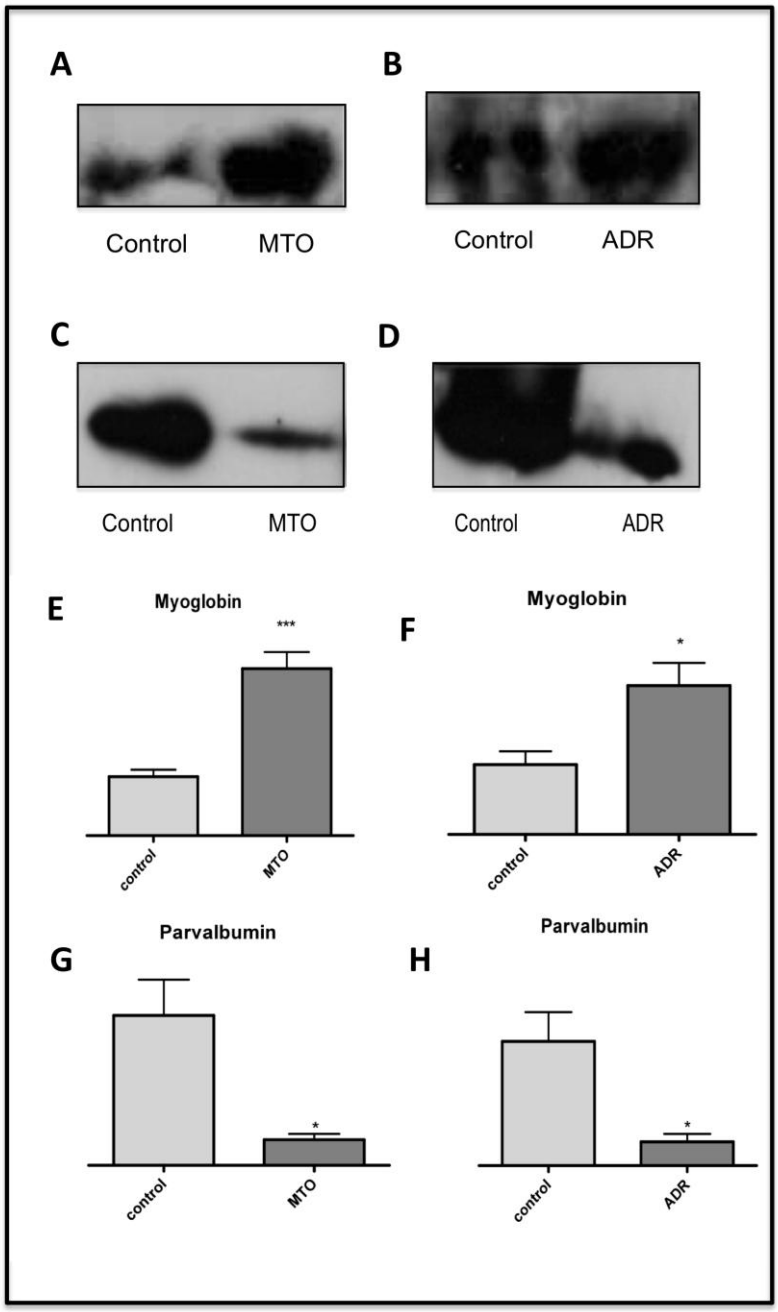

Figure 4.9 1-D Immunoblot analysis of myoglobin and parvalbumin in myotonic muscle MTO and ADR

Shown is the immuno-decorated nitrocellulose bands of 1-D gels from MTO and ADR muscle tissue. Antibodies directed against myoglobin in MTO tissue (A) and ADR tissue (B) and parvalbumin in MTO tissue (G) and ADR tissue (H). Comparative immunoblotting with MTO and ADR tissue versus normal tissue was statistically evaluated using an unpaired Student's t-test (n=4, $p<0.05$,**$p<0.01$) shown in panels for myoglobin (E) and (F) for MTO and ADR respectively and parvalbumin (G) and (H) for MTO and ADR respectively.

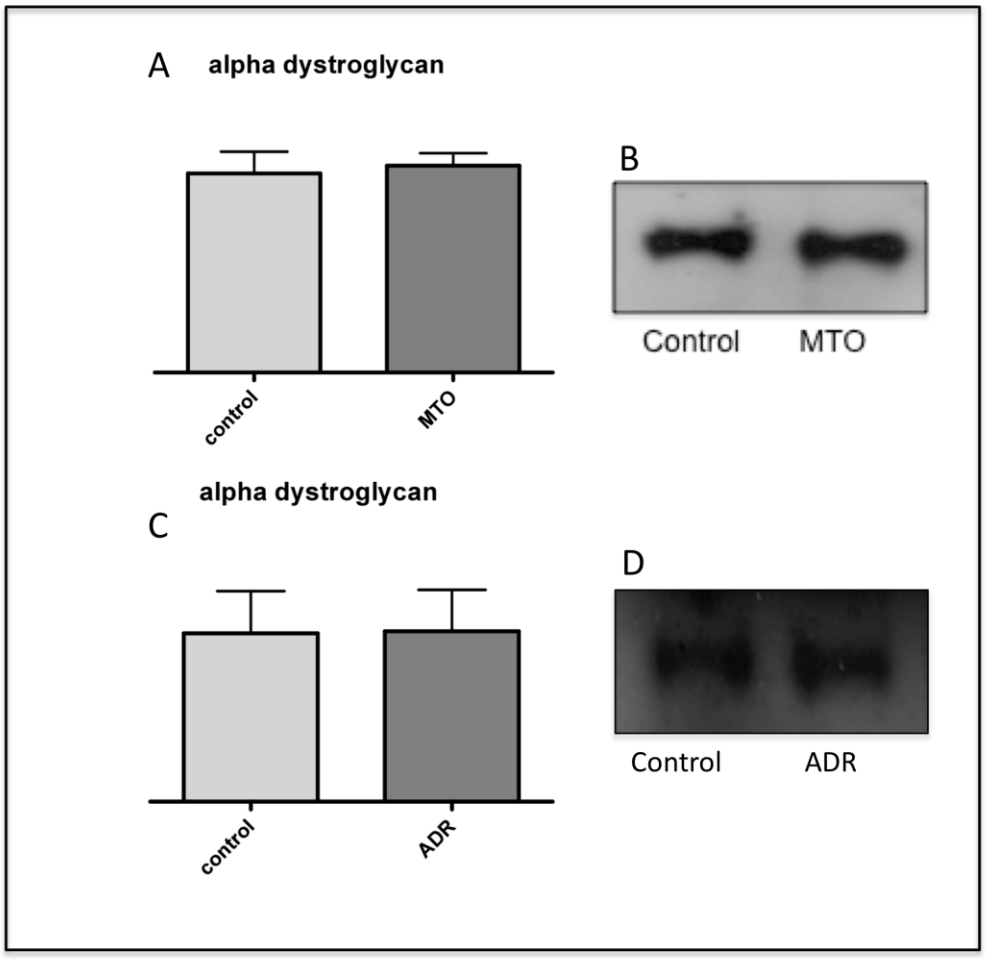

Figure 4.10 1-D immunoblot analysis of alpha dystroglycan in myotonic muscle

Shown is the immuno-decorated nitrocellulose bands. Antibodies were directed against alpha dystroglycan in MTO (B) and ADR muscle (D). Comparative immunoblotting of myotonic muscle versus control muscle was statistically evaluated using an unpaired Student's t-test (n=4) and is graphically shown in panels (A) and (C) for MTO and ADR respectively.

4.3 Discussion

Skeletal muscles from the ADR and MTO phenotype appear to be associated with considerable myotonia-related changes in proteins involved in the excitation-contraction-relaxation cycle, energy metabolism, ion handling, cellular stress response and cellular signaling. An interesting feature in both animal models was the drastic decrease in almost all subspecies of the phosphorylatable fast MLC2f isoform of the myosin light chain that agrees with previous studies of the ADR mouse (Stuhlfauth et al. 1984, Jockusch, et al.1988, Kluxen et al. 1988).

4.3.1 Contractile Apparatus

Previous proteomic studies have shown that isoform changes in myosin light chains represent reliable markers of muscle transformation (Ohlendieck 2010). Chronic low-frequency stimulation of fast rabbit muscle triggers a significant decrease in various MLCf molecules and an increase in slower counterparts (Donoghue et al. 2007). A drastic increase of slow myosin light chain MLC2s was observed in aging rat skeletal muscle, which is indicative of an increased slow fiber population in sarcopenia of old age (Gannon et al. 2009). The reduced density of MLC2 isoforms was seen in both MTO and ADR muscle preparations. In MTO muscle MLC2 phosphorylatable (spot 1,12,15,16,17,20, Table 4.1) was found to have decreased abundances ranging from a 23fold decrease to 7.0 fold. Similarly in ADR muscle preparations MLC2 phosphorylatable (spot 1,7,10,17,28, Table 4.2) was found to have decreased abundances ranging from 18.7 fold to 4.8 fold. A decrease was also seen in MLC2 in ADR muscle (spot 6,8,14,20,24, Table 4.2) ranging from 9.8-fold decrease to 2.7 fold decrease. A similar decrease was seen in MLC3 in ADR and also MTO muscle. MLC3 (spot 14,36, Table 4.1) had decreased abundances of 8.3 and 2.9 respectively in MTO muscle. MLC3 (spot 16, Table 4.2) was found to have a 5.2 fold decrease in ADR muscle. The reduced density of MLC isoforms in ADR and MTO muscle preparations strongly suggests a partial fast-to-slow transition process in myotonia. This transition is further suggested by the immunoblotting of MHC fast and slow isoforms in ADR and MTO muscle preparations shown in Figure 4.7. In addition, this finding confirms the idea that enhanced neuromuscular activity regulates the abundance of this contractile protein (Jockusch et al.1988).

An 8.8 fold decrease in creatine kinase (spot 9, Table 4.1) was seen in MTO muscle preparations. Creatine kinase catalyses the reversible conversion of creatine + MgATP to creatine phosphate + Mg ADP, this reaction can replenish ATP from pools of creatine

phosphate (Ennor et al. 1954). Myosin ATPase preferentially uses ATP supplied by creatine kinase, therefore production of ATP by creatine kinase potentially plays an important role in skeletal muscle contraction (Bessman et al. 1980). The decrease in creatine kinase could have an effect on muscle contraction or could be a consequence of a change in fiber population to a slower oxidative metabolism, as slow type fibers have less creatine kinase (Wallimann et al. 1984).

Both MTO and ADR muscle showed altered abundances of elements of the troponin complex. Both troponin I (spot 6,19,40, Table 4.2) and troponin T (spot 10,26,27,23, Table 4.2) had reduced densities in ADR muscle preparations. MTO muscle preparations had a 10.3 fold decrease in troponin I (spot 5, Table 4.1) but a 6.5 fold increase in troponin T (spot 38, Table 4.1). This conflicting result of troponin T may be an anomaly or an artifact from the lysis process. Tropomyosin the actin binding protein that mediates Ca^{2+} regulation of actomyosin contraction (Nagai et al. 2001), was decreased in both ADR (spot 7,9, Table 4.2) and MTO (spot 13, Table 4.1). The decrease in the structural protein myosin binding protein H in both ADR (spot 28, Table 4.2) and MTO (spot 4, Table 4.1) is also seen. This protein is involved in the interaction with the thick filaments in the A band of the sarcomere. A decrease in actin-capping protein was seen in both ADR (spot 37, Table 4.2) and MTO (spot 19, Table 4.1). This protein regulates the growth of the actin filament by capping the barbed end of growing actin filaments. These findings correlate with previous studies on the contractile properties of myotonic muscle (VanLunteren et al. 2006). VanLunteren and co-workers carried out analysis on diaphragm muscle from ADR mice. This study found CLC-1 deficient diaphragm had impaired isometric force generation compared to wild type. Similarly in MTO mice Entrikin and colleagues (1987) found reduced peak isometric tension in portion to the reduction in muscle weight. Reductions in contractile proteins could contribute to a decrease in force generation during muscle contraction in gastrocnemius muscle in both ADR and MTO muscle.

4.3.2 Muscle transformation

The shift of myosin isoforms as a result of myotonia can be seen in Figure 4.7. The decrease in MHCf in myotonic muscle is coupled with an increase in the expression of the MHCs subunit. A similar differential isoform expression pattern of the Ca^{2+} pump SERCA can be seen in Figure 4.8. Immunodecoration of SERCA isoforms in myotonic muscle show a decrease in the fast SERCA1 isoforms and an increase in the slow SERCA2 isoform. These results correlate well with the idea of muscle transformation from fast-to-slow in myotonic muscle.

4.3.3 Energy metabolism

This proteomic study of myotonic muscle has shown changes in many metabolic enzymes. Albumin is a major plasma protein that is responsible for the extracellular transport of fatty acids, amino-acid storage and osmotic pressure maintenance (Ellmerer et al. 2000). The upregulation of albumin in both ADR (spot 43, Table4.2) and MTO (spot 33, Table4.1) muscle preparations may be due to increased expression or the possible higher capacity of albumin storage by the transformed fibers. The optimum utilization and transportation of free fatty acids seem to be important factors in the aerobic metabolic potential of slower contracting fibers (Kaufmann et al. 1989). In the case of the trifunctional enzyme its beta subunit (spot 11, Table 4.2) was reduced and its alpha subunit increased (spot 48, Table 4.2) in ADR muscle preparations. Similar increases in oxidative phosphorylation enzymes were seen in both ADR and MTO muscle preparations. They can be seen in Table 4.2 and include cytochrome C in ADR muscle (spot 38), ATP succinyl-CoA (spot 39) and ATP synthase (spot 47). Increases in MTO muscle preparations of oxidative phosphorylation enzymes are shown in Table 4.1 and included NADH dehydrogenase (spot 35) and SHDA (spot 41) both are enzymes functioning in oxidative phosphorylation in the mitochondrion. The above changes in myotonic muscle suggest an increase in mitochondrial enzyme activity and a shift to more oxidative metabolic pathway indicative of slower twitching fiber population.

4.3.4 Stress response

The expression of heat shock proteins Hsp70 in ADR (spot 49, Table 4.2) increased 6.4 fold and Hsp90 in MTO (spot 34) by 5.2 fold. Increases in heat shock proteins indicate the response of myotonic muscle to cellular stress. Hsp90 and Hsp 70 act as chaperones during protein unfolding and denaturation by nonphysiological events. Harris and co-workers (2008) found an increase in Hsp90 in soleus muscle after exercise. Similarly Neufer and colleagues (1996) found CLFS of rabbit tibialis anterior resulted in significantly elevated levels of Hsp70. It is also interesting to note that Neufer and co-workers (1996) saw an increase expression of Hsp70 in muscles rich in type 1 fibers. This increase was also accompanied by an increase in Hsp60 in type 1 fibers which is interesting as Hsp60 was found to be increased in MTO*5j muscle preparations. Changes in expression of stress proteins could aid in the remolding process evoked by the sustained contractile activity in myotonic muscle. Hsp 2 (spot 15) and Hsp7 (spot 3) shown in Table 4.1 were both decreased in MTO muscle. Similarly, in ADR 40kDa protein (Hsp40) (spot 4, Table 4.2) was increased in ADR muscle. This increase in heat shock proteins indicates that fiber modifications probably depend heavily on the chaperone function of heat shock proteins.

4.3.5 Other proteins

In addition to the above-discussed alterations in common fiber type-specific markers, many other interesting changes in distinct protein species occurred in the myotonic animal models. The actin binding protein cofilin-2 (spot 39, Table 4.1) was found to be increased 9.3 fold in MTO muscle preparations. Cofilin-2 plays an important role in actin filament dynamics (Ono et al. 1994). This muscle specific isoform is thought to be important for growth of myofibrils in developing and regenerating muscle cells (Thirion et al. 2001, Nakashima et al. 2005). Donoghue and colleagues (2007) investigated muscle adaptation process in response to enhanced neuromuscular activity and found a similar increase of cofilin-2 in stimulated tibialis anterior muscle. The upregulation in cofilin-2 in myotonic transforming fibers could be in response to remodeling of contractile apparatus towards slower twitch properties.

DJ-1 (spot 2, Table 4.1) is decreased drastically in MTO muscle. DJ-1 migrates to mitochondrion during oxidative stress due to actions of chaperones. It is an atypical peroxiredon that protects cells from cell death due to oxidative stress (Chen et al. 2010). An impaired stress response could lead to a detrimental aggregation of misfolded proteins and oxidative damage resulting in dysfunction and muscle weakness seen in myotonic muscle.

Four and a half LIM domain 1 (FHL1) (spot 29, Table 4.2) is characterized by the presence of four and a half highly conserved LIM domains. The LIM domain is a protein-interaction motif and is involved in linking proteins with both actin cytoskeleton and transcriptional machinery (Shathasivam et al. 2010). Today 27 mutations of the gene encoding FHL1 have been recorded and result in at least six different X-linked myopathies (Shathasivam et al. 2010) indicating FHL1 protein is required for normal muscle function.

The reduced density of carbonic anhydrase isoform CA3 (spot 34, Table 4.2) in ADR muscle could be interpreted as a potential impairment of the CO_2-removal mechanism in myotonia. Carbonic anhydrase converts CO_2 into carbonic acid (Geers et al. 2000), therefore its lower expression levels may trigger a reduced availability of this essential hydration reaction that may result in harmful levels of CO_2 in myotonic fibers.

The enzyme disulfide isomerase was found to be increased in ADR muscle, but decreased in MTO. This thiol-disulfide oxidoreductase of the sarcoplasmic reticulum catalyzes the exchange of a disulfide bond with substrates thereby facilitating correct protein folding. The alternate changes in density in ADR and MTO muscle could be potentially used as a differentiating marker of these two different myotonic phenotypes.

4.3.6 Overview of alterations in ADR *vs.* MTO *vs.* MTO*5J

The graphical presentation of Figure 4.11 and Table 4.3 gives an overview of major changes in distinct classes of protein in hyperexcitable muscle tissues as revealed by mass-spectrometry-based proteomics. A striking feature in all animal models was the drastic decreased in a number of subspecies of phosphorylatable fast MLC2f isoform of myosin light chain. Our table shows this reduction along with the metabolic trend of a glycolytic-to-oxidative transformation as well as an increased cellular stress response in hyperexcitable muscles. The direct comparison of the 3 mutants also shows that the concentration changes in proteins are more pronounced in the serve MTO and ADR phentotypes as compared to the milder MTO*5J phenotype.

Table 4.3 List of protein species that exhibit a change in abundance in ADR, MTO and MTO*5J muscle.

Name of Identified Protein	**ADR Fold Change**	**MTO Fold Change**	**MTO*5J Fold Change**
Myosin Light Chain MLC2f, phosphorylatable, fast muscle	-23, -9.5, -8.3, -8.3, -7.2, -7.1, -7.0	-18.7, -9.8, -8.0, -6.1, -4.8, -2.7,	-3.6,
T complex protein 1	-14.0	-10.3	-3.6
Triosephosphate Isomerase	-14.8, -3.8	-4.1	3.7
Troponin T fast skeletal muscle	-5.2, -5.5	8.5, 6.5	6.0
NADH dehydrogenase		5.5	2.9
ATP synthase, mitochondrial	5.1		3.0
Albumin	3.5	4.6	
F-actin capping protein	-2.8	-4.3	
Hsp 27			2.9
Hsp 90		5.2	
Hsp 70	6.4		

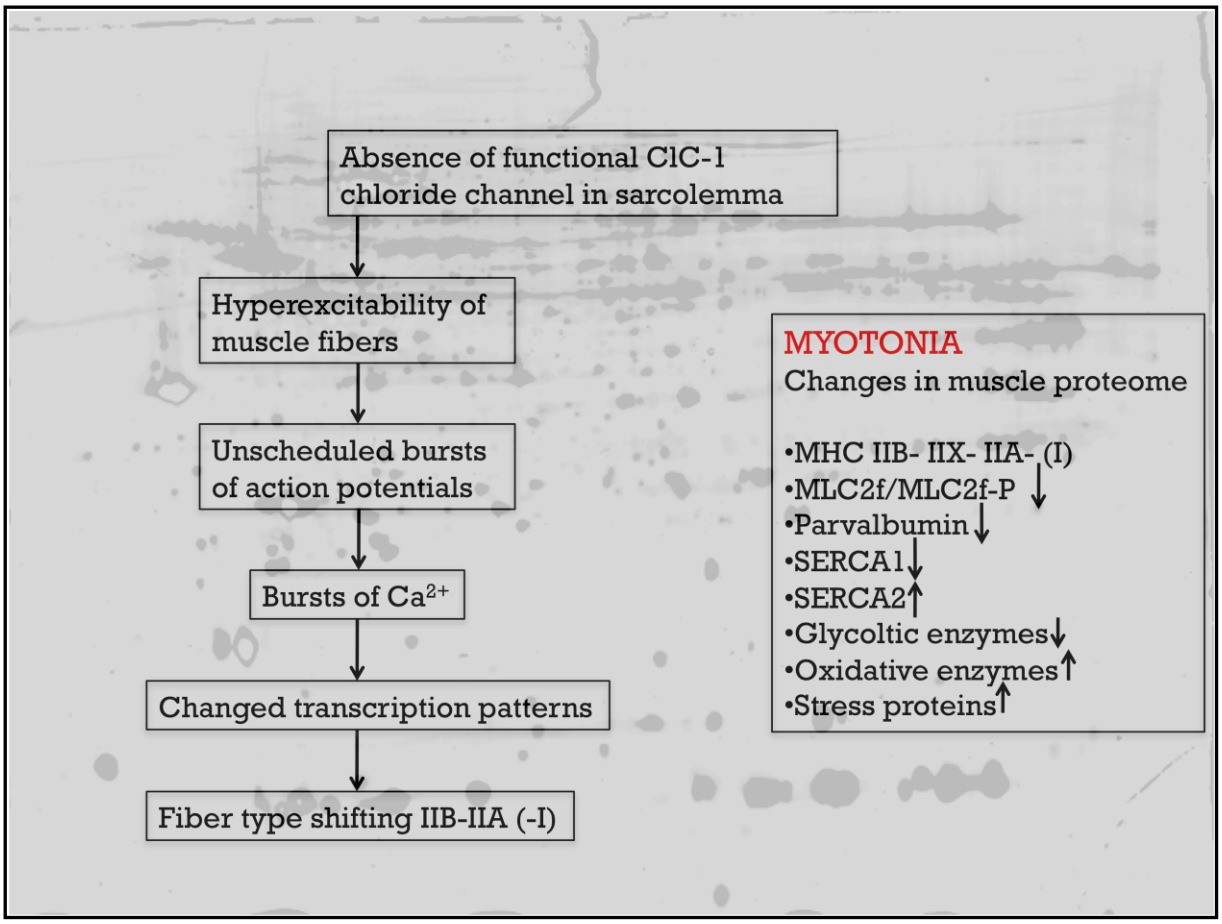

Figure 4.11 Overview of changes in myotonic muscle

A single nucleotide replacement or other event at the DNA level in the *Clc1* gene is sufficient to cause loss of function of the muscular chloride channel CIC-1. In mammalian muscle, CIC-1 is expressed in the sarcolemma of mature muscle, and is required for normal muscle function. Loss of function CIC-1 leads to hyperexcitability of the muscle fiber. Unscheduled bursts of action potentials cause a burst of intracellular Ca^{2+} activities e.g. Ca^{2+}-dependent signaling pathways. In myotonic muscle this results in a change in transcription patterns leading to a fiber shift from fast glycolytic (Type IIB) to fast oxidative (Type IIA) and even to slow (Type I). This fiber type shift is also mirrored at the metabolic level by increases in oxidative enzymes and reduction in glycolytic enzymes. Presumably due to cramps and imbalance of gene expression, there is a considerable cellular stress response in myotonic muscle fibers.

4.5 Conclusion

Myotonia appears to trigger considerable changes in many elements of the contractile apparatus, cellular processes and muscle energy metabolism. Our proteomic finding has shown that a single mutation in a muscle-specific gene that triggers hyperexcitability of the sarcolemma has severe downstream effects on the expression levels of a very large number of genes in contractile tissues. Comparing results from this study with results from chapter 3 indicates that the milder disease progression in the MTO*5J mouse is associated with less pronounced downstream effects on the global muscle proteome complement.

5. DIGE analysis of skeletal muscle affected by motor neuron degeneration

5.1 Introduction

Motor neuron diseases are a heterogeneous group of fatal neurological diseases (Wood-Allum and Shaw 2010). They include spinal muscular atrophy, spinal bulbar muscular atrophy and amyotrophic lateral sclerosis (ALS). Spinal muscular atrophy is an autosomal recessive disorder caused by a mutation in the survival motor neuron SMN1 gene and is characterized by low motor neuron degeneration. Spinal bulbar muscular atrophy is triggered by expansion of a polyglutamine tract in androgen receptor gene and is characterized by slowly progressive motor neuron degeneration with adult-onset. ALS can be sporadic or caused by a genetic mutation. It is the most progressive and frequent form of adult-onset motor neuron disease (Wijesekera and Leigh 2009). ALS is shown to be due to genetic abnormalities in the Cu/Zn superoxide dismutase 1 gene and also the TDP-43 encoding TARDBP gene (Wijesekera and Leigh 2009).

The degeneration of motor neurons leads to weakness of contractile limb, bulbar and respiratory tract. Patients with ALS experience highly progressive paralysis that is usually fatal due to respiratory failure within 2-3 years after bulbar onset or 3-5years after limb onset cases. Today, only one drug has regulatory approval for the treatment of ALS and is called glutamate antagonist riluzole. It prolongs survival time in the treatment of ALS but only by 3-4 months (Miller et al. 2007). This is due to very poor prognosis of patients with ALS. In order to improve prognosis and treatment of ALS it is important that detailed biomedical investigations into its pathogenesis is carried out along with searches for new therapeutic targets.

The wobbler mouse (allele wr) is a recessive mutation mapped to chromosome 11 on the mouse genome and is caused by a mutation in the ubiquitously expressed gene Vps54 (Kaupmann et al. 1992). The gene Vsp54 encodes the vesicular protein sorting factor vps54, which is a component of the GARP complex. The GARP complex is involved in retrograde vesicle transport to the golgi apparatus and plays a crucial role in intracellular transport. Studies where Vsp54 expression was knocked out in mice resulted in embryonic lethality (Schmitt-John et al.2005). The wobbler mouse has rapid disease progression and is an established animal model of human motor neuron disease. It is characterized by cellular abnormalities including muscular atrophy and is a highly valuable model for many aspects of motor degeneration including neuroinflammatory processes.

In this study we have used here fluorescence difference in-gel electrophoresis to analyze global changes in the skeletal muscle proteome from WR versus normal mice.

5.1.2 DIGE

DIGE is a 2-D gel elctrophoresis technique that uses ester cyanine dyes to label proteins before 2-D gel electrophoresis. Today there are three cyanine dyes available comerically; Cy3 (propyl-Cy3 N-hydroxysuccinimide (NHS) ester cyanine), Cy5 (methyl-Cy5 NHS ester cyanine) and Cy2. In this study we have used Cy3 and Cy5. The ester cyanine dyes form a covalent bond with the primary amine of the amino acid lysine and results in an amide linkage between the dye and the protein. Both Cy3 and Cy5 have the same molecular mass and reactive group but different excitation emission spectra (Unlu et al. 1997). The advantage of using these dyes is that they are charge matched to lysine and so ensure negliable shift in pI during the first dimension. They can also detect a minimum of 0.25 ng of protein and can linearly detect protein over greater than 10,000 fold change (Tonge et al. 2001). Another feature of DIGE is the inclusion of an internal pooled standard. The pooled standard is the combination of equal amounts of protein from all samples in the experiment. In this study we used Cy5 as our pooled standard and Cy3 for our individual samples. This means on each strip and then gel an internal pool standard is run along with either a diseased or control sample. As all test samples are labelled with the same dye any dye bias is eliminated. Also as unique excitation and emission spectra are required for both dyes two images are obtained per gel; the internal standard and control/diseased sample. Analysis using Progenesis Same Spot software version 3.2.3 from NonLinear Dynamics (Newcastle Upon Tyne, UK)samples are normalised by comparing samples to pooled standard generating a ratio of spot volume pool:sample. This ratio can then be compared across all gels eliminating technical variation between gels and also reducing the number of gels to be run in the experiment.

5.3 Results

5.3.1 DIGE experimental design

Proteins were separated on a 24cm strip in the pH range of pH3-10. A 50 mg protein sample was fluorescently labelled for each of the protein samples being studied. Normal (n=4)muscle extracts and WR (n=4) muscle extracts were each labelled with Cy3 DIGE Fluor dye and the pooled internal standard with Cy5 DIGE Fluor dye. The 2D-GE separation of fluorescently labelled proteins was carried out by using a total of 100 mg protein per DIGE gel. Two images were obtained from each gel and can be seen in Figure 5.1. Following DIGE analysis analytical gels were then performed to obtain protein samples for mass spectrometric analysis. Figure 5.2 shows a RuBPs stained analytical gel that was used for spot picking for mass spectrometry analysis.

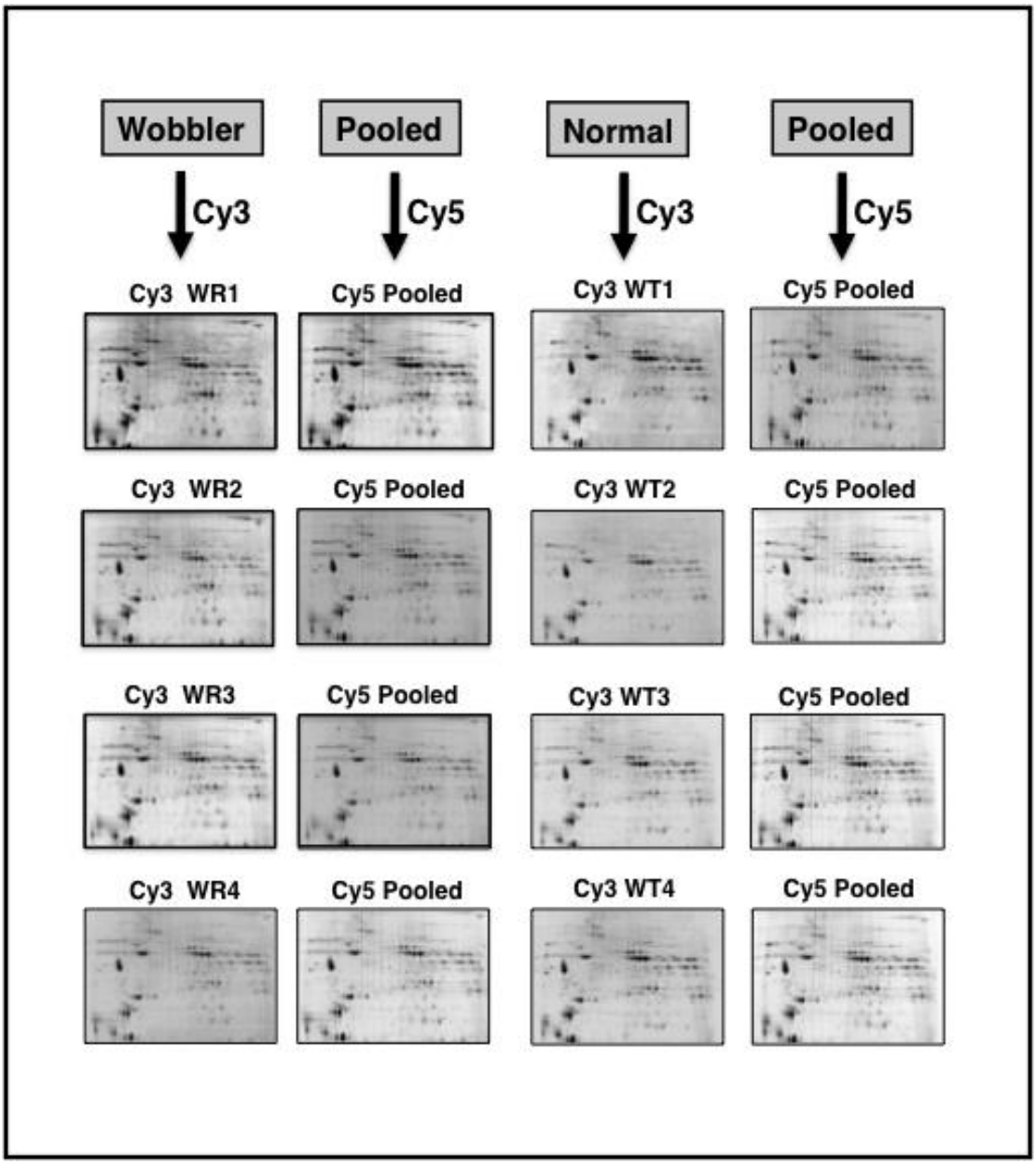

Figure 5.1 2-D gel elctrophoric analysis of wobbler versus control skeletal tissue

Shown is the 2-D DIGE analysis of wobbler versus normal skeletal muscle. Shown are Cy3-labelled gels of total muscle extracts from wobbler (WR1 to WR4) versus normal wild type (WT1 to WT4) mice, as well as Cy5-labelled gels containing pooled standards. DIGE images are shown for the pH 3-10 range.

5.3.2 DIGE analysis of skeletal muscle

The most prominent changes in gene expression in muscles affected by motor neuron degeneration are expected to reflect physiological denervation. In fact, an increase of the mRNA for the a-subunit of the nicotinic acetylcholine receptor, a typical sign of denervation, has been found in WR muscle (Sedehizade et al. 1997). Following differential fluorescent tagging, gel electrophoretic separation, densitometric scanning and image analysis, 24 protein spots were identified in WR muscle tissue that exhibit a significant change in concentration levels. A representative RuBPs master gel is shown for the pH 3-10 range in Figure 5.2. WR-associated changes in the concentration of proteins included two-dimensional spots that covered a p*I*-range from approximately 4.1 (Troponin C) to 8.6 (GAPDH) and ranged in molecular mass from apparent 16 kDa (Cu/Zn superoxide dismutase) to 128 kDa (Myosin binding protein C). The findings from the mass spectrometric identification of the 24 protein spots with a changed abundance are presented in Table 5.1. Expression levels were reduced in the case of 3 protein species and increased for 21 proteins. The spot with the highest relative concentration was found for the glycolytic enzyme aldolase (spot 1, Table 1), followed by GAPDH (spot 2). Other increased proteins are represented by actin (spots 4, 9, 16, 19), desmin (spots 5, 7, 11), myoglobin (spots 6, 12), myozenin (spot 8), troponin C (spot 14), actinin (spot 15), Cu/Zn superoxide dismutase (spot 20) and fast myosin light chain 1f (spot 21). Subtypes of creatine kinase M-type, possibly representing differently phosphorylated isoforms, showed differential changes in a variety of protein spots. Five spots exhibited an increased abundance (spots 3, 10, 13, 17, 18) and one spot a decreased concentration (spot 22). A decrease was shown for 2 proteins spots which both represent fast myosin binding protein C (spots 23, 24).

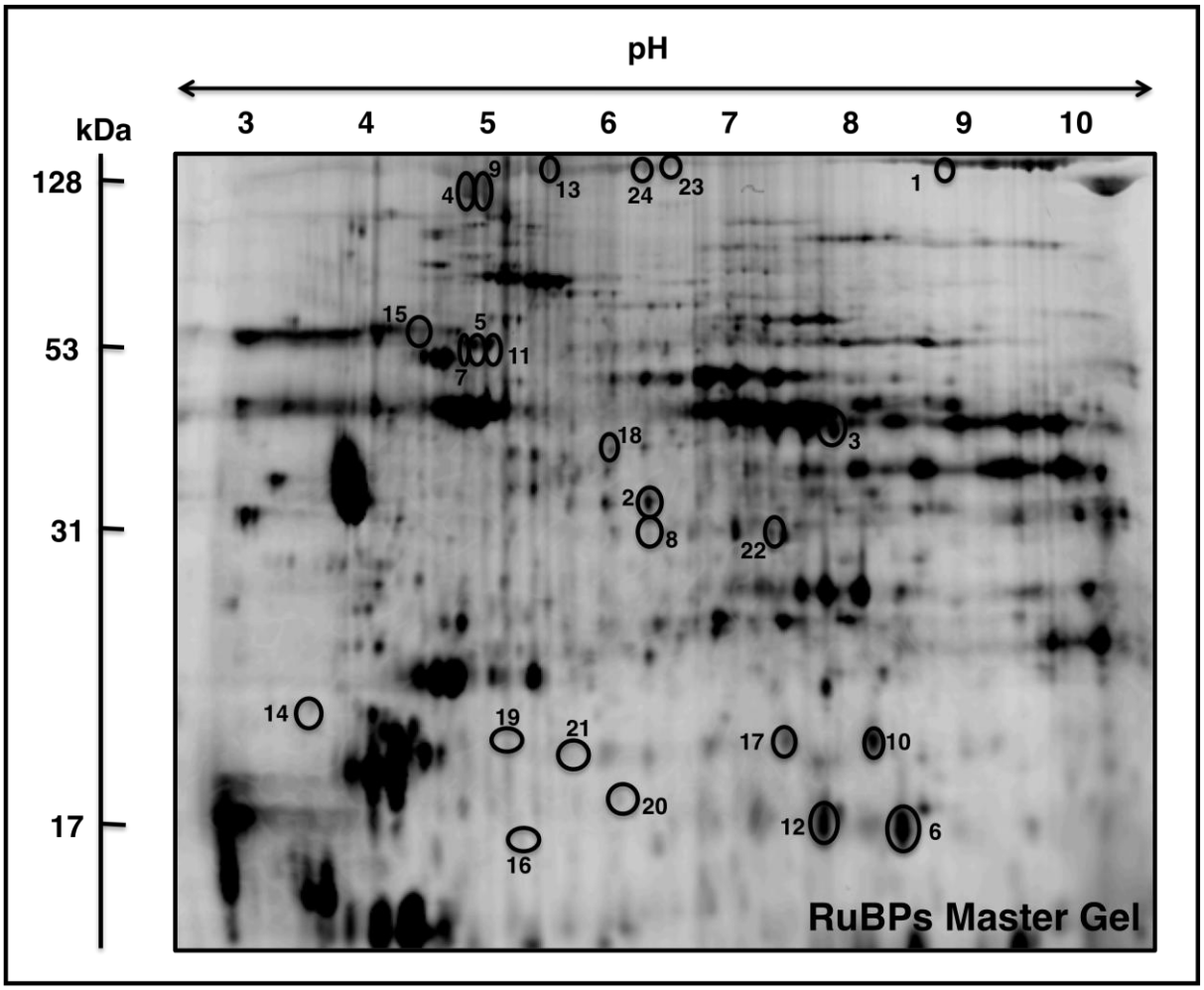

Figure 5.2 DIGE analysis of wobbler versus control tissue

Shown is a RuBPs-labelled master gel of crude tissue extracts from WR muscle tissue covering the pH 3-10 range. Protein spots with a changed concentration in WR preparations are marked by circles and are numbered 1 to 24. See Table 5.1 for a detailed listing of muscle-associated protein species with a changed abundance in the WR mouse model of motor neuron disease. The pH-values of the first dimension gel system and molecular mass standards (in kDa) of the second dimension are indicated on the top and on the left of the panels, respectively.

Table5.1 Proteins with changed abundance identified by LC-MS in WR versus normal skeletal muscle.

Spot no.	**Name of identified protein**	**Accession no.** *	**p*I***	**Molecular mass (kDa)**	**Peptides matched**	**Mascot score****	**Coverage (%)**	**Fold change*****	**Anova**
1	Fructose-bisphosphate aldolase A	gi|6671539|	8.31	39795	2	79	10	0.002	4.5
2	Glyceraldehyde-3-phosphate dehydrogenase	gi|149257623|	8.63	36298	6	101	24	0.002	3.5
3	Creatine kinase M-type	gi|6671762|	6.58	43250	15	447	41	0.006	3.4
4	Actin, alpha-cardiac	gi|387090|	5.23	42043	12	176	32	0.005	3.4
5	Desmin	gi|33563250|	5.21	53523	25	577	57	0.003	3.3
6	Myoglobin	gi|21359820|	7.07	17117	7	249	59	0.007	3.2
7	Desmin	gi|33563250|	5.21	53523	27	475	60	0.004	3
8	Myozenin-1	gi|10946924|	8.57	31438	6	159	25	0.008	3
9	Actin, alpha-cardiac	gi|387090|	5.23	42043	12	185	37	0.009	3
10	Creatine kinase M-type	gi|6671762|	6.58	43250	7	305	20	0.011	2.8
11	Desmin	gi|33563250	5.21	53523	21	369	49	0.008	2.6
12	Myoglobin	gi|21359820|	7.07	17117	7	274	49	0.002	2.6
13	Creatine kinase M-type	gi|6671762|	6.58	43250	5	113	14	0.008	2.3
14	Troponin C, skeletal	gi|6678371|	4.07	18156	6	308	49	0.005	2.2

	muscle								
15	Actinin-3, alpha	gi|7304855|	5.31	103616	14	330	21	0.006	2.1
16	Actin, alpha-cardiac	gi|387090|	5.32	42048	11	89	28	0.013	1.9
17	Creatine kinase M-type	gi|6671762|	6.58	43250	6	102	18	0.007	1.8
18	Creatine kinase M-type	gi|6671762|	6.58	43246	7	295	23	0.011	1.7
19	Actin, alpha	gi|49864|	5.45	38020	8	121	30	0.01	1.7
20	Cu/Zn superoxide dismutase	gi|226471|	6.03	15926	7	156	47	0.005	1.6
21	Myosin light chain 1f	gi|29789016|	4.98	20697	13	187	61	0.013	1.4
22	Creatine kinase M-type	gi|6671762|	6.58	43250	10	152	25	0.004	0.5
23	Myosin binding protein C, fast	gi|20988232|	6.02	128115	14	170	15	0.003	0.4
24	Myosin binding protein C, fast	gi|20988232|	6.02	128100	22	344	26	0.013	0.4

*NCBInr Database, release 20100212

** The mascot score has a 95% confidence level if >49.

*** Wobbler versus normal muscle tissue

5.2.3 Immunoblot validation of DIGE analysis

In order to verify key proteomic findings and to put this study in to perspective with previous analyses of WR muscle tissues, representative immunoblots are shown in Figure 5.3, Figure 5.4. and Figure 5.5 . Immunoblotting shown in Figure 5.3 clearly confirmed our proteomic data and showed a drastically increased abundance of GAPDH and desmin in WR muscle. However, increased levels of Cu/Zn superoxide dismutase shown in Figure 5.4 (B, D) were not significant. Similarly increased levels of myoglobin Figure 5.4 (A, C) shows a slight increase in Wobbler skeletal muscle. Previously published work on mRNA of the cytosolic Ca^{2+}-binding protein parvalbumin showed a drastic decrease in the wobbler (Sedehizade et al. 1997). The immunoblot of parvalbumin versus control in wobbler skeletal tissue shown in Figure 5.5 also agrees with this previously published work.

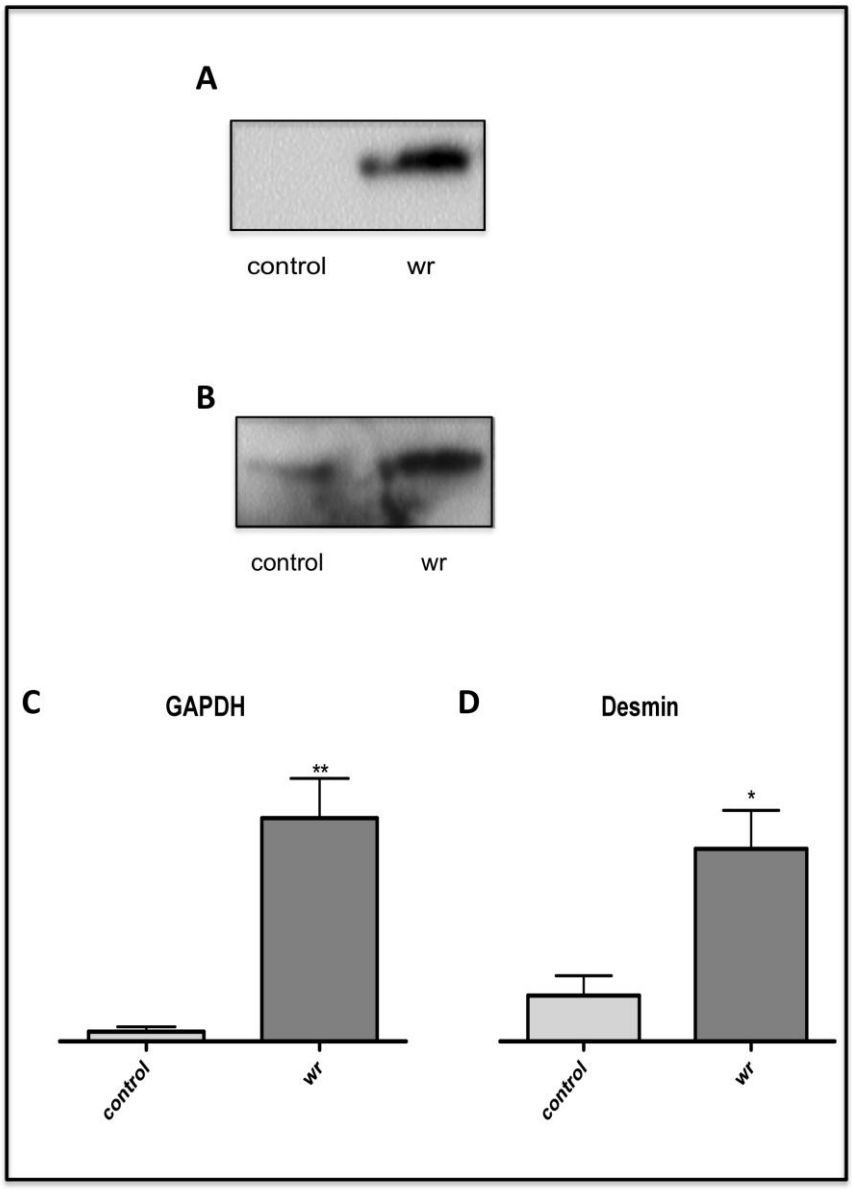

Figure 5.3 Immunoblot analysis of muscle proteins with a differential expression pattern in wobbler fibers

Shown is 1-D immuno-decorated bands and graphical presentation of statisical evaluation of antibody labelling, representing GAPDH (A, C), Desmin (B, D). The comparative blotting was statistically evalutated using an unpaired Student's t-test (n=4, **$p<0.01$,*$p<0.05$).

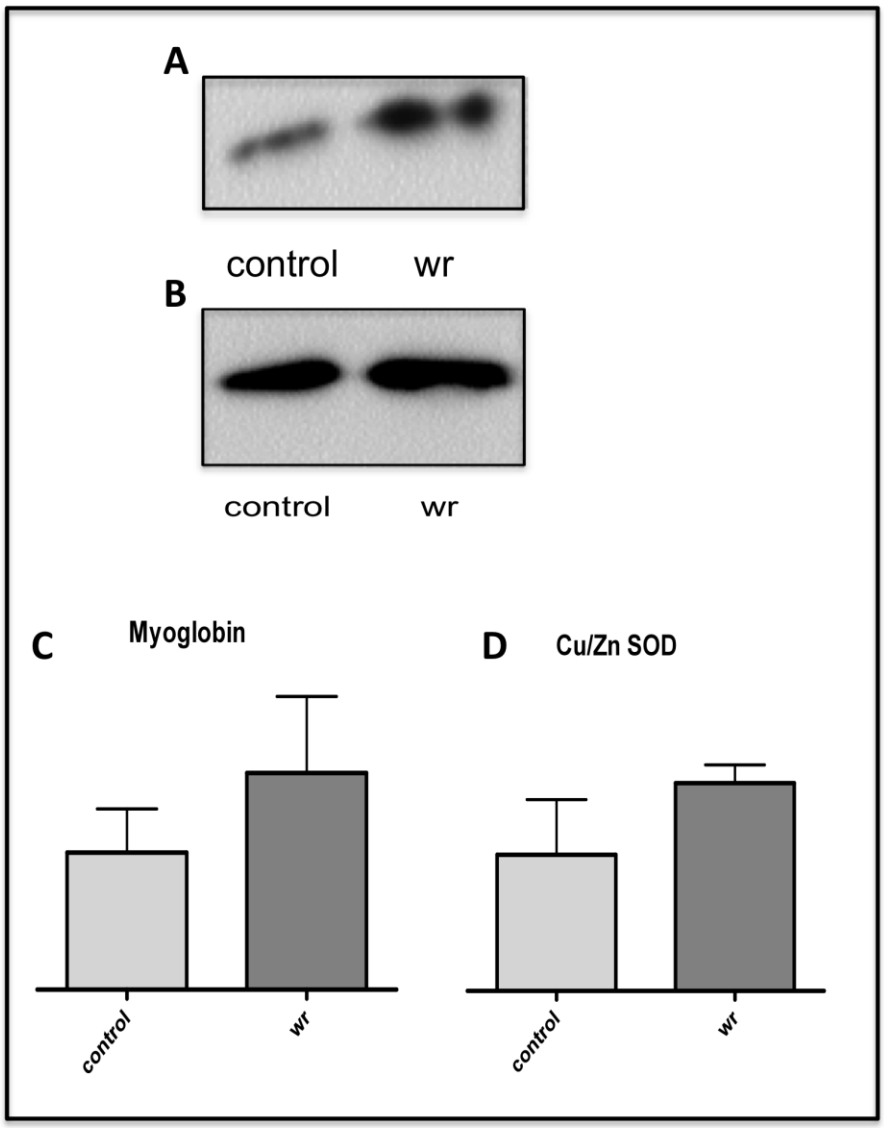

Figure 5.4 immunoblot analysis of Myoglobin and Cu/Zn SOD in wobbler skeletal tissue
Shown is the immuno-decorated band and graphical presentation of statistical evaluation of antibody directed against myoglobin (A,C) and Cu/Zn SOD (B, D). The comparative blotting was statistically evaluated using an unpaired Student's t-test (n=4,*p,0.05).

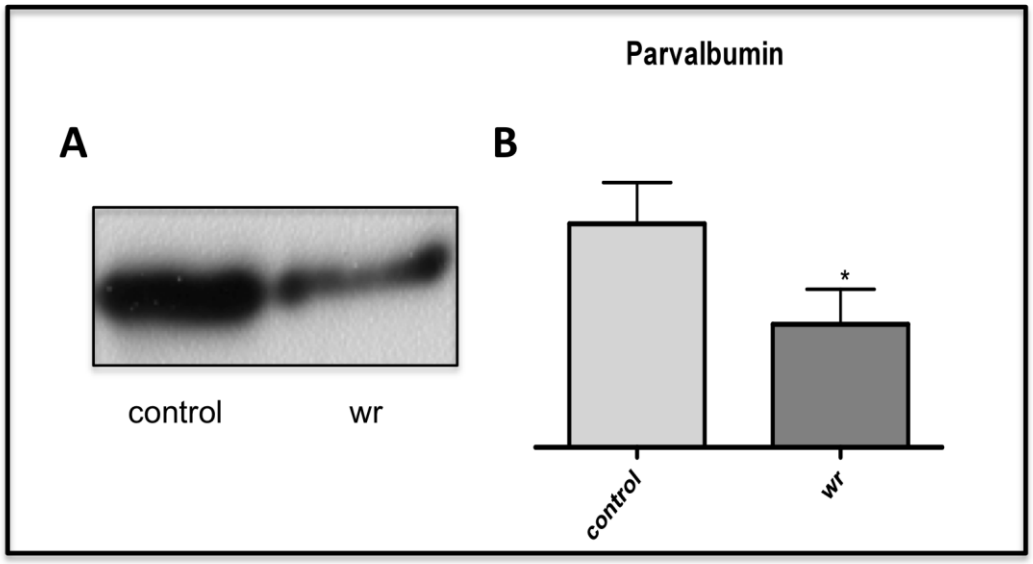

Figure 5.5 Immunoblot analysis of Parvalbumin in wobbler skeletal tissue.
Shown is the immuno-decorated band and graphical presentation of statistical evaluation of antibody directed against parvalbumin (A, B). The comparative blotting was statistically evaluated using an unpaired Student's t-test (n=4, *p,0.05).

5.3 Discussion

The overall objective of our proteomic profiling study of the WR skeletal muscle proteome was the establishment of global effects of motor neuron disease on the protein complement from skeletal muscle tissue. Since conventional protein staining procedures have a limited dynamic range, we employed fluorescence DIGE analysis for the detailed characterisation of global changes in the WR muscle proteome. A total of 24 protein spots were identified in WR muscle tissue that exhibited a significant change in concentration levels. Expression levels were reduced in the case of 3 protein species and increased for 21 proteins. Identified proteins were associated with key metabolic pathways, the contractile apparatus, intermediate filaments and the cellular stress response.

5.3.1 Metabolism

Muscular atrophy is a process in which protein degradation exceeds protein synthesis resulting in a decrease in fiber size, a drastic loss in muscle tissue mass and a decrease in isometric force (Staunton et al. 2011). It is observed in skeletal muscles under certain conditions including: microgravity, traumatic injury, following extended periods of rest or pathological damage to motor neurons (Kandarian et al. 2006). Previous studies have noted muscular atrophy results in an increase in key enzymes in the glycoltic pathway (Li et al. 2005; Sun et al. 2006; Seo et al. 2006). Aldolase A (spot 1) converts fructose 1,6-bisphosphate to glyceraldehyde-3-phosphate and dihydroxyacetone phosphate during glycolysis. Interestingly our second protein with increased abundance in WR muscle was glyceraldehyde-3-phosphate dehydrogenase (GAPDH) which converts glyceraldehyde-3-phosphate to 1,3 bisphosphoglycerate. This drastic increase in GAPDH was clearly confirmed by immunoblotting shown in Figure 5.3 (A).These results agree with previous studies of muscle unloading which results in muscle atrophy (Seo et al. 2006) where enzymes associated with anerobic metabolism showed a significant increase in expression following unloading. Previous work by Sedehizade and co-workers (1997) showed a decrease in the Ca^{2+}-binding protein parvalbumin in WR muscle. Similarly in figure 5.5 immunoblotting confirmed this reduction in parvalbumin in WR skeletal muscle tissue.

Metabolic regulatory protein creatine kinase M chain is presented in multiple spots (Spot 3, 10,13,17,18) this may be due to multiple phosphorylation isoforms. Phosphorylation is a post translational modification whereby phosphate groups are linked to the hydroxyl group of tyrosine, serine or threonine residues (Gannon et al. 2008). Therefore the representation of

creatine kinase as multiple spots on the gel may be due to the addition of one or multiple phosphate groups to the protein affecting its location on the gel. In order to fully determine phosphorylated isoforms of creatine kinase a ProQ diamond stain could be used to assess phosphorylated proteins with changed abundance in WR skeletal tissue. Creatine kinase M can reversibly catalyses the transfer of phosphate between ATP and creatine phosphate. Similar to aldolase A creatine kinase M-type was found to be increased in muscle tissue subjected to unloading (Cros et al. 1999). This overexpression of creatine kinase M-type was seen at early days of unloading and so considered a marker for muscle disuse (Cros et al. 1999). This drastic increase in creatine kinase M-type imply crucial alterations in creatine phosphate metabolism that may be related to metabolic shifts in WR muscle tissue due to muscle disuse due to denervation.

On one hand the decrease in parvalbumin which has been shown to be expressed in fast glycolytic muscle fibers along with an increase in oxygen transporting protein myoglobin (spot 6,12) shown in Figure 5.4 (A), and elvated levels of key glycolytic enzymes on the other indicate that the metabolic transformation in WR muscle is more complex than a unidirectional shift towards an extremely glycolytic phenotype.

5.3.2 Contractile apparatus and intermediate filaments

Changes in the concentration of actin (spot 4,9,16,19), troponin C(spot14), actinin (spot 15), myozenin-1 (spot 8), myosin light chain 1f (spot 21) and myosin binding protein c,fast (spot 23,24) suggest atrophy-related modulations of the contractile apparatus. Skeletal muscle myosin is composed of two heavy chains, two essential light chains (MLC1), and two regulatory light chains (MLC2). Myosin light chains are responsible for force and velocity in muscle fibers (Sato et al. 2009). Therefore the 1.4 fold increase in MLC 1 the fast isoform is expected to happen as a consequence of the lowering of mechanical load with denervated muscle. Myozenin-1 was first described by Takada and co-workers (2001) and was found to bind to a□actinin. Both are major components of Z-lines. □-actinin isoforms function to anchor the actin containing thin filaments (Takada et al. 2001). Changes in proteins of the contractile apparatus may be a result of remodelling due to muscle transformation as a consequence of denervation.

Desmin (spot 5,7,11) is part of the intermediate filament family of proteins that form the fibrous network connecting myofibrils to each other and the plasma membrane from the periphery of the Z-line. Desmin null mice show disorganisation of myofibril architechture and

mutations of the desmin gene underlie certain mutations of muscular dystrophies (Farve et al. 2011). This indicates the importance of desmin for integrity of cytoarchitechture in skeletal muscle cells. The upregulation of desmin could be possibly a compensatory stabilisation of the cytoskeletal network in WR muscle. Similarly increases in the essential contractile protein actin and its achoring proteins actinin and myozenin and the intermediate filament protein desmin on one hand and the decrease in the myosin binding protein C on the other, may be due to contractile remodelling due to fiber transformations in the WR muscle.

5.3.3 Other proteins

The upregulation of anti-oxidant marker Cu/Zn superoxide dismutase (SOD) (spot 20) indicates a need to counter-act cellular damge due to motor neuron degeneration in the WR mouse. Cu/Zn SOD destroys any reactive oxygen species that are produced by the cell. It is interesting that this protein would be increased in the transformed glycoltic WR muscle. Mutations in Cu/Zn SOD have been show in 20% of cases with autosomal dominant FALS and 2% of patients with SALS (Wijesekera and Leigh 2009).

5.4 Conclusions

Studying changes in the WR muscle proteome has the potential to contribute crucial information on disease process during denervation-induced muscular atrophy. The proteomic profiling of muscular atrophy associated with motor neuron disease has revealed key enzymes of the glycolytic pathway and increase contractile proteins, such as actin, troponin C, actinin and myozenin-1. The proteomic data represented supports the general idea of disuse-and atrophy-associated oxidative-to-glycolytic transformation process.

6. Mass Spectrometric identification of sarcoplasmic reticulum proteins by "on membrane" digestion.

6.1 Introduction

In this study we have applied a combination of subcellular fractionation, one-dimensional gradient-gel electrophoresis, on-membrane digestion and MS analysis to determine the complex composition of the sarcoplasmic reticulum (SR) from rabbit skeletal muscle. The SR of skeletal muscle is made of an elaborate system containing integral proteins and large proteins that exist in highly complex supramolecular clusters. Its central role is in the regulation of the excitation-contraction-relaxation cycle and Ca^{2+} homeostasis. Major proteins involved in Ca^{2+}-uptake,Ca^{2+}-shutting, Ca^{2+}-buffering and Ca^{2+}-release are represented by SERCA-type Ca^{2+} pumps including; Ca^{2+}-binding protein sarcalumenin (SAR), high capacity Ca^{2+} binding element calsequestrin and the ryanodine receptor release channel (Ryr). Minor proteins involved in the modulation of excitation-contration coupling include; mitsugumin-29, junctophilin-1, trimeric intracellular cation-selective channel (TRIC-A), JP-45,JP-90, junctin, triadin, the SERCA-regulatory subunits:phospholamban and sarcolipin and the Ryr-associated FKBP12 immunophilins. Primary and secondary defects in Ca^{2+}-homeostasis proteins result in numerous neuromuscular disorders including; malignant hyperthermia, central core disease, Brody's disease and dystrophinopathy. These peripheral and integral Ca^{2+}-regulatory proteins of the SR are maintained as large oligomeric assemblies in muscle fibers which makes them difficult to identify by MS following 2-D gel electrophoresis. Conventional 2-D gel electrophoresis where proteins are separated in the first dimension based on their pI and in the second based on their molecular mass underestimates the presence of integral proteins, very large proteins, proteins with extreme pI values and proteins with low copy number. Subcellular fractionation reduces sample complexcity and so can overcome problems with low abundance proteins. The use of 1-D gradient gels eliminates the exclusion of integral proteins and high molecular mass components. In addition, normal gel-electrophoresis-based proteomics studies use mostly in-gel digestion for generation of peptides to be analyzed by MS technology. However, in-gel trypsination of gel-separated proteins in low digestion efficiency and thus a relatively low yield of proteolyic peptides. This is a problem with low abundance proteins, integral proteins or high molecular mass proteins. In this study in order to address these problems we have used 3-12% large gradient gels for the electrophoretic separation of SR-associated protein complement and on membrane

digestion methods to identify proteins by MS. On membrane trypsination mehods have been applied in various biochemical studies (Aebersold et al. 1987; Luque-Garcia et al. 2008; Towbin et al. 1979; Lewis et al. 2010). In contrast to in-gel trypsination, proteins that are transferred to nitrocellulose sheets are readily accessible to proteases thus increasing digestion efficiency and reducing digestion time making trypsin autolysis at least partically eliminated.

6.2 Results

6.2.1 Subcellular fractionation

Crude microsomal vesicles were prepared from skeletal muscle homogenates by standard differential centrifugation and then the heavy SR fraction was separated from sarcolemma, triads junctions, light SR and mitochondrial debris by sucrose density gradient centrifugation. Subsequently, 3-12% gradient gel electrophoresis was employed to achieve a highly reproducible banding pattern of the protein complement from the SR-enriched fraction. SR proteins were transferred to nitrocellulose membranes and individual bands digested by on-membrane trypsination. The unambiguous identification of SR-associated proteins was achieved by LC-ESI MS/MS analysis.

6.2.2 SDS-PAGE fractionation

The gel electrophoretic separation of the SR fraction resulted in a distinct protein band pattern shown in figure 6.1. As illustrated in the representative gradient gel of Figure 6.3. Ponceau Red staining revealed 35 distinct protein bands, ranging in molecular mass from 12 kDa (S100 Ca^{2+}-binding protein) to 571 kDa (RyR1 SR Ca^{2+}-release channel). Major protein bands were represented by creatine kinase (band 20), CSQ (bands 14 and 15), SERCA Ca^{2+}-ATPase (bands 5, 10 and 11) and the RyR1 isoform of the SR Ca^{2+}-release channel (band 1). Despite repeated attempts to analyze their protease-generated peptide mixtures, 5 proteins bands, i.e. SR bands 3, 16, 19, 29 and 30, could not be identified. In contrast, the most intensively stained protein band of approximately 110 kDa contained 5 distinct groupings of MS hits (bands 10a, 10b, 11a, 11b and 11c). Band 23 could also be subdivided into 2 distinct MS hits (bands 23a and 23b).

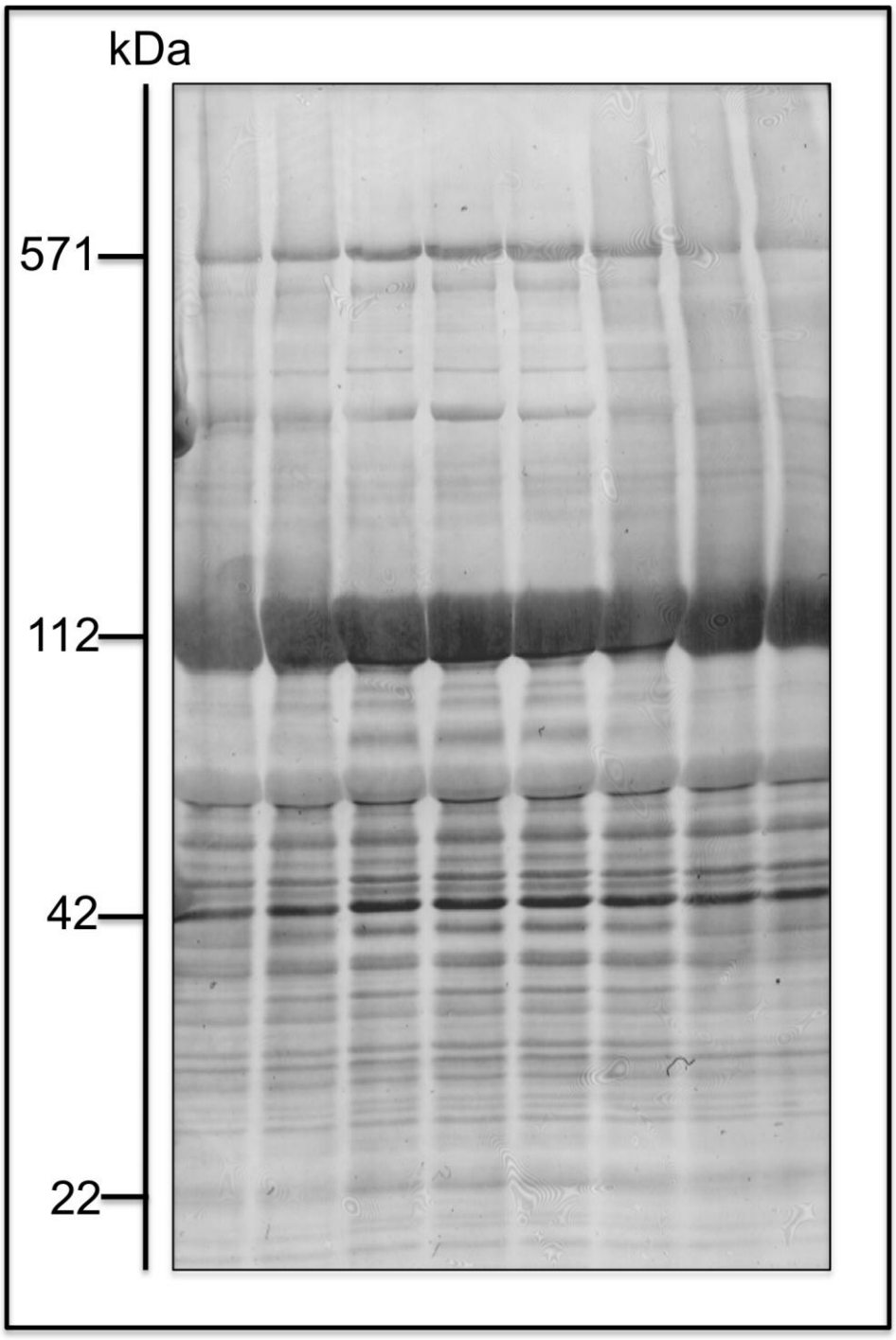

Figure 6.1 Banding pattern of SR 1-dimensional gel.

Shown is the reversible memcode stained distinct banding pattern of SR fraction proteins separated on a 3-12% gradient gel. The multiple lanes represent multiple repeats of the SR fraction.

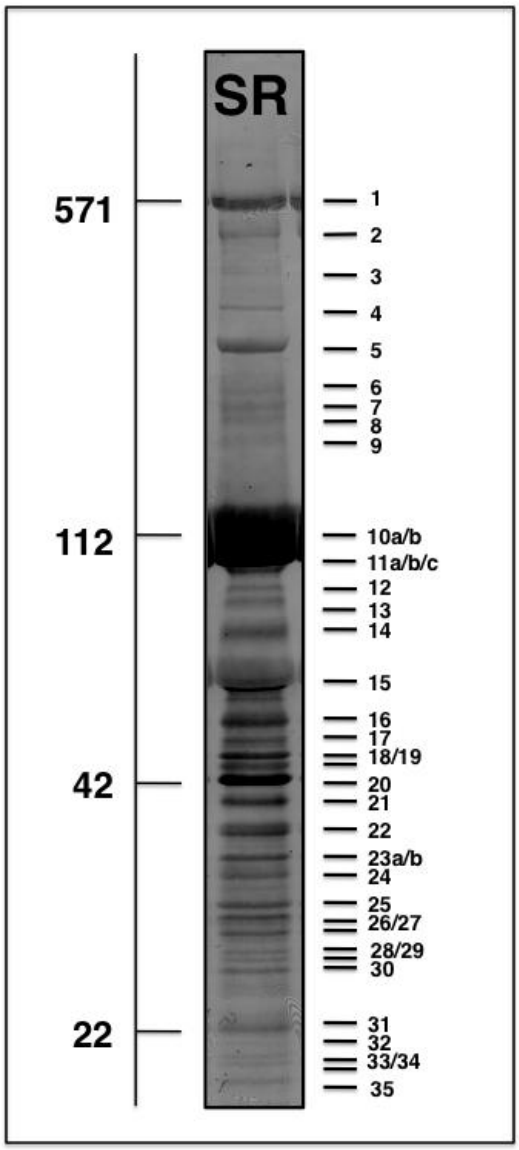

Figure 6.2 One-dimensional master gradient gel.

Shown is a representative Ponceau Red-stained nitrocellulose replica of the electrophoretically separated SR fraction, using a large 3-12% gradient gel system. SR protein bands were numbered 1 to 35 and identified by MS analysis (see: Table 6.1). Molecular mass standards (in kDa) are indicated on the left of the panel.

6.2.3 Identification of sarcoplasmic reticulum proteins by LC/MS

The MS-based identification of the main protein species that represent stained bands following one-dimensional gradient gel electrophoresis is summarized in Table 6.1. Table 6.1 lists identified proteins in the SR fraction from rabbit skeletal muscle as determined by a minimum coverage by two independent peptide sequences. The table gives an overview of the name of identified protein species, peptide sequences, number of matched peptides, the percent sequence coverage, molecular mass, isoelectric point, Mascot score and protein accession number. Clearly identified proteins in the SR fraction were the RyR1 isoform of the Ca^{2+}-release channel (band 1), the SERCA-type Ca^{2+}-pump (bands 4, 5, 8, 9, 10a, 10b, 11a, 11b, 11c), the Ca^{2+}-binding protein CSQ (bands 14 and 15), the 53-GP/SAR protein (band 17), elongation factor 1-alpha (band 18), creatine kinase (band 20), aldolase (band 23a), protein similar to C34G6.1 (band 24), and ADP/ATP translocase 3 (band 3). Some Identified proteins were identified with only one matched peptide and are placed in Table 6.2

Table 6.1. List of MS-identified proteins in the sarcoplasmic reticulum fraction from rabbit skeletal muscle.

Band No.	**Name of identified protein**	**Peptide sequence**	**Peptides matched**	**Coverage (%)**	**Molecular mass (Da)**	**p*I***	**Mascot score**	**Accession No.***
1	Ryanodine receptor RyR1 calcium release channel	LFPAVFVLPTHQNVIQFELGK DPVGGSVEFQ FVPVLK FAVFVNGESVEENANVVVR GEGGSGLLAAIEEAIR LVFDVPILNEFAK DLYALYPLLIR IAELLGMDLASLEITAHNER	7	2	570,723	5.15	194	gi|226386|
4	Sarcoplasmic reticulum calcium ATPase SERCA1	FMEYETDLTFVGVVGMLDPPRK ISLPVIGLDEILK	2	3	111,780	5.14	81	gi|147903853|
5	Calcium-ATPase, Chain	DIVPGDIVEVAVGDKVPADIR ISLPVIGLDEILK	2	3	110,811	5.15	72	gi|18159010|

	A, E2 State							
8	Sarcoplasmic reticulum calcium ATPase SERCA1	FMEYETDLTFVGVVGMLDPPRK ISLPVIGLDEILK	2	3	111,780	5.14	63	gi|147903853|
9	Calcium-ATPase, Chain A, E2 State	DIVPGDIVEVAVGDKVPADIR ISLPVIGLDEILK	2	3	110,811	5.15	72	gi|18159010|
10a	Sarcoplasmic reticulum calcium ATPase SERCA1	DIVPGDIVEVAVGDKVPADIR ALGIVATTGVSTEIGK EFTLEFSR FMEYETDLTFVGVVGMLDPPRK IVEYLQSYDEITAMTGDGVNDAPALKK TASEMVLADDNFSTIVAAVEEGR ALDLTQWLMVLK ISLPVIGLDEILK	8	14	111,780	5.14	205	gi|147903853|
10b	Sarcoplasmic reticulum	DIVPGDIVEVAVGDKVPADLR	2	2	112,101	5.48	38	gi|291405296|

	calcium ATPase	EFTLEFSR						
11a	Calcium-ATPase, Chain A, E2 State	DIVPGDIVEVAVGDKVPADIR VDQSILTGESVSVIK ALGIVATTGVSTEIGK EFTLEFSR RIGIFGENEEVADR IGIFGENEEVADR IVEYLQSYDEITAMTGDGVNDAPALK IVEYLQSYDEITAMTGDGVNDAPALKK TASEMVLADDNFSTIVAAVEEGR ISLPVIGLDEILK	10	13	110,811	5.15	881	gi|18159010|
11b	Sarcoplasmic reticulum calcium ATPase SERCA1	DIVPGDIVEVAVGDKVPADIR VDQSILTGESVSVIK EFTLEFSR RIGIFGENEEVADR IGIFGENEEVADR IVEYLQSYDEITAMTGDGVNDAPALK TASEMVLADDNFSTIVAAVEEGR	8	13	111,780	5.14	881	gi|147903853|

		ISLPVIGLDEILK						
11c	Sarcoplasmic reticulum calcium ATPase	DIVPGDIVEVAVGDKVPADLR EFTLEFSR	2	2	112,101	5.48	38	gi|291405296|
14	Calsequestrin	EEGLDFPEYDGVDR QFEMEELILELAAQVLEDK LGLTEEDSIYVFK	3	12	42,407	3.93	162	gi|157829745|
15	Calsequestrin	QFEMEELILELAAQVLEDK ELQAFENIEDEIK	2	8	42,407	3.93	180	gi|157829745|
17	53 kDa SR glycoprotein / sarcalumenin	EEISLLEDLNQVIENR DFFGINPISSFK AITQELPSLLGSLGLGK	3	9	54,764	6.21	167	gi|623545|
18	Elongation factor 1-alpha	THINIVVIGHVDSGK NIITGTPQDDCAVLIVAAGVGEFEAGIS K	2	11	40,807	6.83	100	gi|74003751|
20	Creatine kinase	NKVTPNGYTLDQCIQTGVDNPGHPFIK GTGGVDTAAVADVYDISNIDR	2	11	48,012	8.46	80	gi|338237|

23a	Aldolase	GVVPLAGTDGETTTQGLDGLSER TVPPAVTGVTFLSGSEEEEGASINLNAI NK	2	14	39,457	9.06	98	gi|229506|
24	Protein similar to C34G6.1	ETRAFLLSSSPGR DDPHSLVALEAMVGLAR	2	2	164,959	6.37	32	gi|73974872|
26	ADP/ATP translocase 3	GAWSNILRGMGGAFVLVLYDELKK GMGGAFVLVLYDELK	2	8	33,078	9.73	58	gi|126325903|

*NCBInr Database, release 20100212

Table 6.2 List of MS-identified proteins from SR fraction that were identified with one peptide matched.

Band No.	Name of identified protein	Peptide Sequence	Peptides Matched	Coverage(%)	kDa	pI	Mascot Score	Accession No.*
2	myosin heavy chain isoform 2b	LASADIETYLLEK	1	1	224021	5.6	55	gi|291405035
6	Nedd4 binding protein 1	FPLLAPLPSIPQNLSMPAQR	1	2	101446	5.72	41	gi|291410221
7	sarcoplasmic reticulum glycoprotein	EEISLLEDLNQVIENR	1	3	54764	6.21	78	gi|623545
12	phosphofructokinase, muscle	LNIIIVAEGAIDR	1	1	94181	7.85	114	gi|291414479
13	heat shock 70kDa protein 5	IEIESFYEGEDFSETLTR	1	2	72314	5.15	68	gi|291408341

21	NADH dehydrogenase (ubiquinone) 1 alpha subcomplex, 10	LLQYADALEHLLSTGQGVVLER	1	6	40716	7.62	51	gi|291414461
22	Fructose-bisphosphate aldolase A	YTPSGQAGAAASESLFIPNQAY	1	11	20702	5.51	70	gi|73976435
23	aldolase C	GVVPLAGTDGETTTQGLDGLSER	2	14	39457	9.06	98	gi|229506
25	dehydrogenase/reductase (SDR family) member 7C	LENLYDALISVADPSK	1	5	35083	8.76	75	gi|291405047
27	trimeric intracellular cation channel type A	GSGVALLSNVEQLLR	1	5	33265	8.64	90	gi|153792068
28	trimeric intracellular cation channel type A	GSGVALLSNVEQLLR	1	5	33265	8.61	93	gi|153792068
32	adenylate kinase 1	IAQPTLLLYVDAGPETMK	1	9	21741	8.72	80	gi|291413541

33	reticulon 2-like	GDGANPFQAYLDVDLTLTR	1	4	50399	4.83	146	gi|291414836
34	S100 calcium binding protein, zeta-like	MPTQLEMAMDTMIRIFHR	1	18	11842	6.1	37	gi|291413610
35	Nedd4 binding protein 1	FPLLAPLPSIPQNLSMPAQR	1	2	101446	5.72	41	gi|291410221

*NCBInr Database, release 20100212

6.2.4 Immunoblot analysis of Ca^{2+} regulatory proteins of the sarcoplasmic reticulum.

For comparative purposes and to verify the electrophoretic position of key Ca^{2+}-handling proteins in one-dimensional gradient gels, immunoblotting of RyR, SERCA, CSQ and SAR are shown in Figure 6.3. The main immuno-decorated band for the SR Ca^{2+}-release channel was shown to be at a molecular mass of approximately 570 kDa (Figure 6.3A), which agrees with the position of the protein band that was identified as the RyR1 isoform by on-membrane digestion (Figure 6.2, Table 6.1). Interestingly, immuno-labeling with a monoclonal antibody to the fast SERCA1 isoform of apparent 112 kDa revealed 3 main bands, probably representing monomers, dimers and tetramers (Figure 6.3B). This finding agrees with the fact that our MS analysis identified several bands with differing molecular mass as SERCA units (Figure 6.3, Table 6.1). Figure 6.3C illustrates antibody labeling of the 63 kDa monomeric CSQ protein and this finding is in agreement with the position of the main MS-identified CSQ band in gradient gels (Figure 6.3, Table 6.1). Immunoblotting of SAR revealed a labeled protein band of approximately 160 kDa (Figure 6.3D). Immunoblotting survey shown in Figure 6.3 agrees with the proteomic characterization of the electrophoretically separated SR fraction.

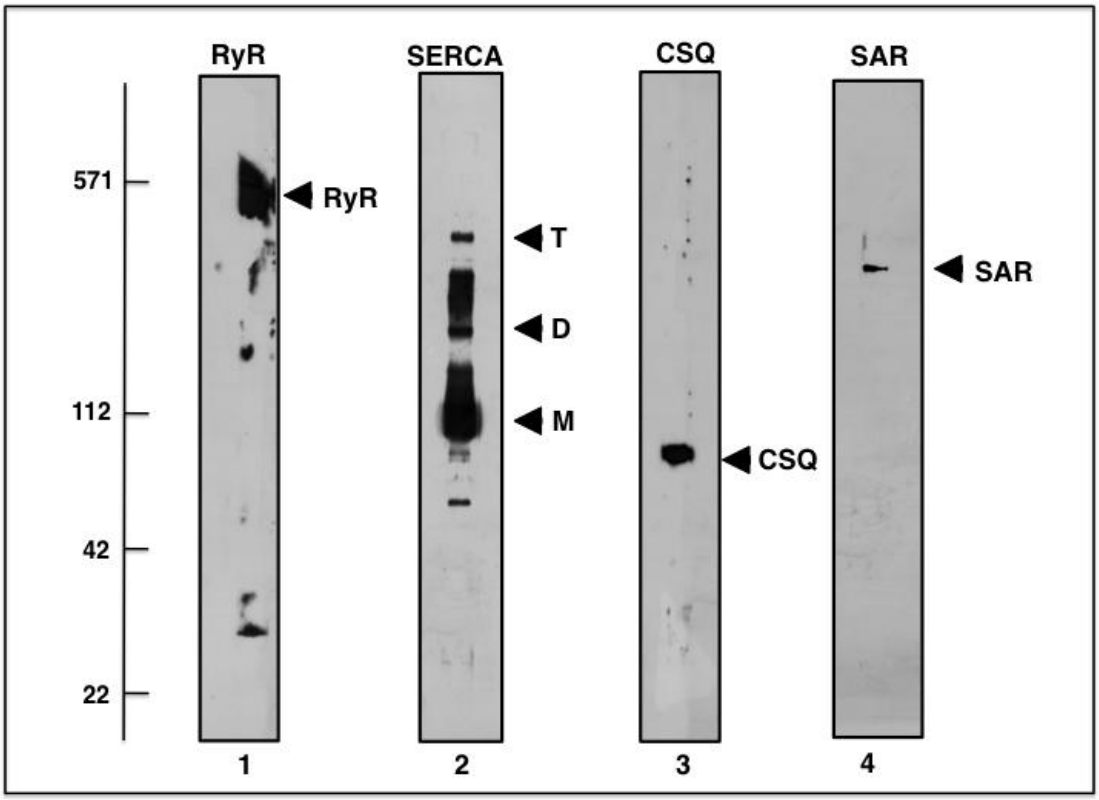

Figure 6.3 Immunoblot analysis of SR-identified proteins.

Shown is 1-D immuno-decorated bands and graphical presentation of antibody labelled SR proteins, representing RyR (1), Sarcoplasmic/endoplasmic Ca^{2+}-ATPase (SERCA) (2), calsequestrin (CSQ) (3) and sarcalumenin (SAR) (4).

6.3 Discussion

Two dimensional gels have been instrumental to the birth and development of proteomics however it is fair to say that hydrophobic proteins, membrane proteins and low abundance proteins are still under represented on 2-D gels. In this study we have used on-membrane digestion as a method to detect integral membrane proteins, high-molecular mass proteins and components of the rabbit skeletal muscle sarcoplasmic reticulum (SR). The MS-based proteomic characterisation of the SR fraction revealed 31 SR-associated protein species. The most highly abundant SR protein, SERCA-type Ca^{2+}-ATPase (Moller et al. 2010) was found to be present in the main 112 kDa band and several other protein bands in the one-dimensional gel. The other main players involved in Ca^{2+}-cycling through the SR, The RyR Ca^{2+}-release channel (band 1), the Ca^{2+}-binding protein CSQ (band 14, 15) and the Ca^{2+}-shuttle element sarcalumenin SAR and its related glycoprotein 53-GP (band 17) were all clearly identified by MS analysis. The on-membrane digestion method has clearly identified the main ion-regulatory elements involved in the energy-dependent Ca^{2+}-release during excitation-contraction coupling (Radermacher et al. 1994), Ca^{2+}-uptake during muscle relaxation (Moller et al. 2010), Ca^{2+}-shutting within the longtitudinal SR tubules (Leberer et al. 1990) and Ca^{2+}-buffering within the lumen of the terminal cisternae region (Royer and Rios 2009).

6.3.1 Glycolytic enzymes

An interesting finding of this MS-based survey of the SR membrane is the identification of the glycolytic enzymes to be present in the SR-enriched subcellular fraction. Both aldolase (band 23) and phosphofructokinase appear to be physically linked to the SR in rabbit skeletal muscle tissue with agrees with previous studies that has demonstrated functional coupling between SR Ca^{2+}-transport and ATP production via the glycolytic pathway (Xu and Becker 1998).

6.4 Conclusions

In conclusion the application of subcellular fractionation to reduce sample complexicity and the use of one-dimensional gradient gel electrophoresis followed by on-membrane digestion and MS analysis has successfully identified a large number of distinct protein species in the SR fraction from rabbit skeletal muscle. On-membrane digestion is shown to be a highly suitable technique for studying integral and high-molecular-mass muscle proteins in subcellular fractions. A high number of muscular disorders are involved with membrane proteins for example the chloride channelopathy myotonia congentia. It may be advantageous to look at protein complexes that are involved in signal transduction pathways that relate muscle membrane hyperexcitability to fiber phenotype. A proteomic study inclusive of high molecular weight proteins unable to enter a 2-D gel with sebsequent mass spectrometric identificationmay give insight into the proteins involved with controlling muscle fiber phenotype.

7. General Discussion

Skeletal muscle is an effector organ that transforms potential energy into contractile force and movement. This movement allows organisms with a means of reacting to its environment. The muscle fibers which make up the tissue are extremely adaptive to numerous external cues, from neuromuscular activity and physical activity to several diseased states.

This proteomic study has focused on the biochemical establishment of secondary effects of myotonia and denervation on the skeletal muscle proteome. Proteomic profiling resulted in the observation of very different fiber type transitions in both diseased states. The long term muscle activity in hyperexcitable muscle due to a single gene defect influenced a multitude of secondary changes in the skeletal muscle proteome. The proteomic profiling of the myotonic animal models ADR, MTO and MTO*5J clearly revealed a drastically perturbed protein expression pattern in the severely affected ADR and MTO muscle, but only moderate changes in mildly diseased MTO*5J animals. Hence, the severity of myotonic symptoms appears to correlate well with quantitative and qualitative alterations in the protein complement of ADR and MTO *vs.* MTO*5J. As seen in Figure 7.1 the loss of sarcolemma Cl^- conductance destabilizes the membrane potential and leads to hyperexcitability of the muscle fiber, the hallmark of myotonia. The unscheduled bursts of action potentials cause bursts of intracellular Ca^{2+} release and cramps. The muscle cramps experienced with myotonia can lead to mechanical stress on the muscle resulting in increased expression of stress proteins. All three animal models displayed increases in stress proteins: MTO*5J (Hsp27), MTO (Hsp 7 and Hsp2), ADR (Hsp 40). The elevated intracellular Ca^{2+} activates Ca^{2+}-dependent signalling pathways e.g. those involving calmodulin/calcineurin and NFAT (shown in Figure 7.1). Activation of these signalling pathways leads to the transcription of the slow gene program. This is seen in myotonic muscle where there is a switch of isoforms of contractile proteins MHC fast to MHC slow along with reduced levels of MLC2f and phosphorylatable MLC2f. The reduced levels of the MHC fast isoform to its slower isoform along with increased levels in oxidative phosphorylation enzymes such as cytochrome c in ADR muscle and NADH in MTO muscle agrees with the idea of myotonia-induced muscle transformation of both the contractile apparatus and muscle metabolism. The findings in chapter 3 and chapter 4 were in line with previous studies of muscle transformation after chronic low-frequency stimulation (Donoghue et al. 2007). In addition to the common fiber-type specific markers, many other

interesting changes occured in the myotonic animal models. Parvalbumin is a soluable Ca^{2+}-binding protein that is present chiefly in the fast-twitch fibers where it plays a role in fast-twitch relaxation (Muntener et al. 1995; Schwaller et al. 1999). The decreased expression of parvalbumin in all three myotonic skeletal tissues could result in a higher concentration of free cytosolic Ca^{2+}. As discussed Ca^{2+} plays an important role in Ca^{2+}-dependent transcriptional pathways e.g. calcineurin. Over expression of parvalbumin in slow fibers resulted in faster twitch contraction and increased relxation time in the slow-twitch soleus muscle, along with a reduction in calcineurin activity (Chin et al. 2003). These findings indicate that parvalbumin expression in fast-twitch fibers act to buffer free cytosolic Ca^{2+} whereby it could prevent its binding to Ca^{2+}-depenpdent pathways such as calcinuerin that activate transcription of the slow gene program. This is clearly seen in our proteomic profiling of skeletal muscle from myotonic mice were expression of slower isoforms of contractile proteins are increased along with increased expression of mitochondrial enzymes indicative of a slow-twitch fiber phenotype. The varying degree of decreased expression of parvalbumin in ADR and MTO *vs.* MTO*5J might be used as a reliable general marker of the severity of myotonia. Similarly with the protein disulfide isomerase was shown to be increased in ADR muscle, but decreased in MTO, and could potentially be used as a differentiating marker of these two different myotonic phenotypes. Further biochemical studies are needed to fully interpret the effects of these changes on gene regulation in skeletal muscle.

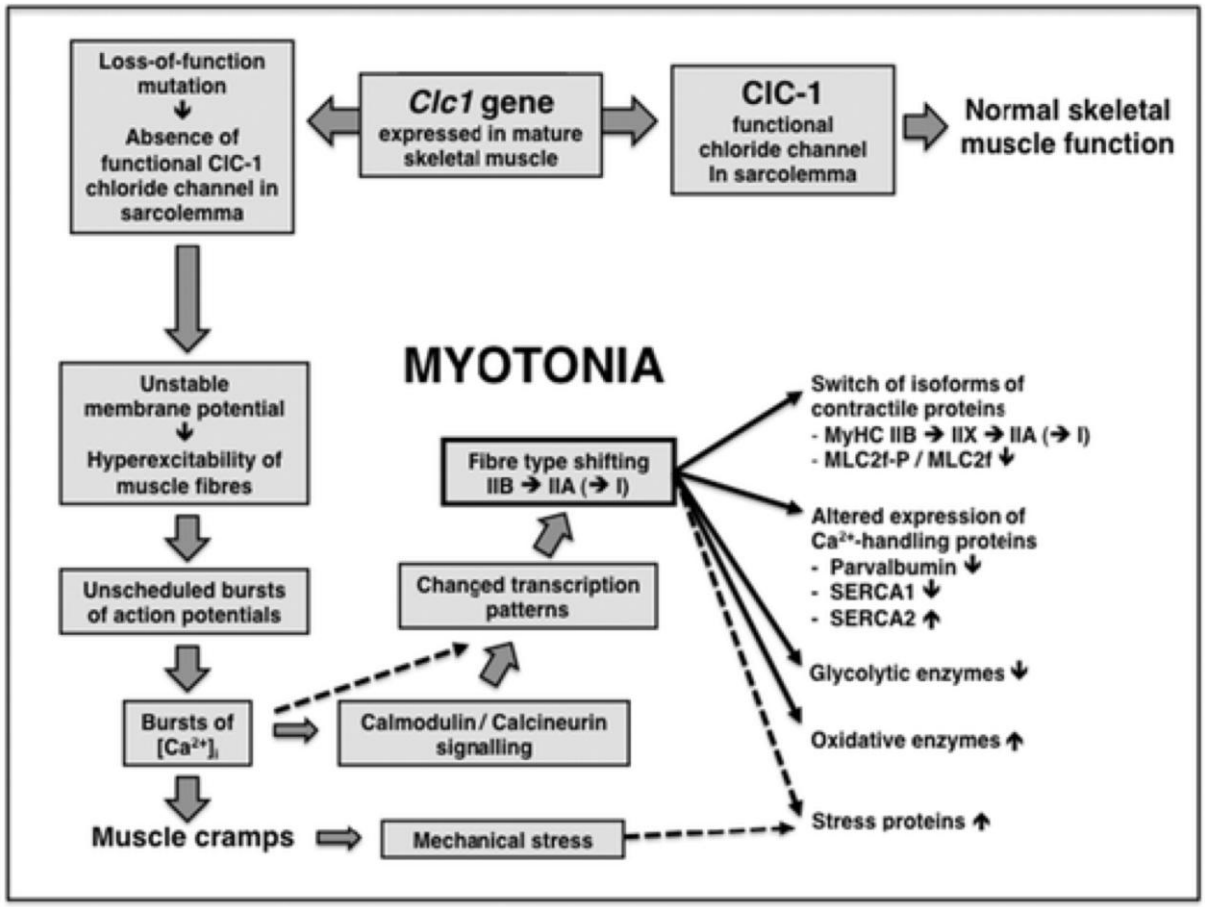

Figure 7.1 Overview of the changes seen in Myotonic skeletal tissue.

Shows an overview of the the changes in myotonic muscle as determined my proteomic profiling. Hyperexcitabilty of skeletal muscle leads to unscheduled bursts of action potentials resulting in bursts of Ca^{2+} concentration. Increased cytosolic Ca^{2+} can influence transcription patterns through calmodulin/calcineurin signalling. Myotonic muscle shows fiber type switching from fast-glycolytic to slow-oxidative fiber phenotype.

The objective to our proteomic profiling study of the WR mouse was the establishment of global effects of motor neuron disease on the protein complement from skeletal muscle tissue. The most prominent changes in gene expression in muscles affected by motor neuron degeneration were expected to reflect physiological denervation. Importantly, the WR pathology is a long-term and continuous process, as opposed to surgical denervation, intrinsic effects of the partial deficiency in VPS54 cause proteome-wide alterations in skeletal muscle as shown in Figure 7.2. Following differential fluorescent tagging, gel electrophoretic

separation, densitometric scanning and image analysis, 24 protein spots were identified in WR muscle tissue that exhibit a significant change in concentration levels. Expression levels were reduced in the case of 3 protein species and increased for 21 proteins. In contrast to myotonic mouse muscle, in which there is a shift from the dominant myosin heavy chain (MHC) isoform IIB to IIX and IIA , in WR muscle there is an opposite shift to an even higher proportion of MHC IIB and a glycolytic phenotype. The highest increases in WR muscle was found for the glycolytic enzyme aldolase followed by GAPDH. These two enzymes with an increased concentration reflect a shift towards an extreme glycolytic muscle fiber type. Similar to myotonic muscle the skeletal tissue from the WR mouse showed a significant decrease in the Ca^{2+}-binding protein parvalbumin. It is interesting that the WR skeletal muscle shows a shift towards glycolytic metabolism indicative of fast-twitch fibers yet they have decreased expression of parvalbumin at the mRNA level (Sedehizade et al. 1997) and protein level (Staunton et al. 2011). Perhaps this protein could be used as a biomarker for both muscle excitabiltiy and motor neuron degeneration in skeletal muscle. Both diseases show drastic fiber type switiching yet a similar decrease in the Ca^{2+}-binding protein parvalbumin.

Future work is needed to determine the signalling pathways involved in fiber type switching in order to gain a better understanding of Ca^{2+}- dependent signalling pathways that determine gene expression in fast-twitch and slow-twitch muscle. Perhaps the use of muscle cell lines e.g. C2C12 (Kane et al. 2009) could be used to further understand the cellular signalling pathways that control fiber-specific genes.

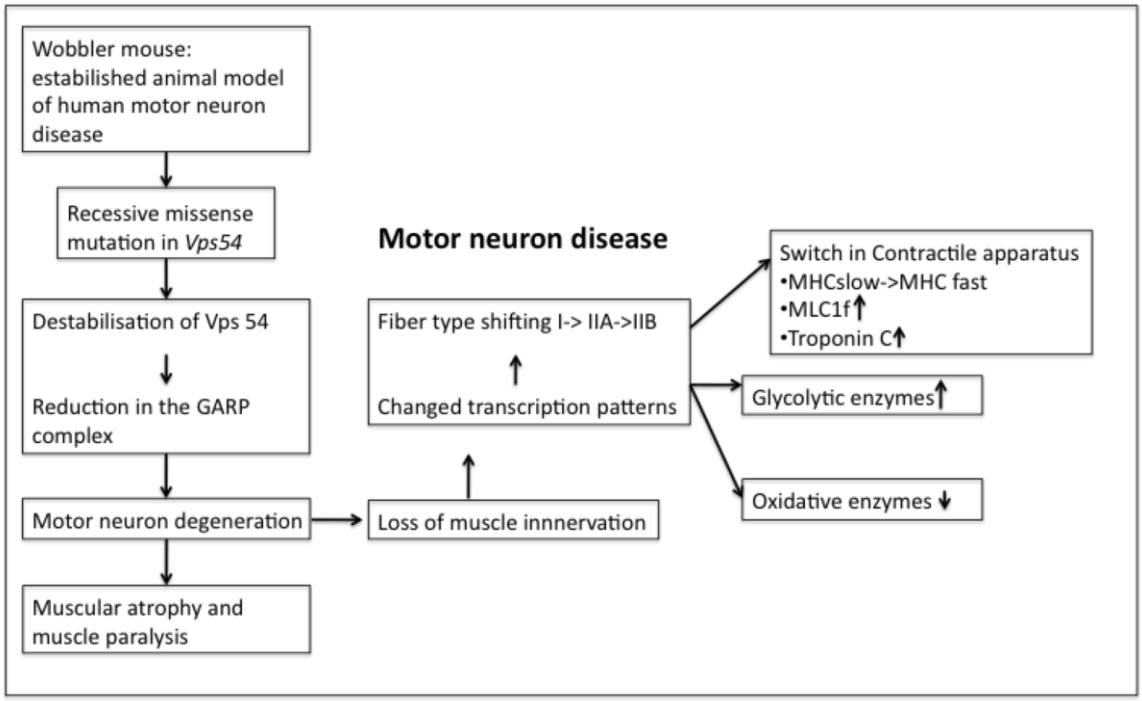

Figure 7.2 Overview of changes observed in the Wobbler skeletal tissue.

Shows the overall changes observed in the Wobbler skeletal tissue. The destabilisation of Vsp54 protein leads to a reduced concentration of the GARP complex resulting in motor neuron degeneration and impaired spermiogenesis in the Wobbler mouse. Muscle denervation results in fiber type switching from slow oxidative to fast glycolytic fiber phenotype. The proteomic profiling from the Wobbler skeletal tissue shows a drastic increase in glycolytic enzymes along with increases in the fast MLC of the contractile apparatus.

Proteomic studies have shown that mass spectrometry-based technologies can be used for studying a representative proportion of muscle proteins involved in contraction, metabolism, cellular stress response or calcium regulation. However, there are limitations to this method with respect to studying the entire proteome. High molecular weight proteins, membrane proteins and low abundance proteins can be difficult to detect in polyacrylamide gels due to pore size, hydrophobic nature and dynamic range. A mulitude of approaches have been attempted in order resolve these problems, from gel-free approaches or shot gun proteomics. In chapter 6 we attempted to optimise the on-membrane digestion of SR-associated proteins. Since the abundant SR membrane system plays a key role in excitation-contraction-relaxation

cycles and because SR proteins are involved in numerous human diseases (MacLennan et al. 2011), the establishment of a complete list of SR-associated proteins will be extremely useful for the evaluation of novel biomarker signatures of neuromuscular disorders and the identification of new therapeutic targets to treat channelopathies.

Bibiolography

Abersold, R. H., J. Leavitt, R. A. Saavedra, L. E. Hood and S. B. Kent. 1987. Internal amino acid sequence of proteins separated by one-or two dimensional gel elctrophoresis after in situ protease digestion on nitrocellulose. Proc Natl Acad Sci U S A 84(20): 6970-4.

Abersold, R., and M. Seilhamer. 2003. Mass Spectrometry-based proteomics. Nature 422(6928): 198-207.

Adrian, R. H., and S. H. Bryant. 1974. On the repetitive discharge in myotonic muscle fibers. J Physiol 240: 505-515.

Agbulut, O., P. Noirez, G. Butler-Browne, and H. Jockusch. 2004. Specific isomyosin proportions in hyperexcitable and physiologically denervated mouse muscle. FEBS Lett. 561(1-3): 191-194.

Anderson, L., and J. Seilhamer. 1997. A comparison of skelected mRNA and protein abundances in human liver. Electrophoresis 18(3-4): 533-7.

Bacou, F., P. Rouanet, C. Barjot, C. Janmot, P. Vigneron, and A. D'Albis. 1996. Expression of myosin isoforms in denervated, cross-reinnervated, and electrically stimulated rabbit muscles. Eur J Biochem 236(2): 539-47.

Bárány, M. 1990. ATPase activity of myosin correlated with speed of muscle shortening. J Gen. Physiol. 50(6): 197-218.

Barber, S. C., and P. J. Shaw. 2010. Oxidative stress in ALS: key role in motor neuron injury and therapeutic target. Free Radic Biol Med. 48(5): 629-41.

Bastone, A., E. Fumagalli, P. Bigini, P. Perini, D. Bernardinello, A. Cagnotto, I. Mereghetti, D. Curti, M. Salmona, and T. Mennini. 2009. Proteomic profiling of cervical and lumbar spinal cord reveals potential protective mechanisms in the wobbler mouse, a model of motor neuron degeneration. J Proteome Res 8(11): 5229-40.

Beghi, E., T. Mennini, C. Bendotti, P. Bigini, G. Logroscino, A. Chió, O. Hardimann, D. Mitchell, R. Swingler, B. J. Traynor, and A. Al-Chalabi. 2007. The heterogeneity of amytrophic lateral sclerosis: a possible explaination of the treatment failure. Current Medicinal Chemistry 14(30): 3185-3200.

Berkes, C. A., and S. J. Tapscott. 2005. MyoD and the transcriptional control of myogenesis. Semin Cell Dev Biol. 16(4-5): 585-95.

Berchtold, M. W., H. Brinkmeier, and M. Muntener. 2000. Calcium ion in skeletal muscle: its crucial role for muscle function, plasticity, and disease. Physiol Rev 80(3): 1215-65.

Bessmann, S. P., W. C. Yang, P. J. Geiger, and S. Erickson-Viitanen. 1980. Intimate coupling of creatine phosphokinase and myofibrillar adenosinetriphosphate. Biochem Biophys Res Commun. 96(3): 1414-20.

Bordet, T., B. Buisson, M. Michaud, C. Drouot, P. Galéa, P. Delaage, N. P. Akentiera, A. S. Evers, D. F. Covey, M. A. Ostuni, J. J. Lacapère, C. Massaad, M. Schumacher, E. M. Steidl, D. Maux, M. Delaage, C. E. Henderson, and R. M Pruss. 2007. Idenfication and characterisation of cholest-4-en-3-on, oxime (TRO19622). A novel drug candidate for amytrophic laterial sclerosis. J Pharmacol Exp Ther 322(2): 709-20.

Bottinelli, R., S. Schiaffino, and C. Reggiani. 1991. Force-velocity relations and myosin heavy chain isoform compositions of skinned fibers from rat skeletal muscle. J Physiol. 437: 655-72.

Bottinelli, R., R. Betto, S. Schiaffino, and C. Reggiani. 1994a. Maximum shortening velocity and coexistance of myosin heavy chain isoforms in single skinned fast fibers of rat skeletal muscle. J Muscle Res Cell Motil. 15(4): 413-419.

Botinelli, R., M. Canepari, C. Reggiani, and G.J. Stienen. 1994. Myofibrillar ATPase activity during isometric contraction and isomyosin composition in rat single skinned muscle fibers. J Physiol 481(3): 663-75.

Bradd, S. J., M. J. Dunn. 1993. Analysis of membrane proteins by western blotting and enhanced chemiluminescence. Methods Mol. Biol. 19: 211-218.

Bradford, M.M. 1976. A rapid and senititive method for the quantitation of microgram quantities of protein utilising the principle of protein-dye binding. Anal Biochem 72: 248-254.

Bryant, S. H., and A. Morales-Aguilera. 1971. Chloride channel in normal and myotonic muscle fibers and the action of monocarboxylic aromatic acids. J Physiol. 219(2): 367-83.

Buller, A. J., A. C. Dornhorst, R. Edwards, D. Kerr, and R. F. Whelan. 1959. Fast and slow muscles in mammals. Nature 183(4674): 1516-7.

Caiozzo, V. J., R. E. Herrick, and K. M. Baldwin. 1992. Response of slow and fast muscle to hypothyroidism: maximal shortening velocity and myosin isoforms. Am J Physiol. 263: C86-C94.

Catz, O. S., L. M. Fisher, and D. B. Kelley. 1995. Androgen regulation of a laryngeal-specific myosin heavy chain mRNA isoform whose expression is sexually differenciated. Dev Biol 171(2): 448-57.

Celio, M. R., and C. W. Heizmann. 1982. Calcium-binding protein parvalbumin is associated with fast contracting muscle fibers. Nature 297(5866): 504-6.

Chen, X. L., L. Zhou, J. Yang, F. R. Shen, S. P. Zhao, Y. L. Wang. 2010. Heptocellular carcinoma-associated protein markers investigated by MALDI-TOF MS. Mol Med Report 3(4): 589-96.

Chen, G., S. Carroll, D. Racay, J. Dick, D. Pette, I. Traub, G. Vrbova, P. Eggli, M. Celio, and B. Schwaller. 2001. Deficiency in parvalbumin increases fatigue resistance in fast-twitch muscle and upregulates mitochondria. Am J Physiol. 281(1): C114-22.

Chevallet, M., S. Luche, and T. Rabilloud. 2006. Silver staining of proteins in polyacrylamide gels. Nat Protoc 1(4): 1852-8.

Chin, E. R., E. N. Olson, J. A. Richardson, Q. Yang, C. Humphries, J. M. Shelton, H. Wai, W. Zhu, R. Bassel-Duby, and R. S. Williams. 1998. A calcineurin-dependent transcriptional pathway controls skeletal muscle fiber type. Genes Dev. 12: 2499-2509.

Chin, E. R., R. W. Grange, F. Viau, A. R. Simard, C. Humphries, J. Shelton, R. Bassel-Duby, R. S. Williams, and R. N. Michel. 2003. Alterations in slow-twitch muscle phenotype in transgenic mice overexpressing the Ca^{2+} buffering protein parvalbumin. J Physiol 547 (2): 649-663.

Clark, K. A., A. S. McElhinny, M. C. Beckerle, and C. C Gregorio. 2002. Striated muscle cytoarchitecture: an intricate web of form and function. Annu Rev Cell Biol. 18: 637-706.

Conjard, A., M. Peuker, and D. Pette. 1998. Energy state and myosin heavy chain isoforms in single fibers of normal and transforming rabbit muscles. Pflugers Arch. 436(6): 962-969.

Cros, N., J. Muller, S. Bouju, G. Piétu, C. Jacquet, J. J. Léger, J. F. Marini, and C. A. Dechesne. 1999. Upregulation of M-creatine kinase and glyceraldehyde 3-phosphate dehydrogenase: two markers of muscle disuse. Am J Physiol. 276(2): R308-16.

Donoghue, P., S. Ribaric, B. Moran, V. Cebasek, I. Erzen, and K. Ohlendieck. 2004. Early effects of denervation on Ca(2+)-handling proteins in skeletal muscle. Int J Med 13(6): 767-72.

Donoghue, P., P. Doran, P. Dowling, and K. Ohlendieck. 2005. Differential expression of the fast skeletal muscle proteome following chronic low-frequency stimulation. Biochem Biophys Acta 1752(2): 166-76.

Donoghue, P., P. Doran, K. Wynne, K. Pedersen, M. J. Dunn, and K. Ohlendieck. 2007. Proteomic profiling of chronic low-frequencing stimulated fast muscle. Proteomics 7(18): 3417-30.

Doran, P., P. Dowling, J. Lohan, K. McDonnell, S. Poetsch, and K. Ohlendieck. 2004. Subproteomics analysis of Ca+-binding proteins demonstrates decreased calsequestrin expression in dystrophic mouse skeletal muscle. Eur J Biochem 271(19): 3943-52.

Dutka, T. L., R. M. Murphy, D. G. Stephenson, and D. G. Lamb. 2008. Chloride conductance in the transverse tubular system of rat skeletal muscle fibers: importance in the excitation-contraction coupling and fatigue. J Physiol. 586(3): 875-887.

Dutzler, R., E. B. Campbell, M. Cadene, B. T. Chalt, and R. Mackinnon. 2002. X-Ray structure of a CIC chloride channel at the 3.0 Å reveals the molecular basis of anion selectivity. Nature 415(6869): 287-94.

Ellmerer, M., L. Schaupp, G. A. Brunner, G. Sendlhofer, A. Wutte, P. Wach, and T. R. Pieber. 2000. Measurement of interstitial albumin in human skeletal muscle and adipose tissue by open-flow microperfusion. Am J Physiol Endocrinol Metab. 278(2): E352-6.

Ennor, A. H., and H. Rosenberg. 1954. Some properties of creatine phosphokinase. Biochem J. 57(2): 203-12.

Entrikin, R. K., R. T. Abresch, R. B. Sharman, D. B. Larson, and N. A. Levine. 1987. Contractile and EMG studies of murine mytonia (mto) and muscular dystrophy (dy/dy). Muscle Nerve 10(4): 293-8.

Fahlke, C. 2000. Molecular mechanisms of ion conduction in CIC-type chloride channels: lessons from disease-causing mutations. Kidney Int. 57(3): 780-6.

Fahlke, C., and R. Rüdel. 1995. Chloride currents across the membrane of mammalian skeletal muscle fibers. J Physiol. 484(2): 355-68.

Fahlke, C., C. L. Beck, and A. L. George Jr. 1997. A mutation in autosomal dominant myotonia congenita affects pore properties of the muscle chloride channel. Proc Natl Acad Sci U S A 94(6): 2729-34.

Farley, J. M., and P. R. Miles. 1977. Role of depolarisation in acetylcholine-induced contractions of dog trachealis muscle. J Pharmacol Exp Ther 201(1): 199-205.

Farve, B., Y. Schneider, P. Lingasamy, J. E. Bouameur, N. Begré, Y. Gontier, M. F. Steiner-Champliaud, M. A. Frias, L. Borradori, and L. Fontao. 2011. Plectin interacts with the rod domain of type III intermediate filament proteins desmin and vimentin. Eur J Cell Biol. 90(5): 390-400.

Fitts, R. H., W. W. Winder, M. M. Brooke, K. K. Kaiser, and J. O. Holloszy. 1980. Contractile, biochemical and histochemical properties of thyrotoxic rat soleus muscle. Am J Physiol 238: C15-C20.

Froemming, G. R., B. E. Murray, S. Harmon, D. Pette, and K. Ohlendieck. 2000. Comparative analysis of the isoform expression pattern of Ca(2+)- regulatory membrane proteins in fast-twitch, slow-twitch, cardiac, neonatal and chronic low-frequency stimulated muscle fibers. Biochem Biophys Acta 1466(1-2): 151-68.

Gannon, J., P. Doran, A. Kirwan, and K. Ohlendieck. 2009. Drastic increase of myosin light chain MLC-2 in senescent skeletal muscles indicates fast-to-slow fiber transition in sarcopenia of old age. Eur J Cell Biol 88(11): 685-700.

Geers, C., and G. Cros. 2000. Carbon dioxide transport and carbonic anhydrase in blood and muscle. Physiol Rev. 80(2): 681-715.

George, A. L. Jr, M. A. Crackower, J. A. Abdalla, A. J. Hudson, and G. C. Ebers. 1993. Molecular basis of Thomsen's disease (autosomal dominant myotonia congenita). Nat. Genet. 3(4): 305-10.

Goldberg, A. L. 1967. Work-induced growth of skeletal muscle in normal and hypophysectomised rats. Am J Physiol. 213: 1193-1198.

Goodall, E. F., and K. E. Morrison.2006. Amytrophic Lateral Sclerosis (motor neuron disease): proposed mechanisms and pathways to treatment. Expert Rev Mol Med. 8(11): 1-22.

Gorza, L., K. Gundersen, T. Lømo, S. Schiaffino, and K. H. Westgaard. 1988. Slow-to-fast transformation of denervated soleus muscles by chronic high-frequency stimulation in the rat. J Physiol. 402: 627-49.

Gregory, P., R. B. Low, and W. S. Stirewalt. 1986. Changes in skeletal muscle myosin isoenzymes with hypertrophy and exercise. Biochem J 238: 55-63.

Gregory, P., J. Gagnon, D. A. Essig, S. K. Reid, G. Prior, and R. Zak. 1990. Differential regulation of actin and myosin isenzymes synthesis in functionally overloaded skeletal muscle. Biochem J 265: 525-532.

Groen, A. J., and K. S. Lilley. 2010. Proteomics of totall membranes and subcellular membranes. Expert Review of Proteomics 7(6): 867-878.

Gurnett, C. A., S. D. Kahl, R. D. Anderson, and K. P. Campbell. 1995. Absence of the skeletal muscle sarcolemma chloride channel CIC-1 in myotonic mice. J Biol Chem. 270(16): 9035-8.

Gutmann, E., and V. Hanzlíková. 1970. Effect of androgens on histochemical fiber type differentiation in the temporal muscle of the guinea pig. Histochemie 24: 287-291.

Harris, M. B., B. M. Mitchell, S.G. Sood, K. C. Webb, and R. C. Venema. 2008. Increased nitric oxide synthase activity and Hsp 90 associated with skeletal muscle following chronic exercise. Eur J Appl Physiol 104(5): 795-802.

Heller, A. H., E. M. Eicher, M. Hallett, and K. L. Sidman. 1982. Myotonia, a new inherited muscle disease in mice. J Neurosci 2:924-933.

Hodgkin, A. L., and P. Horowicz. 1960. Potassium contractures in single muscle fibers. J Physiol 153: 386-430.

Holzbaur, E. L., and M. K. Tokito. 1996. Localisation of the DCTN1 gene encoding p150 glued to human chromosome 2p13 by fluorescence in situ hybridisation. Genomics 31(3): 398-9.

Huxley, H., and J. Hanson. 1954. Changes in the cross sections of muscle during contraction and stretch and their structural interpretation. Nature 173(4412): 973-976.

Huxley, H. 2004. Fifty years of muscle and the sliding filament hypothesis. Eur. J. Biochem. 271: 1403-1415.

Jakubiec-Puka, A., J. Kordowska, C. Catani, and U. Carraro. 1990. Myosin heavy chain isoform composition in striated muscle after denervation and self-reinnervation. Eur J Biochem 193(3): 623-628.

Jänkälä, H., V. P. Marjola, N. E. Petersen and M. Märkönen. 1997. Myosin heavy chain mRNA transform to faster isoforms in immobilised skeletal muscle: a quantitative PCR study. J Appl Physiol 82: 977-982.

Jentsch, T. J. 2002. Chloride channels are different. Nature 415(6869): 276-7.

Jentsch, T. J., K. Steinmeyer, and G. Schwarz. 1990. Primary structure of Torpedo marmorata chloride channel isolated by expression cloning in Xenopus oocytes. Nature 348(6301): 510-4.

Jentsch, T. J., I. Neagoe, and O. Scheel. 2005. CLC chloride channels and transporters. Curr Opin Neurobiol. 15(3): 319-25.

Jockusch, H., K. Bertmam, and S. Schenk. 1998. The genes for two neuromuscular diseases of the mouse “arrested development of righting response”, adr, and “myotonia”, mto, are allelic. Genet Res. 5: 203-205.

Jurkat-Rott, K., H. Lerche, F. Lehmann-Horn. 2002. Skeletal muscle channelopathies. J Neurol 249: 1493-1502.

Kandarian, S. C., and R. W. Jackman. 2006. Intracellular signalling during skeletal muscle atrophy. Muscle Nerve 33(2): 155-65.

Kane, M. A., C. E. Kasper, and J. F. Kalinich. 2009. The use of established skeletal muscle cell lines to assess potential toxicity from embedded metal fragments. Toxicol in Vitro. 23(2): 356-9.

Katz, A., and K. Sahlin. 1988. Regulation of lactic acid production during exercise. J Appl Physiol. 65(2): 509-518.

Kaufmann, M., J. A. Simoneau, J. H. Veerkamp, and D. Pette. 1989. Electrostimulation-induced increases in fatty acid-binding protein and myoglobin in rat fast-twitch muscle and comparison with tissue levels in the heart. FEBS Lett. 245(1-2): 181-4.

Kaufmann, K., D. Simon-Chazottes, J. L. Guenet, and H. Jockusch. 1992. Wobbler, a mutation affecting motorneuron survival and gonadal functions in the mouse, maps to chromosome 11. Genomics 13: 39-43.

Kloche, R., K. Steinmeyer, T. J. Jentsch, and H. Jockusch. 1994. Role of innervation, excitabilty and myogenic factors in the expression of the muscular chloride channel ClC-1. A study of normal and myotonic muscle. J Biol Chem. 269 (44): 27635-9.

Kluxen, F. W., F. Schöffl, M. W. Berchtold, and H. Jockusch. 1988. Opposite regulation of the mRNAs for parvalbumin and p19/6.8 in myotonic mouse muscle. Eur J Biochem. 176(1): 153-8.

Koch, M. C., K. Ricker, M. Otto, F. Wolf, B. Zoll, C. Lorenz, K. Steinmeyer, and T. J Jentsch. 1993. Evidence for genetic homogeneity in autosomal recessive generalised myotonia (Becker). J Med Genet. 30(11): 914-7.

Kunita, R., A. Otomo, H. Mizumura, K. Suzuki, J. Showguchi-Miyata, Y. Yanagisawa, S. Hadano, J. E. Ikeda. 2004. Homo-oligomerisation of ALS2 through its unique carboxyl-terminal regions is essential for the ALS2-associated Rab5 guaine nucleotide exchange activity and its regulatory function on endosome trafficking. J Biol Chem. 279(37): 38626-35.

Kuzma-Kozakiewicz, M., and H. Kwiecinski. 2001. New therapeutic targets for amytrophic lateral sclerosis. Expert Opin. Targets 15(2): 127-143.

Lacomblez, L., G. Bensimon, P. N. Leigh, P. Guillet, and V. Meininger. 1996. Dose-ranging study of riluzole in amytrophic lateral sclerosis. ALS/Riluzole study group II. Lancet 347(9013): 1425-31.

Laemmli, U.K. 1970. Cleavage of structural proteins during the assembly of the head of bacteriophage T4. Nature 227(5259): 680-5.

Leberer, E., B. G. Timms, K. P. Campbell, and D. H. MacLennan. 1990. Purification, calcium-binding properties, and ultrastructural localisation of the 53'000- and 160'000 (sarcalumenin)- dalton glycoproteins of the sarcoplasmic reticulum. J Biol Chem 265: 10118-10124.

Lehmann-Horn, F., and K. Jurkatt-Rott. 1999. Voltage-gated ion channels and hereditary disease. Physiol Rev. 79(4): 1317-72.

Lewis, C. And K. Ohlendieck. 2010. Mass spectrometric identification of dystrophin isoform Dp427 by on-membrane digestion of sarcolemma from skeletal muscle. Anal iochem. 404(2): 197-203.

Li, Z. B., M. Lehar, R. Samlan, and P. W. Flint. 2005. Proteomic analysis of rat laryngeal muscle following denervation. Proteomics 5: 4764-4776.

Lin, J., H. Wu, D. T. Tarr, C. Y. Zhag, and Z. Wu. 2002. Transcriptional co-activator PGC-1 alpha drives the formation of slow-twitch muscle fibers. Nature 418: 797-801.

Locke, M., and E. G. Noble. 1995. Stress proteins: the exercise response. Can J Appl Physiol. 20: 155-167.

Lömo, T., R. H. Westgaard, and H. A. Dahl. 1974. Contractile properties of muscle: control by pattern of muscle activity in the rat. Proc R Soc Lond Bio Sci 187 (1086): 99-103.

Lui, Y., and J. M. Steinacker. 2001. Changes in skeletal muscle heat shock proteins: pathological significane. Front Biosci. 1(6): 12-25.

Luque-Garica, J. L., G. Zhou, D. S. Spellman, T. T. Sun, and T. A. Neubert. 2008. Analysis of electroblotted proteins by mass spectrometry: protein identification after western blotting. Mol Cell Proteomics 7(2): 308-14.

MacLennan, D. H., and E. Zvaritch. 2011. Mechanistic models for muscle diseases and disorders originating in thesarcoplasmic reticulum. Biochim Biophys Acta (in press).

Mankodi, A. 2008. Myotonic disorders. Neurol India 56(3): 298-304.

Mankodi, A. and C. A. Thornton. 2002. Myotonic Syndromes. Curr Opin Neurol. 15(5): 545-52.

Matthews, E., D. Fialho, S. V. Tan, S. L. Venance, S. C. Cannon, D. Sternberg, B. Fontaine, A. A. Amato, R. J. Barohn, R. C. Griggs, M. G. Hanna, and CINCH Investigators, 2010. Muscle channelopthies: does the predicted channel gating pore offer new treatment insights for hypokalaemic periodic paralysis? Brain 133(1) 9-22.

McCullagh, K. J., E. Calabria, G. Pallafacchina, S. Ciciliot, A. L. Serrano, C. Argentini, J. M. Kalhorde, T. Lømo, S. Schiaffino. 2004. NFAT is a nerve activity sensor in skeletal muscle and controls activity-dependent myosin switching. Proc Natl Acad Sci U S A 101(29): 10590-5.

Mehrke, G., H. Brinkmeier, and H. Jockusch. 1988. The myotonic mouse mutant ADR: electrophysiology of the muscle fiber. Muscle and nerve 11: 440-446.

Meisler, M. H., C. Russ, K. T. Montgomery, M. Greenway, S. Ennis, O. Hardiman, D. A. Figiewicz, N. R. Quenneville, E. Conibear, and R. H. Brown jr. 2008. Evaluation of the golgi trafficking protein VPS54 (wobbler) as a candidate for ALS. Amytroph Lateral Scler 9 (3): 141-8.

Meyer, M., D. M. C. Gonzalez, L. I. Garay, G. G. Monachelli, A. Lima, P. Roig, R. Guennoun, M. Schumacher, and A. F. De Nicola. 2010. Stage dependent effects of progesterone on motorneurons and glial cells of the wobbler mouse spinal cord degeneration. Cell Mol Neurobiol. 30 (1):123-35.

Miller, R. G., J. D. Mitchell, M. Lyon, and D. H. Moore. 2007. Riluzole for Amytrophic lateral sclerosis (ALS)/ motor neiron disease (MND). Cochrane Database Syst Rev 1: CD001447.

Moller, J. V., C. Olesen, A. M. Winther, and P. Nissen. 2010. The sarcoplasmic Ca2+-ATPase: design of a perfect chemi-osmotic pump. Q. Rev. Biophys 43: 501-566.

Muntener, M., L. Käser, J. Weber, and M. W. Berchtold. 1995. Increase of skeletal muscle relaxation speed by direct injection of parvalbumin cDNA. Proc. Natl. Acad. Sci. USA 92: 6504-6508.

Murgia, M., A. L. Serrano, E. Calabria, G. Pallafacchina, T. Lømo, and S. Schiaffino. 2000. Ras is involved in nerve-activity-dependent regulation of muscle genes. Naure Cell Bio 2(3): 142-147.

Nagai, S. M., J. R. Pearlstone, C. S. Farah, F. C. Reinach, L. B. Smillie, and R. S. Hodges. 2001. Structural and functional studies on Troponin I and Troponin C interactions. J Cell Biochem 83(1): 33-46.

Nakashima, K., N. Sato, T. Nakagaki, H. Abe, S. Ono, T. Obinata. 2005. Two mouse cofilin isoforms, muscle type (MCF) and non muscle type (NMCF), interact with F-actin with different efficiencies. J Biochem 138(4): 519-26.

Neufer, P. D., G. O. Ordway, G. A. Hand, J. M. Shelton, J. A. Richardson, I. J. Benjamin and R. S. Williams. 1996. Continuous contractile activity induces fiber type specific expression of Hsp 70 in skeletal muscle. Am J Physiol 271: C1828-C1837.

Neufer, P. D., and I. J. Benjamin. 1996. Differential expression of □-crystallin and Hsp 27 in skeletal muscle during continuous contractile activity. Relationship to myogenic regulatory factors. J Biol Chem. 271(39): 24089-95.

Neuhoff, V., N. Arold, D. Taube, and W. Ehrhardt. 1988. Improved staining of proteins in polyacrylamide gels including isoelectric focusing gels with clear background at nanogram sensitivity using coomassie brilliant blue G-250 and R-250. Electrophoresis 9(6): 255-62.

O'Farrell, P. H. 1975. High resolution two-dimensional electrophoresis of proteins. J Biol Chem 250(10): 4007-21.

Ohlendieck, K. 2010. Proteomics of skeletal muscle glycolysis. Biochem Biophys Acta. 1804(1): 2089-2101.

Ohlendieck, K., J. M. Ervasti, J. B. Snook, and K. P. Campbell. 1991. Dystrophin-glycoprotein complex is highly enriched in isolated skeletal muscle sarcolemma. J. Cell Biol. 112: 135-148.

Ohlendieck, K., G. R. Frömming, B. E. Murray, P. B. Maguire, E. Leisner, I. Traub, and D. Pette. 1999. Effects of chronic low-frequency stimulation on Ca2+-regulatory membrane proteins in rabbit fast muscle. Pflugers Arch. 438(5): 700-8.

Ono, S., N. Minami, H. Abe, and T. Obinata. 1994. Characterisation of a novel cofilin isoform that is predominantly xpressed in mammalian skeletal muscle. J Biol Chem. 269(21): 15280-6.

Pattullo, M. C., M. A. Cotter, N. E. Cameron, and J. A. Barry. 1992. Effects of lengthened immobilisation on functional and histochemical properties of rabbit tibialis anterior muscle. Exp Physiol. 77: 433-442.

Pérez-Victoria F. J., G. Abascal-Palacios, I Tascón, A. Kajara, J.G. Magadán, E. P. Pioro, J. S. Bonifacino, and A. Hierro. 2010. Structural basis for the wobbler mouse neurodegenerative disorder caused by mutation in the Vsp54 subunit of the GARP complex. Proc Natl Acad Sci U S A 107(29): 12860-5.

Peter, J. B., R. J. Barnard, V. R. Edgerton, C. A Gillespie, and K. E. Stempel. 1972. Metabolic profiles of three fiber types of skeletal muscle in guinea pigs and rabbits. Biochemistry. 11(14): 2627-33.

Pette, D. 2001. Historical perspectives: plasticity of mammalian skeletal muscle. J Appl Physiol. 90(3): 119-24.

Pette, D., B. U. Ramirez, W. Müller, R. Simon, G. U. Exner, and R. Hildebrand. 1975. Influence of intermittent long-term stimulation on contractile, histochemical and metabolic properties of fiber populations in fast and slow rabbit muscles. Pflugers Arch. 361(1): 1-7.

Pette, D., and R. S. Staron. 1990. Cellular and molecular diversities of mammalian skeletal muscle fibers. Rev Physiol Biochem Pharmacol. 116: 1-76.

Pette, D., and R. S. Staron. 2000. Muscle isoforms, muscle fiber types, and transitions. Microscopy Research and Technique 50(6): 500-509.

Planells-Cases, R., and T. J. Jentsch. 2009. Chloride channelopathies. Biochim Biophys Acta 1792(3): 173-89.

Pratt, J., J. Rataud, F. Bardot, M. Roux, J. C. Blanchard, P. M. Laduron, and J. M. Stutzmann. 1992. Neuroprotective action of riluzole in rodent models of global and focal cerebral ischaemia. Neurosci Lett. 140(2): 225-30.

Proenza, C., J. O'Brien, J. Nakai, S. Mukherjee, P. D. Allen, and K. G. Beam. 2002. Identification of a region of the Ryr1 that participates in allosteric coupling with the alpha 1s (car 1.1) II- III loop. The Journal of Biological Chemistry 277(8): 6530-6535.

Pusch, M. 2002. Myotonia caused by mutations in the muscle chloride channel gene CLCN1. Hum Mutat. 19(4): 423-34.

Rabilloud, T., J. M. Strub, S. Luche, A. Dorsselaer, and J. Lunardi. 2001. A comparison between Sypro Ruby and ruthenium II tris(bathophenanthroline disulfonate) as fluorescent stains for protein detection in gels. Proteomics 1(5): 699-704.

Racay, P., P. Gregory, and B. Schwaller. 2006. Parvalbumin deficiency in fast-twitch fibers leads to increased "slow-twitch type" mitochondria, but does not affect the expression of fiber specific proteins. FEBS Journal 273: 96-108.

Radermacher, M., V. Rao, R. Grassucci, J. Frank, A.P. Timerman, S. Fleischer, and T. Wagenknecht. 1994. Cryo-electron microscopy and three-dimensional reconstruction of the calcium re;ease channel/ryanodine receptor from skeletal muscle. J Cell Biol 127: 411-423.

Reininghaus, J., E. M. Füchtbauer, K. Bertram, and H. Jockusch. 1988. The myotonic mouse mutant ADR: phyiologically denervated mouse muscle. FEBS Lett. 561(1-3): 191-194.

Rosen, D. R., T. Siddique, D. Patterson, D. A. Figlewicz, P. Sapp, A. Hentati, D. Donaldson, J. Goto, J. P. O'regan, H. X. Deng. 1993. Mutations in Cu/Zn superoxide dismutase gene are associated with familian amytrophic lateral sclerosis. Nature 362(6415): 59-62.

Rossi, A. E., and R. T. Dirksen. 2006. Sarcoplasmic reticulum: the dynamic calcium governer of muscle. Muscle Nerve 33(6): 715-31.

Rothstein, J. D., and R. W. Kundel. 1995. Neuroprotective strategies in a model of chronic glutamate-mediated motor neuron toxicity. J Neurochem 65(2): 643-51.

Royer, L., and E. Rois. 2009. Deconstructing calsequestion. Complex buffering in the calcium store of skeletal muscle. J Physiol. 587: 3101-3111.

Rüdel, R., R. Dengler, K. Ricker, A. Haass, and W. Emser. 1980. Improved therapy of myotonia with the lidocaine derivative tocainde. J Neurol 222(4): 275-8.

Salmons, S., and G. Vrbova. 1969. The influence of activity on some contractile characteristics of mammalian fast and slow muscles. J Physiol 201(3): 535-549.

Sathasivam, S. 2010. Motor neurone disease: clinical features, diagnosis, diagnostic pitfalls and prognostic markers. Singapore Med J. 51(5): 367-72.

Saviane, C., F. Conti, M. Pusch. 1999. The muscular chloride channel CiC-1 has a double barreled apparance that is differentially affected in dominant and recessive myotonia. J Gen Physiol. 113: 457-467.

Schiaffino, S., and C. Regfiani. 1996. Molecular diversity of myofibrillar proteins: gene regulation and functional significance. Physiol Rev. 76(2): 371-423.

Schiaffino, S., and C. Reggiani. 1994. Myosin isoforms in mammalian skeletal muscle. J Appl Physiol. 77(2) 493-501.

Schmidt-Rose, T., and T. J. Jentsch. 1997. Transmembrane topology of a CIC chloride channel. Proc Natl Acad Sci U S A 94: 7633-7638.

Schmitt-John, T., C. Drepper, A. Mußmann, P. Hahn, M. Kutilmann, C. Thiel, M. Hafner, A. Lengeling, P. Heimann, J. M. Jones, M. M. Meisler, and H. Jockusch. 2005. Mutation of Vsp54 causes motor neuron disease and defective spermiogenesis in the wobbler mouse. Nature genetics 37 (11): 1213-5.

Schwaller, B., J. Dick, G. Dhoot, S. Carroll, G. Vrbova, P. Nicotera, D. Pette, A. Wyss, H. Bluethmann, W. Hunziker, and M. R. Celio. 1999. Prolonged contraction-relaxation cycle of fast-twitch muscles in parvalbumin knockout mice. Am J Physiol 276: C395-C403.

Sedehizade, F., R. Kloche, and H. Jockusch. 1997. Expression of nerve-regulated genes in muscles of mouse mutants affected by spinal muscular atrophies and muscular dystrophies. Muscle Nerve 20(2): 186-94.

Seo, Y., K. Lee, K. Park, K. Bae, and I. Choi. 2006. A proteomic assessment of muscle contractile alterations during unloading and reloading. J Biochem 139(1): 71-80.

Shaw, P. J. 2005. Molecular and cellular pathways of neurodegeneration in motor neurone disease. J Neurol Neurosurg Psychiatry 76: 1046-1057.

Shaw, P. J., V. Forrest, P. G. Ince, J. P. Richardson, and M. J. Wastell. 1995. CSF and plasma amino acid levels in motor neuron disease: elevation of CSF glutamate in a subset of patients. Neurodegeneration 4: 209-216.

Shigemoto, K., S. Kubo, S. Mori, S. Yamada, T. Akiyoshi, and T. Miyazaki. 2010. Muscle weakness and neuromuscular junctions in aging and disease. Geriatr gerontol Int. 10(1): S137-S147.

Squire, J. M., and E. P. Morris. 1998. A new look at thin filament regulation in vertebrate skeletal muscle. The FASEB Journal 12: 761-771.

Staron, R. S., and D. Pette. 1986. Correlation between myofibrillar ATPase activity and myosin heavy chain composition in rabbit muscle fibers. Histochemistry 86(1): 19-23.

Staron, R. S. 1997. Human skeletal muscle fiber types: delineation, development, and distribution. Can J Appl Physiol. 22(4): 307-27.

Staron, R. S., W. J. Kraemer, R. S. Mikida, D. W. Reed, J. D. Murray, G. E. R. Campos, and S. E. Gordon. 1998. Comparison of soleus muscles from rats exposed to microgavity for 10 versus 14 days. Histochem Cell Bio 110: 73-80.

Staunton L , Jockusch H , Ohlendieck K . 2011. Proteomic analysis of muscle affected by motor neuron degeneration; the wobbler mouse model of amyotrophic lateral sclerosis. Biochem Biophys Res Commun. 406 (4): 595-600.

Staunton L , Donoghue P , Mullen E , Manning G , Ohlendieck K . 2010. DIGE analysis of rat skeletal muscle proteins using nonionic detergent phase extraction of young adult versus aged gastrocnemius tissue. J. Proteomics. 73 (8): 1441-1453.

Steinmeyer, K., R. Kloche, C. Ortland, M. Gronemeier, H. Jockusch, S. Gründer, and T. J. Jentsch. 1991. Inactivation of muscle chloride channel by transposon insertion in myotonic mice. Nature 354(6351): 304-8.

Stuhlfauth, I., J. Reininghaus, H. Jockusch, and C. W. Heizmann. 1984. Calcium-binding protein, parvalbumin is reduced in mutant mammalian muscle with abnormal contractile properties. Proc Natl Acad Sci U S A 81(15): 4814-8.

Sun, H., J. Liu, F. Ding, M. Wang, M. Lui, and X. Gu. 2006. Investigation of differentially expressed proteins in rat gastrocnemius muscle during denervation-reinnervation. J. Muscle Res. Cell. Motil. 27: 241-250.

Takada, F., D. L. Vander Woude, H. Q. Tong, T. G. Thompson, S. C. Watkins, L. M. Kundel, and A. H. Beggs. 2001. Myozenin an alpha-actin-actinin- and gamma-filamin- binding protein of skeletal muscle Z lines. Proc Natl Sci U S A 98(4): 1595-600.

Thirion, C., K. Stucka, B. Mendel, A. Gruhler, M. Jaksch, K. J. Nowak, N. Binz, N. G. Laing, and H. Lochmüller. 2001. Characterisation of human muscle type cofilin (CFL2) in normal and regenerating muscle. Eur J Biochem 268(12): 3473-82.

Tobacman, L. S. 1996. Thin filament-mediated regulation of cardiac contraction. Ann. Rev. Physiol. 58: 447-481.

Tonge, R., J. Shaw, B. Middleton, R. Rowlinson, S. R. Rayner, J. Young, F. Pogan, E. Hawkins, I. Curvie, and M. Davison. 2001. Validation and development of fluorescence two-dimensional differential gel electrophoresis proteomic technology. Proteomics 1(3): 377-96.

Towbin, M., T. Staehelin, and J. Gordon. 1979. Electrophoresis transfer of proteins from polyacrylamide gels to nitrocellulose sheets: protein identification after western blotting. Mol Cell Proteomics 7(2): 308-14.

Trentham, D. R., C. H. McMurray, and C. L. Pogson. 1969. The active chemical state of D-glyceraldehyde 3-phosphate in its reactions with D-glyceraldehyde 3 –phosphate dehydrogenase, aldolase, and triose phosphate isomerase. Biochem J. 114(1): 19-24.

Unlu, M., M. E. Morgan, and J. S. Minden. 1997. Difference gel electrophoresis: a single gel method for detecting changes in protein extracts. Electrophoreis 18(11): 2017-7.

Valentine, J. S., P. A. Doucette, and S. Z. Potter. 2005. Copper- Zinc Superoxide Dismutase and Amytrophic Lateral Sclerosis. Annu Rev. Biochem 74: 563-93.

Van Lunteren, M., M. Moyer, and P. Leahy. 2006. Gene expression profiling of diaphragm muscle isometric contractile properties. Respir Physiol Neurobiol 155(3): 220-6.

Waldegger, S., and T. J. Jentsch. 2000. From tonus to tonicity: physiology of CIC chloride channels. J Am Soc Nephrol 11: 1331-1339.

Wallimann, T., T. Schlösser, and M. M. Eppenberger. 1984. Function of the M-line-bound creatine kinase as intramyofibrillar ATP regeneration at the receiving end of the phosphorylcreatine shuttle in muscle. J Biol Chem 259(8): 5238-46.

Wang, Y. X., C. L. Zhag, R. T. Yu, H. R. Cho, M. C. Nelson, C. K. Bayuga-Ocampo, J. Ham, H. Kang, and R. M. Evans. 2004. Regulation of muscle fiber type and running endurance by PPAK delta. Plos Biol. 2(10): 1532-1539.

Watkins, W. J., and D. C. Watts. 1984. Biological features of the new A2G-adr mouse mutant with abnormal muscle function. Laboratory Animals 18: 1-6.

Weiss A., S. Schiaffino, and L. A. Leinwand. 1999. Comparative sequence analysis of the complete human sarcomeric myosin heavy chain family: implications for functional diversity. J. Mol. Med. 290(1): 61-75.

Westerblad, H., J. D. Bruton, and A. Katz. 2010. Skeletal muscle: energy metabolism, fiber types, fatigue and adaptability. Experimental Cell Research 316(18): 3093-3099.

Wheeler, T. M. 2008. Myotonic dystrophy: therapeutic strategies for the future. Neurotherapeutics 5(4): 592-600.

Wijesekera, L. C., and P. N. Leigh. 2009. Amytrophic Lateral Sclerosis. Orphanet J Rare Dis 4:3.

Xu, K. Y., and L. C. Becker. 1998. Ultastructural localisation of glycolytic enzymes on sarcoplasmic reticulum vesticles. J Histochem Cytochem 46: 419-427.

Yamashita, M., and J. B. Fenn. 1983. Electrospray ion source, Another variation on the free-jet theme. The Journal Of Physical Chemistry. 88(20): 4451-4459.

Zhu, S., I. G. Starrorskaya, M. Drozda, B. Y. Kim, V. Ona, M. Li, S. Sarang, A. S. Lui, D. M. Hartley, D. C. Wu, S. Gullans, R. J. Ferrante, S. Przedborski, B. S. Kristal, and R. M. Friediander. 2002. Minocycline inhibits cytochrome c release and delays progression of amytrophic lateral sclerosis in mice. Nature 417(6884): 74-8.

Appendix

Peer-reviewed Publications